A Molecular Dynamics Study of the Tribological Properties of Diamond Like Carbon

by

Mathew M Swisher

Submitted to the Department of Mechanical Engineering
in partial fulfillment of the requirements for the degree of

Doctor of Philosophy in Mechanical Engineering and Computation

at the

MASSACHUSETTS INSTITUTE OF TECHNOLOGY

September 2020

Author .....
Department of Mechanical Engineering
August 14, 2020

Certified by .....
Nicolas G. Hadjiconstantinou
Professor of Mechanical Engineering
Thesis Supervisor

Accepted by .....
Nicolas G. Hadjiconstantinou
Chairman, Department Committee on Graduate Theses
Co-Director, Computational Science and Engineering

Accepted by .....
Youssef M. Marzouk
Co-Director, Computational Science and Engineering

A Molecular Dynamics Study of the Tribological Properties of Diamond Like Carbon

by

Mathew M Swisher

Submitted to the Department of Mechanical Engineering
on August 14, 2020, in partial fulfillment of the
requirements for the degree of
Doctor of Philosophy in Mechanical Engineering and Computation

Abstract

Diamond like carbon (DLC) is an attractive choice as a coating for mechanical components, because of its excellent wear resistance and very low coefficient of friction. We use molecular dynamics (MD) simulations with a reactive force field (ReaxFF) to study the friction and wear between DLC counterfaces, both in comparison to and in contact with steel counterfaces. We show that the tribological properties of DLC in dry sliding friction are heavily dependent on both the structure of the DLC as well as the passivation layer that forms on the sliding counterfaces under different environmental conditions, and that when optimizing for the lowest COF the best structure for the DLC depends on the type of passivation layer. We also find that, by preventing bonding across the counterfaces as the thin film of lubricant is squeezed out at the point of contact, the passivation layer is instrumental in the material's ability to resist scuffing and wear. Additionally, we find that the strength and hardness of DLC makes damaging the passivation layer due to contact forces unlikely under real world conditions.

Finally, we use MD simulations to study in more detail the transition from lubricated to dry friction, and in particular, the role of DLC surface chemistry and the resulting passivation layer in this transition. Our work shows that the frictional force can be described quite accurately across the transition from pure slip (dry friction) to the purely hydrodynamic regime using a simple model which superposes the two effects, provided it also accounts for any immobile fluid layers at the fluid-solid interface. We show that, for water lubrication, the transition from the pure slip to the purely hydrodynamic regime occurs at smaller lengthscales in DLC counterfaces compared with steel.

Thesis Supervisor: Nicolas G. Hadjiconstantinou
Title: Professor of Mechanical Engineering

Acknowledgments

I would like to start by thanking my advisor, Prof. Nicolas Hadjiconstantinou. Not only for his knowledge and insight, but also for his kindness, patience, and good humor. I consider myself extremely lucky to have had such a wonderful advisor.

I would also like to thank Dr. Tian Tian and Prof. Ken Kamrin for being a part of my PhD committee. Their suggestions and advice have been particularly helpful and greatly appreciated.

Additionally, I would like to thank Drs Hans-Jürgen Füßer, Enrique Lizarraga-Garcia, and Philipp Köser for many useful discussions and suggestions. Their input on how DLC is used and performs in real world applications was invaluable and helped this research find its direction.

I am thankful to all my friends and lab mates: Rounaq Basu, Rohan Banerjee, Michael Boutilier, Nisha Chandramoorthy, Mojtaba Forghani, Colin Landon, Evan Massaro, J.-P. Peraud, and Gerald Wang. Their friendship has made living and working at MIT an incredible and wonderful experience that I will never forget.

This research was sponsored by the Consortium on Lubrication in Internal Combustion Engines with additional support from Argonne National Laboratory and the US Department of Energy. The consortium members were Daimler, Mahle, MTU Friedrichshafen, PSA Peugeot Citroën, Renault, Shell, Toyota, Volkswagen, Volvo Cars, Volvo Trucks and Weichai Power.

Contents

List of Figures

Chapter 1

Introduction

Diamond like carbon (DLC) [1, 2] is an attractive choice as a coating for mechanical components. For example, DLC is typically used for reducing abrasive wear in a variety of applications as varied as internal combustion engines [3, 4], coatings on hard disk drives [5], and medical implants [6, 7]. Particular interest has focused on characterizing the tribological properties between DLC and other common materials found in mechanical components, such as steel [8, 9, 10]. Previous work reveals that DLC exhibits both excellent wear resistance as well as a very low coefficient of friction (COF) [1, 2, 11, 12]. Laboratory experiments have established a range of values for both the wear rate and the COF [11, 12]. These experiments also highlight the fact that many factors can affect the measured tribological properties of the material. Some of the more obvious examples include the bulk properties of DLC, such as the percentage of sp^3 bonds or the percentage of hydrogen in the DLC; however, there are also other less obvious factors such as the environment the DLC is being tested in. For example, the relative humidity the experiment is performed at can have a dramatic impact on the resulting COF measured [11]. As we show in this thesis, many of the answers to these questions lie in the nature of the interactions *between* materials, that is, interface structure and properties are very important.

Friction and wear are fundamentally molecular-level processes. In the case of DLC, in addition to its own structure, molecular considerations extend to its passivation layer which is in contact with the opposing surface ("counterface"). Currently, the

molecular mechanisms leading to the observed experimental behavior involving DLC remain poorly understood. Particularly intriguing are experimental data suggesting considerable sensitivity to ambient conditions [13, 11, 14]. It is widely speculated that these phenomena are driven by physicochemical interactions at the interface between the DLC and the counterface. Understanding the fundamental physics behind these phenomena is of vital importance for determining if DLC is an appropriate choice in a given environment. Additionally, this knowledge can be used to optimize existing systems for fully exploiting DLC properties.

Currently the main method that has been applied to study the tribological properties of DLC on the atomistic level is quantum molecular dynamics (QMD) simulation [30, 51, 22]. This method, which features first principles quantum mechanical modeling to capture the interactions between atoms in the system, is highly accurate and is able to simulate all of the chemical reactions occurring in a simulation; at the same time, it is also very computationally expensive. As such, it is currently impossible to perform simulations containing enough atoms to simulate some of the important phenomena of practical interest (e.g. wear, scuffing, and lubrication).

In this thesis we use classical molecular dynamics (MD) simulation that exploits the recently-developed reactive potential models to study the atomistic mechanics underlying the properties of DLC under a variety of conditions of interest in the context of tribological applications. With this in mind, whenever possible, the simulations in this work provide direct comparisons to analogous simulations involving steel counterfaces.

Reactive potentials [19, 20, 21] combine many of the benefits of ab-initio techniques with the computational efficiency of traditional classical MD simulations and have made it possible to perform sufficiently large simulations (e.g. 10,000-100,000 atoms) without resorting to massively parallel computing resources, while still modeling the chemical reactions occurring in the system with reasonable accuracy. In the present thesis we use the ReaxFF potential [41, 40, 46, 54], which is described in more detail in section 2.3.3. The thesis outline is as follows.

In Chapter 2 we provide background material on nanoscale friction and DLC

properties; we also review some of the general methods used in this thesis including MD simulation, the Reax Force Field, and the methods used to create atomistic models of DLC.

In Chapter 3 we use atomistic simulations to measure the COF for DLC counterfaces in dry sliding friction. We specifically investigate the effect of the DLC structure (e.g. sp^3 percentage) and environmental conditions which influence the passivation layer that forms on the counterface. The simulation results are compared with those for steel counterfaces as well as experimental results (for both materials) where those are available.

In Chapter 4 we use MD simulations to study the friction and wear between pairs of DLC, steel, and mixed surface counterfaces in sliding contact. We consider water, n-eicosane, and 9-octyl-eicosane lubricants, paying particular attention to the passivation layer they induce on the sliding solid surfaces, and how they influence the bonding and wear that is experienced by the different combinations of surfaces. Using these simulation results, we study the failure modes of the various surfaces in order to gain insight into what makes DLC an effective coating for reducing friction and wear.

In Chapter 5 we use atomistic simulations to study the transition from lubricated to dry friction in much greater detail. This is done by simulating like surface pairs of DLC and steel counterfaces that are separated by a lubricating layer of various thicknesses that are then subjected to Couette flow. This enables us to compare how the thin fluid films of the model lubricants behave relative to the theoretical models as well as the known properties of the fluid. In particular, we are interested in modeling the transition between the three expected regimes of nanoconfined flow and how the interactions between the model lubricants and the surfaces influence these transitions.

Finally, in Chapter 6, we summarize the results from the previous chapters and offer suggestions for future work.

Chapter 2

Background

2.1 Nanoscale Tribology

Friction and the associated Amontons law [16] is one of the most fundamental and well-studied problems in the history of science. Although energy dissipation due to friction can be explained at a basic level using simple terms, as we do below, models that are sufficiently accurate to be used for engineering design are typically very specific, complex and in many cases remain empirical. In this thesis we aim to provide fundamental understanding towards the development of such models for DLC and will be using high-fidelity MD simulations to obtain the required insight.

Before we embark on this task, we provide a brief review of the basic understanding of frictional processes between molecularly smooth surfaces through van der Waals and electrostatic forces when in close sliding contact [16, 17, 18]. These studies suggest that the energy dissipation associated with friction can be illustrated using the following simplified mechanism [16], which considers atoms/molecules at the interface of two surfaces in sliding contact as shown in Figure 2-1.

Consider two particles (A and B, figure 2-1, part a) at the interface of the two surfaces; due to the relative motion of the two surfaces, they are approaching each other but start far enough away from each other for their interaction to be negligible. Next in part b, due to the translation of the upper surface, the two particles get closer which results in mutual repulsion, causing particle A to move up and to the left and

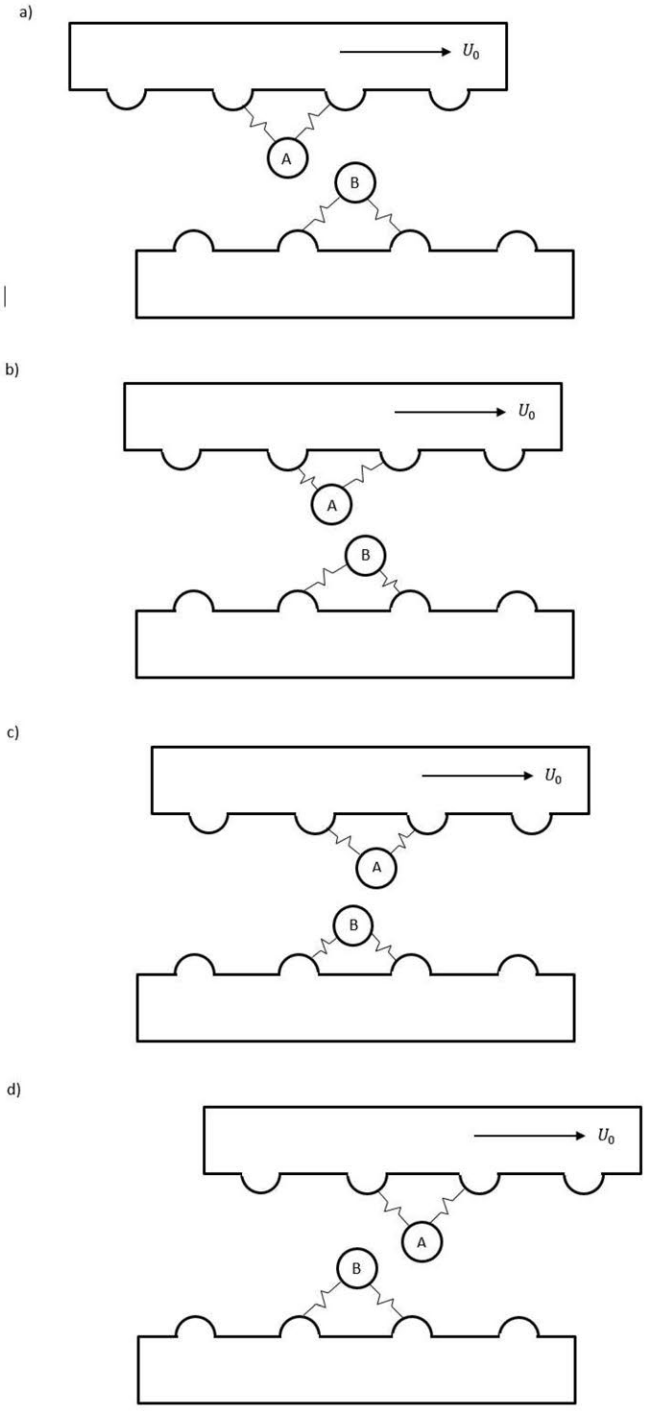

Figure 2-1: Simplified mechanism through which atomistic friction, manifesting itself as dissipation of energy, is caused by the motion of atoms at the material interface. Upper surface is moving at constant velocity U_0 and lower surface is held stationary. As the bonds between particles A and B with their respective surfaces deform, potential energy is stored. This energy is then converted back into kinetic energy after the particles pass the point of minimum separation, and is ultimately dissipated by subsequent collisions with other atoms.

particle B to move down and to the right (by a fraction of the typical intermolecular distance). In addition to exerting a force on both surfaces, the motion of particle A and particle B away from their starting positions results in both of these particles storing potential energy in their bonds with their respective surfaces. Then in part c, the two particles pass the location of their minimum separation. At this point the direction of the repulsion in the horizontal direction has reversed and the two particles are finally able to move back towards their equilibrium positions. Once this happens in part d, the stored potential energy can be converted into kinetic energy of the two molecules, which is then dissipated into the bulk and becomes heat when those, now fast-moving, molecules collide with other molecules in their immediate vicinity.

Normally, the potential energy stored when the particles move apart is provided by the normal load keeping the two materials in contact. However, even in the absence of chemical bonding at the interface, longer range molecular forces, such as van der Waals forces as well as electrostatic (Coulomb) forces, result in adhesion between the two surfaces, which also contributes to the work done (and thus, ultimately, dissipation). In other words, adhesion plays a role both in determining the COF and wear via molecular interactions occurring at the contact interface, but by causing an attraction between the two materials that increases the effective load on the system. The latter, however, is generally not observed when dealing with real surfaces. This is because real materials are rough, making the percentage of the contact area where the two materials are close enough for molecular interactions to be significant a small fraction of the total area.

Smooth-surface friction and wear rates of various types of DLC have been widely studied in the literature using ab-initio MD simulations [23, 24, 22]. While these simulations are quite accurate, due to the intermolecular forces being calculated directly from quantum mechanics, their extreme computational cost greatly limits the size of the computational domain that can be simulated using reasonable computational resources. The small size of these simulations makes modeling important tribological phenomena like wear and lubrication very difficult or impossible. However, these studies do predict that DLC in contact with a DLC counterface should provide some

of the smallest known COF values for dry sliding (less than 0.07), due to minimal surface roughness and weak adhesion between surfaces [28, 16]. However, while laboratory experiments [1, 2, 27, 28] have demonstrated that DLC surfaces can achieve a low COF, they have not been able to consistently reproduce the very low COF values predicted in these earlier studies except under very specific circumstances.

The most likely cause of this disagreement is the highly idealized conditions in these simulations. In addition to assuming perfectly flat DLC surfaces, there are also some unrealistic assumptions being made about the passivation layer and the ambient conditions. For example, the carbon atoms at the DLC surface will be perfectly passivated with hydrogen atoms, however the ambient conditions needed to generate that passivation layer are not considered in these computational studies. Additionally, little effort has been made to simulate DLC with sub-optimal but realistic passivation layers, such as DLC that has become oxidized due to prolonged exposure to oxygen in the atmosphere. In this thesis, we address this by incorporating the chemical interactions between the two counterfaces, the surrounding environment, and any lubricants used into the model to more closely simulate the interaction between real surfaces. This is vital for allowing us to accurately observe how the tribological properties of DLC function at the molecular level.

2.2 Diamond Like Carbon

DLC is a type of amorphous carbon material that can exhibit a range of properties depending on how the carbon atoms it is comprised of are bonded together [2, 26]. This is usually quantified as the percentage of sp^3 bonded carbon atoms. More sp^3 bonded carbon atoms results in a denser coating that is similar to diamond. DLC comprised of more than 60% sp^3 is generally referred to as tetrahedral amorphous carbon (ta-C). Materials with sp^3 percentages below 40% are usually considered to be amorphous carbon (a-C). Additionally, the properties of DLC can also be modified by the inclusion of fillers such as hydrogen.

High sp^3 DLC has a number of properties that are similar to diamond, such

as high hardness and low chemical activity in most environments. In laboratory and industrial settings it has been shown [2, 3] that applying a layer of DLC to a mechanical component can greatly extend the lifetime of the part by reducing the amount of friction at the interface as well as the associated wear. However, the efficacy of this process can vary significantly in lab experiments and in real world applications, even for very similar types of DLC. For example, measurements of the COF of unlubricated hydrogen-free tetrahedral amorphous DLC can range between 0.05 and 0.20, solely based on the relative humidity at which the experiment was performed [27, 29, 30].

These variations are thought [30]-[35] to be heavily dependent on the surface chemistry of DLC and the properties of the passivation layer that forms based on environmental conditions, such as the amount of oxygen or water vapor in the air, or the composition of any lubricants to which the DLC surface is exposed to. As a result, understanding how the passivation layer interacts with a lubricant is of great importance for gaining molecular insight into the origin of the excellent tribological properties exhibited by DLC.

Current computational research into the surface chemistry and passivation of DLC has generally been focused on relatively small quantum chemical simulations. These simulations are able to accurately study how different passivation layers form and how effective these layers are at reducing the COF [30, 36]. Additionally, quantum molecular dynamics (QMD) simulations were recently used to identify why organic friction modifiers were able to induce super-lubricity in ta-C [37]. While these techniques are powerful, they are unable to scale up to the simulation sizes and length scales necessary for measuring wear, even at the atomic level. Recently, molecular dynamics (MD) simulations utilizing a reactive potential [38, 40] have been used to study nanoscale friction in amorphous carbon films [31, 32]. In these studies, they modeled the dry sliding friction between large molecularly smooth hydrogenated amorphous carbon (a-C:H) surfaces. From their computational experiments they were able to show that temperature and normal load during sliding friction influenced the length of time for the COF to reach a constant value (the running-in time) of the counter-

faces. They were also able to conclude that this behavior was a result of structural changes at the surface of the DLC and its passivation layer.

Although significantly more expensive than non-reactive potentials, reactive potentials are significantly more computationally efficient than ab-initio (quantum chemical) simulations while still offering reasonable chemical accuracy, thus enabling otherwise infeasible simulations while striking a good balance between efficiency and fidelity. Using these techniques will allow us to accurately model both the DLC and its surface chemistry, and enable us to study how these physicochemical interactions impact the friction and wear of DLC in several different environments and with a selection of test lubricants.

2.3 General Methods

In this section we briefly discuss the main computational techniques we leverage in this thesis.

2.3.1 Molecular Dynamics

Molecular dynamics is a technique for modeling the behavior of a system consisting of an ensemble of atomic particles using the classical Newtonian equations of motion. The motion of each atom in the simulation is tracked through time by determining the forces acting upon it using an interatomic potential and then numerically integrating in time to obtain its position at the next timestep of the simulation.

In this work the MD simulations were performed using LAMMPS (large scale atomistic/molecular massively parallel simulator), an open source package developed by Sandia National Laboratories that is highly optimized for running MD simulations across many CPU cores or even GPUs [42, 38, 56].

In order to integrate the equations of motion in time, LAMMPS uses the Velocity Verlet algorithm [43]. This algorithm is preferred because it reduces the total number of mathematical operations needed to update each of the atom positions compared to many other numerical integration schemes. These forces acting on each of the atoms

in a given simulation can come from a several different sources including van der Waals, electrostatic, chemical bonds, as well as constraints placed on the simulation.

In this thesis, the forces resulting from van der Waals effects, electrostatics, and chemical bonds are all calculated according to ReaxFF. This potential model is discussed in more detail in section 2.3.3 below. While this potential model has many useful features, it is also very computationally expensive. Fortunately, LAMMPS enables us to take advantage of a number of standard techniques to improve the performance of the simulations in this work.

For example, in order to reduce the number of calculations performed when calculating the next timestep of a simulation, the ReaxFF implementation features a cutoff distance of 10 angstroms, which means that forces between atoms farther away than 10 angstroms are set to zero. Coupled to cell lists (binning), which group all atoms into cells slightly larger than the cutoff distance (12 angstroms on each side). Using this approximation prevents us from having to calculate the distances or forces between atoms that are not in the same or an adjacent cell. This reduces the computational complexity of performing the MD calculation from $O(N^2)$ (when using a neighbor list) to $O(NN_c)$, where N_c is the number of atoms per cell. This improvement is particularly important for large simulations such as those in this work, because N_c is dependent on the number density of the atoms in the simulation rather than the total size of the simulation. This means that for increasingly large simulations the scaling becomes $O(N)$.

A second technique that brings considerable computational benefit is parallel processing, which takes makes best use of the processing capabilities of state of the art multi-core CPUs. This is done using several approaches. The most straightforward amounts to dividing the simulation domain into a grid of smaller boxes and assigning each of these boxes to a Message Passing Interface (MPI) node [38]. While the definition of nodes has become more complicated with the advent of high core and thread count computer processors, the concept is that each node runs on a subset of the available computing hardware (either on one or more servers). In general, approximately one node is used per physical CPU core; however other configurations may be

more efficient in specific circumstances. Each node calculates the forces and updates the positions for all of the atoms in its box before relaying the updated information the other MPI nodes. The size of these boxes is periodically adjusted so that the number of atoms per MPI node remains relatively even. However, the efficiency gain from this technique eventually becomes limited by the communication overhead. On the other hand, we can take advantage of Open Multi Processing (OpenMP), which allows for additional multi-threading within each of the MPI nodes [39].

2.3.2 General simulation geometry

The general simulation setup consists of two counterfaces in relative motion (see Figures 2-2 and 2-3) with and without lubricant, to simulate lubricated and dry sliding friction, respectively. These counterfaces are composed of several layers of atoms, including a control surface, a temperature control layer and the main body of the material. In some cases (see below), atoms near the point of contact are endowed with a different identity so that they can be used (as a group) to measure the stress tensor/pressure at that location.

Two different geometries are used in this work. For simulations of dry sliding friction or Couette flow (in Chapter 3 and Chapter 5), we use the flat counterfaces as shown in Figure 2-2. For simulations of thin film lubrication and wear (Chapter 4) we introduce an asperity via the sinusoidal counterface shown in Figure 2-3.

All simulations in this work are performed at a fixed temperature of 350K. The temperature was kept constant by using a Nose Hoover thermostat [44, 45], which simulates an external heat reservoir and exchanges kinetic energy between the system of interest and the reservoir. This enables the removal of the excess kinetic energy generated due to friction. To avoid any artifacts from the thermostat, the latter is only used on the atoms in the temperature control layer of each counterface while data is being collected.

Additional constraints on the simulation include the imposition of constant velocities or constant external forces on the 'control surface' portion of the counterfaces. Assigning constant velocities is necessary for achieving relative translation between

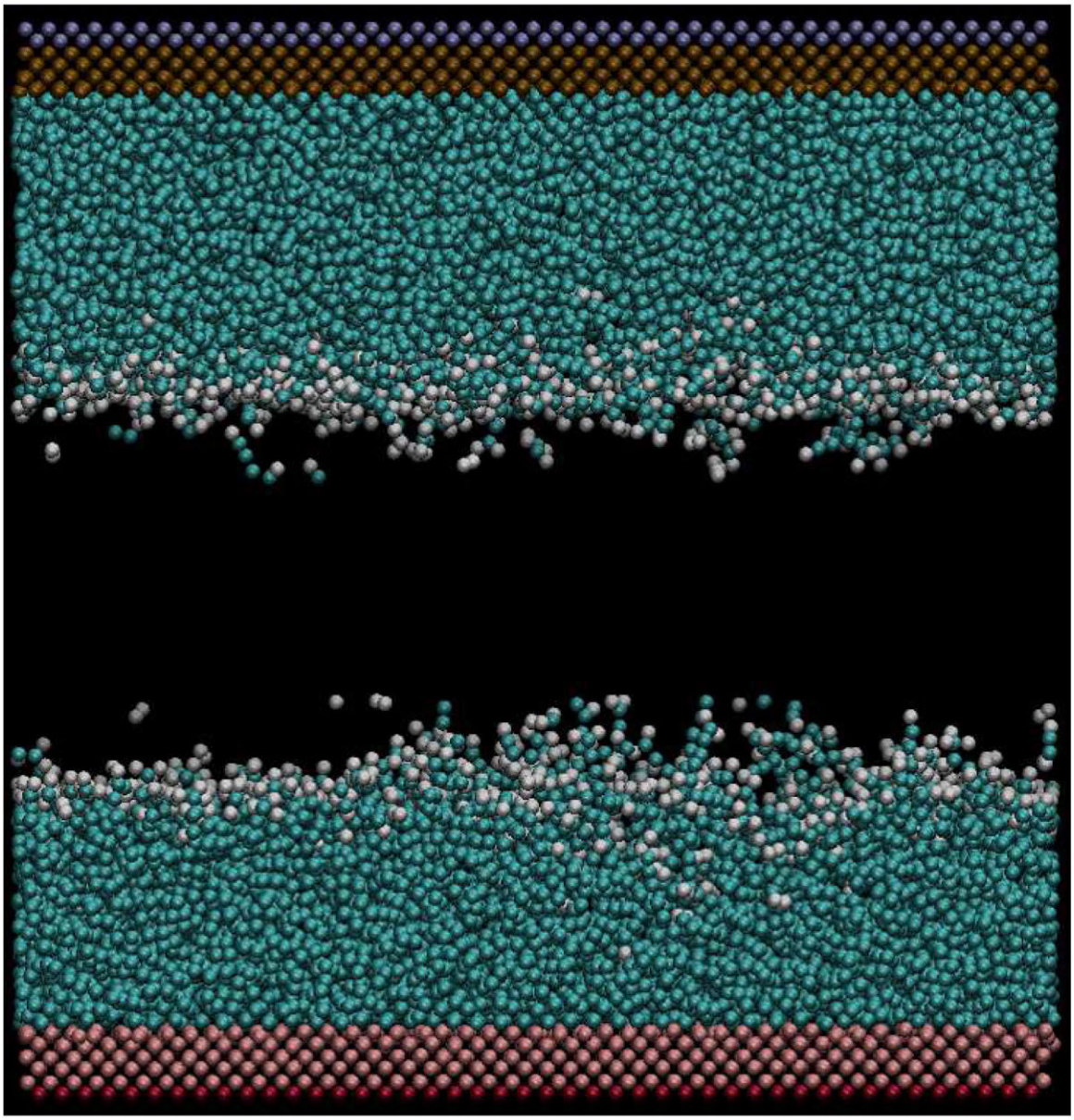

Figure 2-2: Initial simulation setup for flat DLC counterfaces. The atoms used to apply external forces are shown in red, the atoms held stationary are shown in pale blue, temperature control layers of atoms are shown in pink and brown, and the atoms making up the main body of the counterface are shown in teal. The atoms making up the two passivation layers are shown in white.

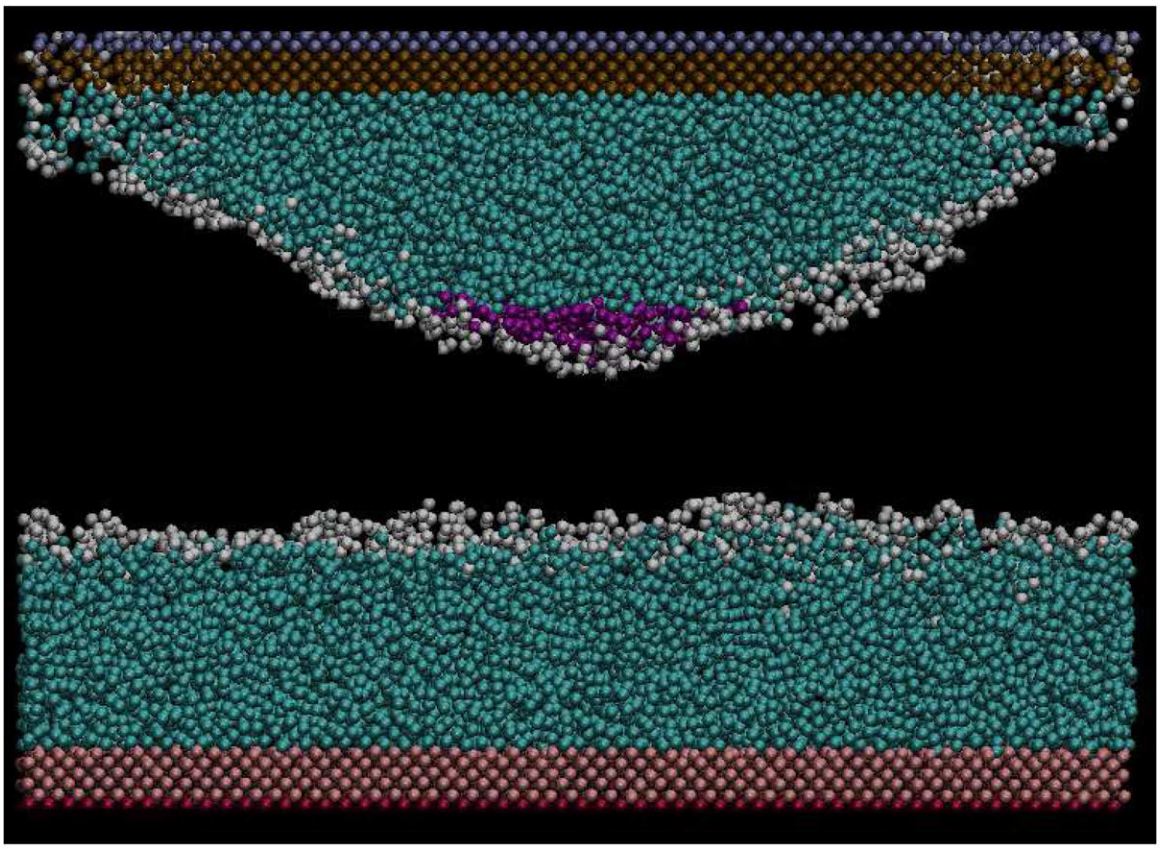

Figure 2-3: Initial simulation setup for a counterface with an asperity. Atoms used to apply external forces are shown in red, temperature control layers of atoms are shown in blue and atoms making up the main body of the counterface are shown in purple. The (main body) atoms used to calculate the stress at the tip of the model asperity are shown in purple. The passivation layers are shown in white.

the counterfaces, while applying a constant external force allows, *in principle* the imposition of a desirable nominal pressure (see below). Relative motion is achieved by immobilizing one counterface and moving the other at a fixed rate.

The nominal pressure is applied by assigning an additional force to all of the atoms in a given control surface. This results in the load being evenly distributed across all the atoms in the control surface, while keeping the atoms the positions of the atoms frozen relative to the other atoms in the layer. In this work, we generally use this constraint in combination with a prescribed (constant) horizontal velocity, which enables us to measure the horizontal forces acting required to cause the (horizontal) motion and from that calculate the frictional force.

In the cases where we prescribe both the horizontal and vertical velocities, we can get a measurement of both the friction force and the nominal pressure. However, the nominal pressure, although useful, is a poor approximation of the actual pressure at the point of contact. To obtain a better measure of the pressure at the point of contact, we sample the stress tensor of a small number of atoms near the point of contact, which we call the stress measurement region.

The stress measurement region is at the bottom tip of the asperity containing 250 atoms and is used to calculate the stress tensor at the contact point (see figure 2-3). This region of includes the bottom 2(DLC)/3(Steel) angstroms of the asperity. While these atoms may eventually move as the material wears, we empirically concluded from our simulations that in general, they do not leave the area of contact between the two surfaces, and are thus expected to produce reliable measurements of the stress at the contact point. The stress tensor at the tip can then be used to calculate the pressure at the tip of the model asperity as well as the shear stress at the tip.

We recall that all measurements in MD simulation are subject to statistical noise, due to the small number of molecules present in the averaging volume [25]. To reduce the statistical uncertainty in our measurements we use time averaging to the extent allowed by our simulations. In steady simulations, such as those in Chapter 3 and in Chapter 5, after the equilibration period the simulation reaches a steady state and results can be averaged in time. The simulations of Chapter 4, however, are inherently

unsteady both due to the relative lateral motion of the counterfaces (which leads to compression) and the resulting wear.

For Chapter 3 and Chapter 5, all of the data from after the equilibration period was averaged and the standard deviation was found using the bootstrap method. For the data presented in Chapter 4, the data from every period of 5000 timesteps (1 picosecond) was averaged together and recorded. The length of this period was chosen based on the autocorrelation of the force acting on the asperities. It was found that the force data required up to 5000 timesteps (1ps) for 95% confidence that the datapoints were no longer correlated. Based on this, the data used in the analysis presented in this work was time averaged into 5000 timestep blocks.

Additionally, for all the simulations presented in this work, the coordinates of the atoms in each simulation were recorded every 5000 timesteps to be used for visualization and wear analysis. In Chapter 3 and Chapter 5, the simulations used a minimum of 2 million timesteps to ensure that equilibration was reached and an additional 2 million timesteps of sampling after reaching equilibrium. For simulations with larger lubricant layers, the equilibrium and sampling time was increased to ensure statistically significant results (up to 4 million timesteps for equilibration and 6 million timesteps for data collection).

For the unsteady simulations in Chapter 4, the simulations were generally around 3 to 5 million timesteps long, with the total length of the simulation depending on when catastrophic material failure occurred in the bulk material.

2.3.3 Reax Force Field

ReaxFF is a high fidelity reactive potential that allows us to perform simulations that capture the dissociation and recombination processes that occur during wear and scuffing, including tribochemical reactions between the solid surfaces, the passivation layers, and the lubricants, on a significantly larger scale than would be possible using ab-initio quantum-mechanical calculations.

ReaxFF was created to bridge the gap between ab-initio techniques like QMD and MD simulations using empirical force fields. While QMD methods are highly

accurate and theoretically capable of simulating any chemical system, their prohibitive computational cost means that they are typically limited to a small number of atoms. Unlike traditional force fields which require chemical bonds to be explicitly defined, ReaxFF is able to simulate chemical reactions because it allows for the breaking and formation of chemical bonds throughout the MD simulation [40, 46]. ReaxFF is able to allow for this by using the concept of bond order (BO), a continuous function that represents the number of bonds according to molecular orbital theory, instead of predefined chemical bonds between atoms. One of the benefits of this approach is that it makes ReaxFF a very general potential model that is in theory capable of accurately simulating a wide range of materials, including carbon based compounds, metals, and hydrocarbons.

More specifically, ReaxFF uses a description of the bond order as well as terms which describe the polarizable charge in the system to model both the reactive and the nonreactive interactions between systems of atoms in the simulation. The bond order (BO) between two atoms (i, j) can be written as an explicit function of the distance between those atoms r_{ij} as follows

$$\begin{aligned} BO_{ij} &= BO_{ij}^{\sigma} + BO_{ij}^{\pi} + BO_{ij}^{\pi\pi} \\ &= \exp\left[p_{bo1}\left(\frac{r_{ij}}{r_0^{\sigma}}\right)^{p_{bo2}}\right] + \exp\left[p_{bo3}\left(\frac{r_{ij}}{r_0^{\pi}}\right)^{p_{bo4}}\right] + \exp\left[p_{bo5}\left(\frac{r_{ij}}{r_0^{\pi\pi}}\right)^{p_{bo6}}\right] \end{aligned} \tag{2.1}$$

where BO_{ij}^{σ} is the number of σ bonds between atoms i and j, BO_{ij}^{π} is the number of π bonds between atoms i and j, and $BO_{ij}^{\pi\pi}$ is the number of $\pi\pi$ bonds between atoms i and j. These BO terms depend on r_{ij} and the equilibrium bond length for a bond of a given type (r_0^{σ}, r_0^{π}, and $r_0^{\pi\pi}$, respectively); p_{bo1} through p_{bo6} are empirical fitting parameters defined in the potential model. The BO calculated according to the above expression is then corrected by removing the contribution of any unrealistically weak bonds.

The BO formulation allows the simulation to track which atoms are bonded and apply an energy penalty for any atoms that have an unrealistic number of bonds based on their type (see discussion of equation 2.2 below). Another important feature of

the BO is that it is a continuous function. This means that even as the bond between two atoms transitions between the σ, π, and $\pi\pi$ orbitals, ReaxFF is able to generate a differentiable potential energy surface. This is critical for being able to calculate the interatomic forces between two atoms as these transitions occur.

Within ReaxFF, the potential energy of the system can be represented by the following equation:

$$E_{system} = E_{bond}+E_{over}+E_{under}+E_{angle}+E_{tors}+E_{LP}+E_{Hbond}+E_{VDW}+E_{Coulomb} \quad (2.2)$$

where the total system energy is comprised of nine different components. E_{bond} is the sum of the energy from all of the covalent bonds which have formed between all the atoms in the system. E_{over} is an energy penalty which is used to discourage atoms from forming too many bonds with other atoms, i.e. being overcoordinated. Similarly, E_{under} is an energy penalty on atoms which are undercoordinated. E_{angle} is the energy contribution from changing the angle between three bonded atoms, or 3-body terms, and E_{tors} is the energy from changing the dihedral angle associated with a bonded group of four atoms. E_{LP} is the energy resulting from lone pair electrons, and E_{Hbond} is the energy from any hydrogen bonds occurring in the system. Additionally, there are two types of long range sources of potential energy that affect every atom in the system, van Der Waals forces and Coulomb electrostatic interactions. However, it is important to note that in ReaxFF these interactions are shielded in cases where atoms are very close to each other.

The potential energy resulting from the van der Waals in the system are included in E_{VDW}. ReaxFF models this potential energy using the Morse Potential:

$$E_{VDW} = \sum D_0 \left[\exp^{-2\alpha(r_{ij}-r_0)} - 2\exp^{-\alpha(r_{ij}-r_0)}\right] \quad (2.3)$$

where r_{ij} is the current separation between atoms i and j, r_0 is the equilibrium separation, D_0 is the depth of the energy well, and α is the width of the energy well.

The potential energy resulting from electrostatics ($E_{Coulomb}$) is calculated from

Coulomb's Law and is given by

$$E_{Coulomb} = \sum \frac{1}{4\pi\epsilon_0} \frac{q_i q_j}{r_{ij}} \tag{2.4}$$

where r_{ij} is the current separation between atoms i and j, ϵ_0 is the permittivity of free space, and q_i is the charge of atom i. Additionally, ReaxFF updates the electrostatic charges on each atom every timestep using a geometry dependent charge equilibration (QEq) [55, 56, 57]. This method works by minimizing the electrostatic energy in the system by adjusting the partial charges on each of the individual atoms, based on the surrounding atoms and any interactions with them.

Each of these energy terms has numerous parameters that need to be defined for a given ReaxFF model in order for it to be able to model the bonded and non-bonded interactions of a particular material accurately. In this work we make use of two different ReaxFF models depending on the conditions being simulated. Generally we make use of the C/H/O/Fe/S/Cr model from the combustion branch of ReaxFF models [40, 46, 54]. This model is specialized in modeling carbon based materials, hydrocarbons, and their oxidization. The model is also capable of simulating iron surfaces, as well as wusite (FeO) and hematite (Fe_2O_3).

Additionally, we make use of a second ReaxFF potential model for Fe/C/H/O ReaxFF model created by Zou, van Duin, and Sorescu [47]. This model is based on the aqueous branch of ReaxFF models, which specializes in accurately simulating liquid water, and was built upon and incorporates the features of many earlier ReaxFF models [40, 46, 52, 53, 54]. It was designed to be able to accurately simulate iron, iron carbide, and common types of iron oxide bulk material and surfaces in contact with water. While this model was not specifically designed to simulate carbon based materials; however, it still retains the core features of the original ReaxFF formulation and the later base aqueous model for ReaxFF which allow for it to model diamond and graphene lattices. To verify that this potential could in fact accurately simulate the tribological properties of DLC surfaces we ran additional simulations comparing the friction properties of DLC surfaces when modeled with both ReaxFF models. From

our results we found that the friction force between DLC surfaces for each model were within 7% and within the margin of error for our simulations. While this model was not specifically designed to simulate carbon based materials, our test simulations showed that the friction results for DLC surfaces were within the margin of error when comparing the two potentials. As a result, we believe that the accuracy of this model is sufficient (with either DLC or steel surfaces) to be used in simulations where the focus is on the the behavior of liquid water in Chapter 5.

2.3.4 Modeling Counterfaces in Molecular Dynamics

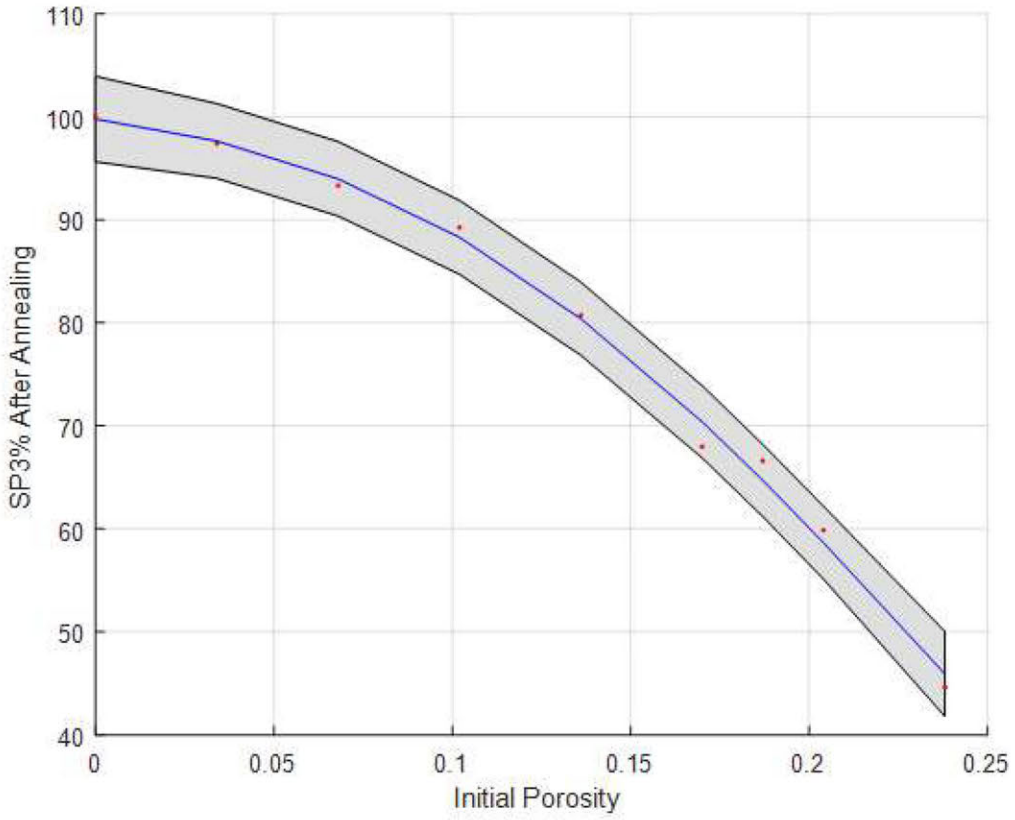

Figure 2-4: The final sp^3 percentage of the DLC is controlled by the initial percentage of atoms removed from the diamond lattice (porosity). A 95% confidence interval is indicated in gray.

In order to create a realistic model of DLC counterfaces we started with a bulk simulation of carbon atoms in diamond lattice. A fraction of the atoms from this

lattice was randomly removed to reduce the density of the material. The material was then annealed by heating to 4000K for 2ns to allow the porous diamond lattice to melt. The material was then quenched by quickly cooling the carbon atoms from 4000K to 350K over 9ns (approximately the time for light to travel 3 meters). This was done to prevent the carbon atoms from forming larger crystal structures and instead turn the material into an amorphous solid. The fraction of sp^3 bonds in the resulting material is quantified using the ReaxFF bond order calculation [46].

This process is repeated several times to generate a relation between the initial porosity created in the diamond lattice and the final sp^3 percentage after quenching. The resulting data is shown in figure 2-4. This relation allows us to consistently generate new bulk DLC models with the desired ratio of sp^2 to sp^3 hybridized bonds. Unless mentioned otherwise, DLC counterfaces used in this thesis featured 68% sp^3 bonded carbon atoms.

In addition to generating sample models of DLC, we also developed steel counterfaces for performing comparisons between the two materials. The steel material model used in this work was created starting from an iron body centered cubic (bcc) lattice. Carbon atoms were then randomly added until a 0.1 percent of carbon atoms by weight was reached. The material was then melted and cooled following a similar process to the bulk DLC. After cooling, the steel returned to a bcc lattice structure. The combination of a bcc lattice and the amount of carbon present indicates that the steel model has formed a mixture of ferrite and a small number of cementite (iron carbide) molecules. These cementite molecules are dispersed throughout the bulk steel.

After producing a bulk volume of each material, upper and lower counterfaces were cut from this bulk. As described in section 2.3.2, we use two different counterface geometries in this work. To create the flat counterfaces (similar to Figure 2-2) used in Chapter 3 and Chapter 5, the bulk material was cut into a simple rectangular shape and initially measure 100 angstroms by 40 angstroms by 25 angstroms in the x, y, and z directions respectively. For the geometry featuring an asperity (shown in Figure 2-3), the lower counterface has a simple rectangular shape and initially measures 100

angstroms by 40 angstroms by 23 angstroms in the x, y, and z directions, while the upper counterface is cut into a sinusoidal shape that models the tip of an asperity, and has maximum initial dimensions of 100 angstroms by 40 angstroms by 27 angstroms.

While surfaces being simulated are quite large and computationally expensive for a MD simulation using a reactive potential model, the overall dimensions of the simulations are still small in real terms. For example, the grains of DLC resulting from chemical vapor deposition techniques range from the order of hundreds to thousands of angstroms depending on the technique used to manufacture the DLC [48, 49]. The counterfaces in these simulations can be thought of as segments of individual grains of either DLC or Steel.

Pristine counterfaces are very reactive and quickly form passivation layers when exposed to any environment. The passivation layer composition is primarily determined by the environment. For example, DLC placed in a hydrocarbon environment will eventually develop a hydrogen passivation layer [36, 37, 51]. To simulate this effect we modeled different passivation layers for each type of counterface. This was done by exposing the DLC surfaces to unbonded atoms that would be found in the test conditions. These test conditions varied according to the ambient conditions being simulated.

To model the passivation layer that would be created on the surface of the DLC when exposed to hydrocarbons, we simulated pristine DLC counterfaces exposed to an excess of unbonded hydrogen atoms for 20ps until all of the hydrogen had bonded to the surfaces or formed hydrogen gas. This resulted in a thin layer of hydrogen atoms bonded to the DLC surface. Excess H_2 molecules between the surfaces were removed to facilitate placing the much larger hydrocarbon molecules in the simulation for testing. An identical process was followed using oxygen atoms in order to generate models of DLC counterfaces passivated with oxygen.

In order to model the passivation layer for DLC when exposed to water, the pristine DLC counterfaces were exposed to an excess of unbonded hydrogen and oxygen atoms (in a 2:1 ratio). The simulation was then run for 20ps until all of the unbonded atoms had reacted with the surfaces or each other. This resulted

in a passivation layer that had a thickness of approximately 3 angstroms and was composed of hydrogen, oxygen, and hydroxyl groups.

For the steel counterfaces, the passivation layers were generated in a similar fashion. When exposed to an excess oxygen atoms, the oxygen reacted with the iron atoms to form a passivation layer of iron oxide. This resulted in a passivation layer with a thickness of 10 angstroms on each surface, which is significantly thinner than the typical iron oxide layer that is on the order of several hundreds of angstroms thick [50]. Unfortunately, simulating passivation layers of this thickness is not computationally feasible. On the other hand, the layer simulated here is sufficiently thick to prevent the underlying unoxidized steel from having a direct effect on the interactions being studied at the contact point and is therefore sufficiently realistic for the purposes of this work. When generating the passivation layer that would form when exposed to water the surface was instead exposed to a mixture of hydrogen and oxygen atoms. The oxygen and a smaller quantity of hydrogen atoms reacted with the iron atoms to form a passivation layer that was primarily iron oxide and of approximately the same thickness.

To model the passivation layer that would form on the steel surface when exposed to hydrocarbons in an oxygen-free environment, we simulated the pristine steel counterface exposed to an excess of unbonded hydrogen atoms for 20ps. This resulted in a monolayer of hydrogen which was approximately 2 angstroms thick. Excess H_2 molecules between the surfaces were removed to facilitate placing the much larger hydrocarbon molecules in the simulation for testing.

Chapter 3

Dry Sliding Friction

3.1 Introduction

The tribological properties of DLC can be influenced by a number of factors. One of the important factors in determining the physical properties of a given DLC sample is the percentage of sp^3-bonded carbon atoms. As discussed in section 2.2, increasing the percentage of sp^3 bonded carbon in the DLC increases the material hardness, making it generally more diamond like, while reducing the sp^3 percentage makes the DLC more graphite like. However, there are other environmental factors that can dramatically change the friction properties of the material.

By changing the type of elements present in the environment around a DLC surface, we can change the makeup of the passivation layer that forms on new or freshly worn DLC surfaces. In this thesis we are primarily interested in three different types of passivation layers. The first is a hydrogen passivation layer that forms when the surface is exposed to a hydrogen rich environment, such as when lubricated with alkanes or other hydrocarbons. The second is a plain oxidized surface that occurs when a surface is exposed to dry air. The third is a mixture of these two cases which occurs when DLC is exposed to water, and will be looked at in detail in Chapters 4 and 5. As discussed in Section 2.1, an important cause of friction when observing the mechanics on the nanoscopic scale is adhesion between the two surfaces [16].

In this chapter, we will be verifying that these simulations can accurately model

the friction forces between two counterfaces in dry sliding contact. Additionally, we will study the effect of the sp^3 percentage and composition of the passivation layer on the friction force, adhesion between the surfaces, and the coefficient of friction. Furthermore, we will also be studying how the DLC sp^3 percentage and the makeup of the passivation layer interact to affect the tribological properties of the counterfaces.

3.2 Methods

Our setup follows the general setup described for flat counterfaces in section 2.3.4. We now discuss elements of this setup that are specific to the present simulations.

In order to generate relative motion, the control surface of the upper counterface is held in a fixed position, while the control surface of the lower counterface is translated at a constant velocity of 25 m/s in the x direction. Additionally, a constant normal force is applied to the lower counterface's control surface to bring the two surfaces into dry sliding contact.

3.2.1 Measuring the COF

As explained in section 2.1, one particular challenge associated with simulating friction at the nanoscale is that for the systems amenable to simulation, adhesion forces between the counterfaces become of the same order of magnitude or larger than the external normal forces applied to the system. These forces arise from van der Waals interactions. Under normal circumstances these attractive and repulsive surface forces are negligible because real world surfaces are not atomically smooth. However, when simulating these surfaces at the nanoscale their average separation at contact can be on the order of a single angstrom.

To demonstrate this we can approximate these surfaces as two semi-infinite flat plates. The macroscopic van der Waals attraction between the two plates is given by:

$$F_{VDW} = \frac{CA}{6\pi d^3} \tag{3.1}$$

where C is the Hamaker constant for the two materials, A is the surface area, and d is the distance separating the two plates [58]. This force can become very large as the distance between the two surfaces decreases towards zero.

Additionally, it is also possible for there to be other long range forces that impact the adhesion between surfaces. More specifically, charged particles in the passivation layers can exert electrostatic forces. This force is likely to be repulsive, because of the similar makeup of passivation layers formed in a given environment. Considering two charged particles, one on either surface, the electrostatic repulsion between them is given by

$$F_{Elecrostatic} = \frac{Q^2}{4\pi\epsilon_0 r^2} \tag{3.2}$$

where Q_1 and Q_2 are the charges of each particle, ϵ_0 is the vacuum permittivity, and r is the distance between the particles. Calculating the total repulsive force between the two surfaces requires integrating over all particle pairs. However, the resulting electrostatic forces from these calculations can change significantly as those charged particles move in time. Due to this complexity, we calculate the contribution of these adhesive and repulsive forces using a different approach, namely by writing

$$F_{friction} = \mu \left(F_{applied} + F_{adhesion} \right) \tag{3.3}$$

where $F_{friction}$ is the friction force, $F_{applied}$ is the normal force being applied to the control surface, and μ is the coefficient of friction. Here, $F_{adhesion}$ is the combined adhesive force made up of the van der Waals and electrostatic forces. For example, attraction between the two surfaces is indicated by a positive value for $F_{adhesion}$ and a negative value indicates repulsion between the surfaces. Additionally, we define $F_{NetNormalLoad} = F_{applied} + F_{adhesion}$, which is the net load in the normal direction at the interface. It is also important to note that a $F_{NetNormalLoad}$ of less than zero indicates that the repulsion between the surfaces is strong enough to prevent the surfaces from making contact, which will result in approximately zero friction.

In order to measure the COF for a given combination of surfaces using equation 3.3, the friction force needs to be calculated at several different applied pressures.

Then the resulting friction force and applied load data can be fit to equation 3.3, in order to calculate both the adhesive force and the coefficient of friction.

3.3 Results

We performed simulations with DLC, steel, or mixed counterfaces with either a hydrogen passivation layer or an oxygen passivation layer. The counterfaces were placed into dry sliding contact and the resulting forces on the control surfaces were measured. Below we discuss the results for each combination of surfaces with both types of passivation layer. DLC simulations were run at a variety of sp^3 percentages to determine the effect on friction between the surfaces.

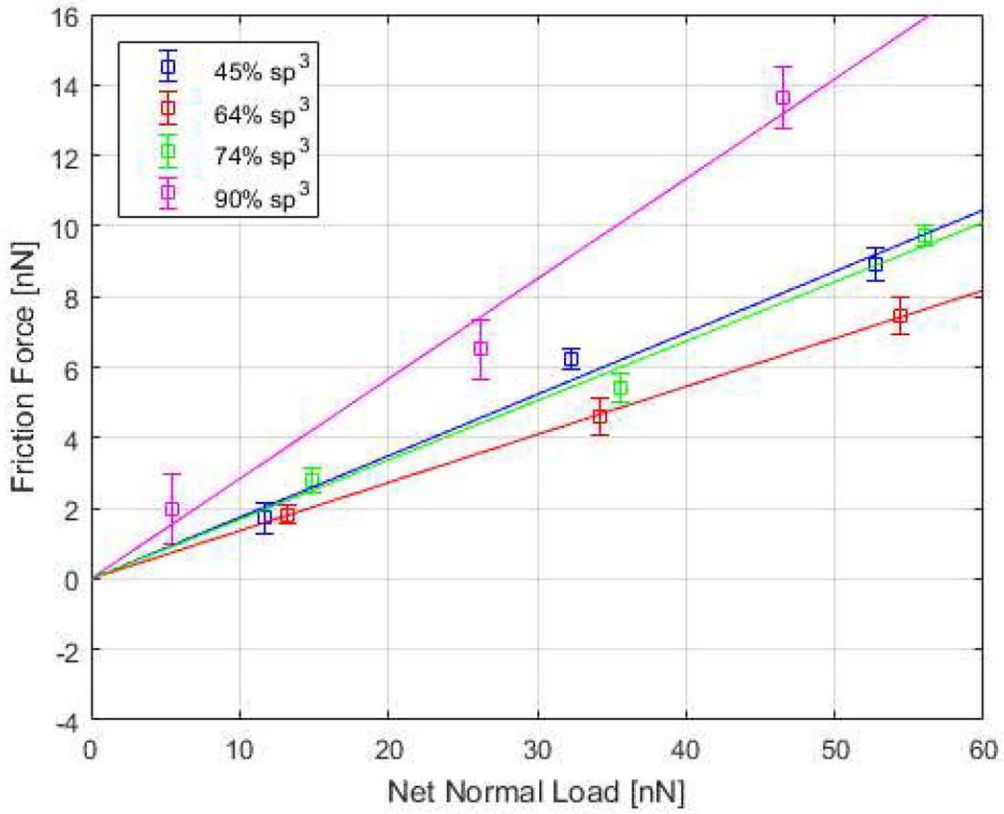

Figure 3-1: Friction force measured from upper control surface versus net normal load at the interface, for two DLC surfaces passivated with hydrogen. Results shown for a range of sp^3 percentages.

3.3.1 DLC - Hydrogen Passivation

The simulation results for two DLC counterfaces with hydrogen passivation layers in sliding contact are shown in figures 3-1. The friction data was recorded for four different DLC samples with a range of sp^3 percentages. The friction force for each set of DLC counterfaces was measured with three different normal forces applied to the bottom surfaces. As expected, the measured friction force increases linearly as the applied load in the normal direction is increased. As the sp^3 percentage was changed, we found there to be a slight variation in the adhesion force. The values for $F_{adhesion}$ where found to vary between each of the surface pairs and were in the range of ± 5 nN.

From the linear fits shown in Figure 3-1, we can determine that an sp^3 percentage of 45% resulted in a COF of 0.17 ± 0.02. When the sp^3 percentage was increased to 64% and 74%, there was not a significant change in the COF. From fitting the data we were able to calculate a COF of 0.14 ± 0.02 and 0.16 ± 0.01 respectively. However, when testing with an sp^3 percentage of 90% the COF was determined to be significantly higher, at 0.25 ± 0.03. This trend indicates that more graphite like DLC surfaces with lower sp^3 percentages can result in low COF values, when passivated with hydrogen. Similarly, the COF will increase when the DLC has a high sp^3 percentage and is more diamond like. This reduced COF at low sp^3 percentage is likely due to the DLC surface being softer and more amorphous, which allows for the hydrogen atoms in the passivation layer to have more flexibility and move out of each otherï£¡s way during sliding contact.

The values obtained for the COF of two hydrogen-passivated DLC surfaces in dry sliding contact are in general agreement with the experimental values found in the literature, which range from 0.10 to 0.25 [60, 59]. However, in many of these sources, there is ambiguity in the exact sp^3 percentage of the DLC, which makes direct comparisons difficult.

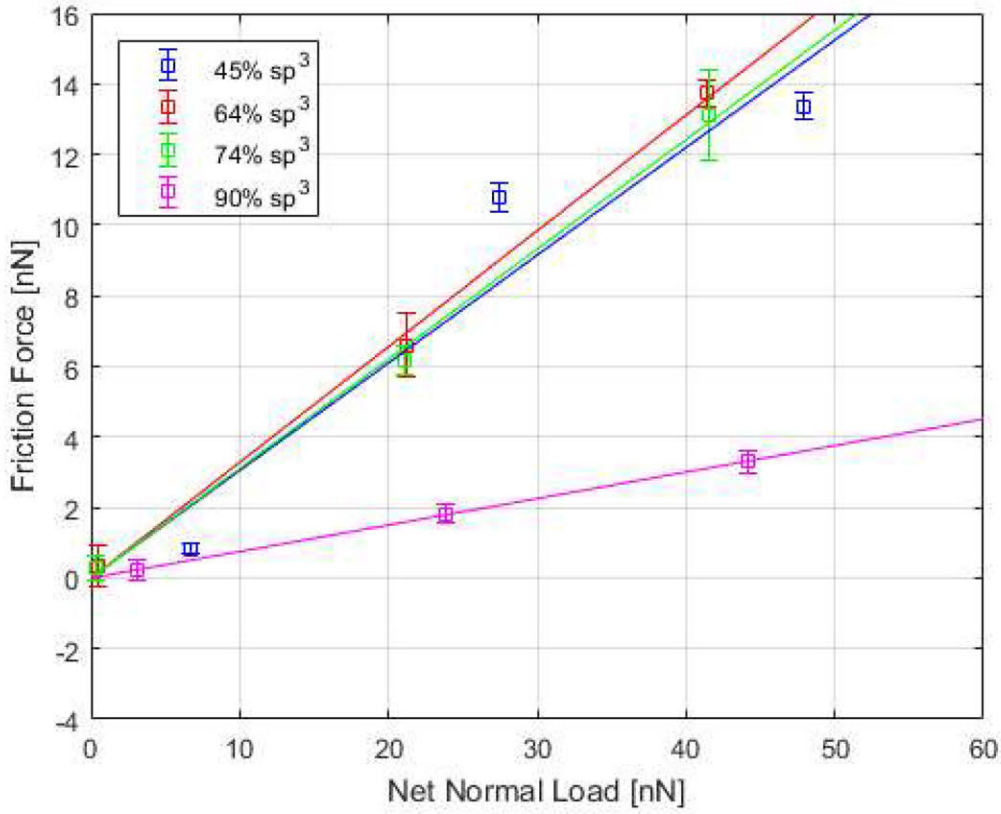

Figure 3-2: Friction force measured from upper control surface versus net normal load at the interface, for two DLC surfaces passivated with oxygen. Results shown for a range of sp^3 percentages.

3.3.2 DLC - Oxygen Passivation

The simulation results for two DLC counterfaces with oxygen passivation layers in sliding contact are shown in figures 3-2. The friction data was recorded for four different DLC samples with a range of sp^3 percentages. The friction force for each set of DLC counterfaces was measured with three different normal forces applied to the bottom surfaces. As expected, the measured friction force increased linearly as the applied load in the normal direction was increased. The values for $F_{adhesion}$ where found to vary between each of the surface pairs and ranged from -2 nN to -9 nN, which indicates a repulsive force in between the two surfaces.

From the linear fits shown in Figure 3-1, we can determine that an sp^3 percentage of 45% resulted in a COF of 0.29 ± 0.03. When the sp^3 percentage was increased

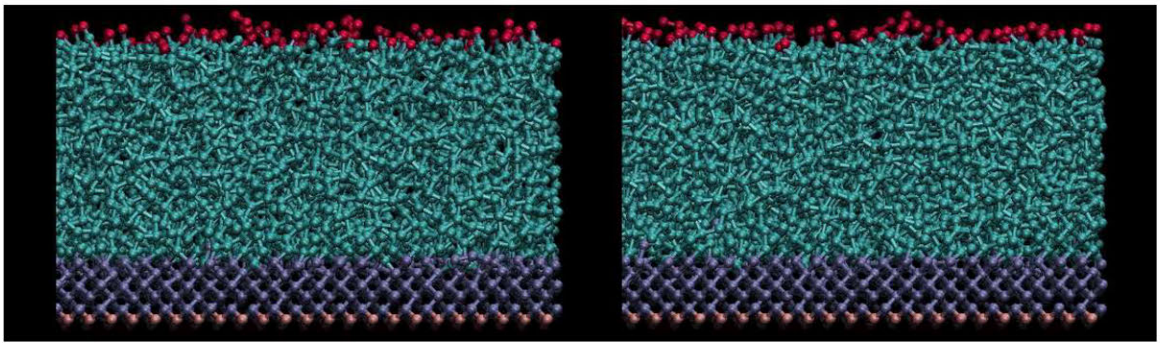

Figure 3-3: Comparison of the passivation layer and structure of 45% sp^3 DLC (left) and 90% sp^3 DLC (right) surfaces passivated with oxygen. The control surface is shown in pink, the temperature control layer is shown in dark blue, the bulk DLC is shown in cyan, and the oxygen atoms are shown in red.

to 64% and 74%, we were able to calculate a COF of 0.31 ± 0.02 and 0.27 ± 0.01 respectively. However, when testing with an sp^3 percentage of 90% the COF was determined to be significantly lower, at 0.07 ± 0.03. This trend is the reverse of what was observed with hydrogen passivated DLC. In the present case, having a harder and more diamond like DLC allowed for a lower COF than was obtained with lower sp^3 percentages. From the simulations, this appeared to result from the increased rigidity of the passivation layer, preventing the charged oxygen atoms from deflecting away from each other, and resulted in higher levels of repulsion between the oxygen atoms. This keeps the surfaces from making as close a contact and reduces the amount of interaction between the surfaces. The relative softness of the lower sp^3 percentage DLCs and their passivation layers can be observed from their structures shown in figure 3-3, where there are more and longer chains of double bonded carbon atoms terminated by oxygen in the 45% sp^3 surface compared to the 90% sp^3 surface.

The values obtained for the COF of two oxygen-passivated DLC surfaces in dry sliding contact agree with the experimental values found for the COF in the literature, which ranged from 0.15 to 0.37 [60, 14]. However, in many of these sources, there is ambiguity in the exact sp^3 percentage of the DLC, which makes direct comparisons difficult.

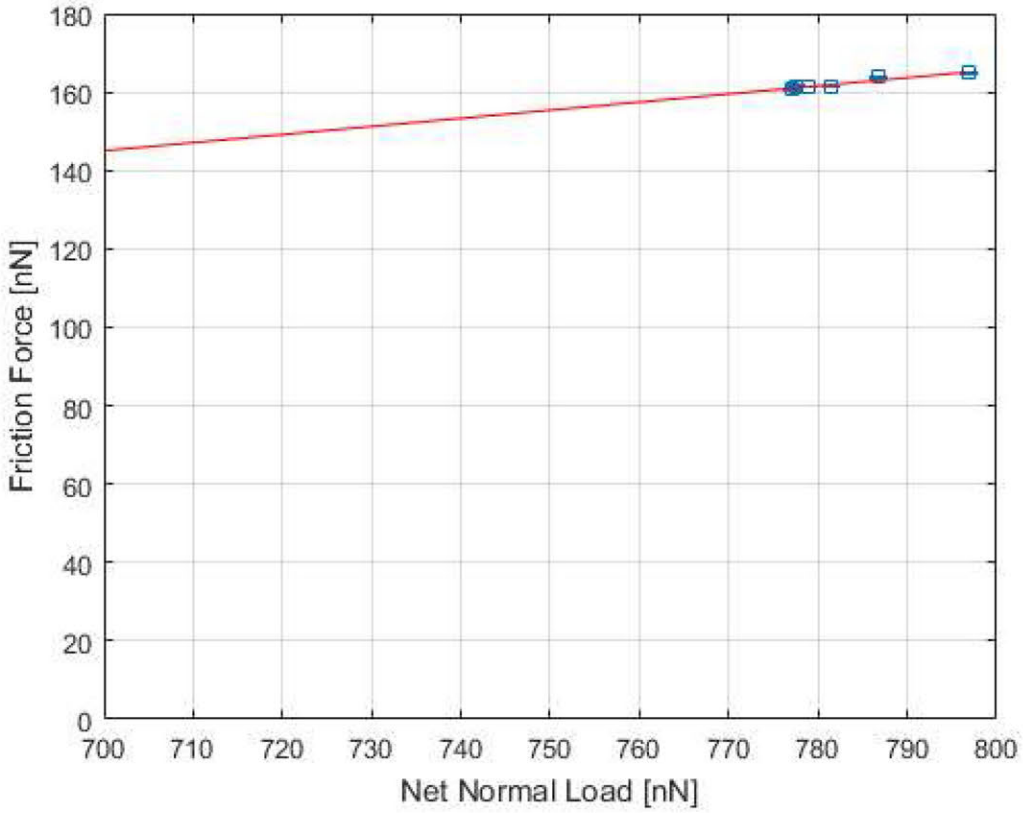

Figure 3-4: Friction force measured from upper control surface versus net normal load at the interface, for two steel surfaces passivated with hydrogen in dry sliding contact.

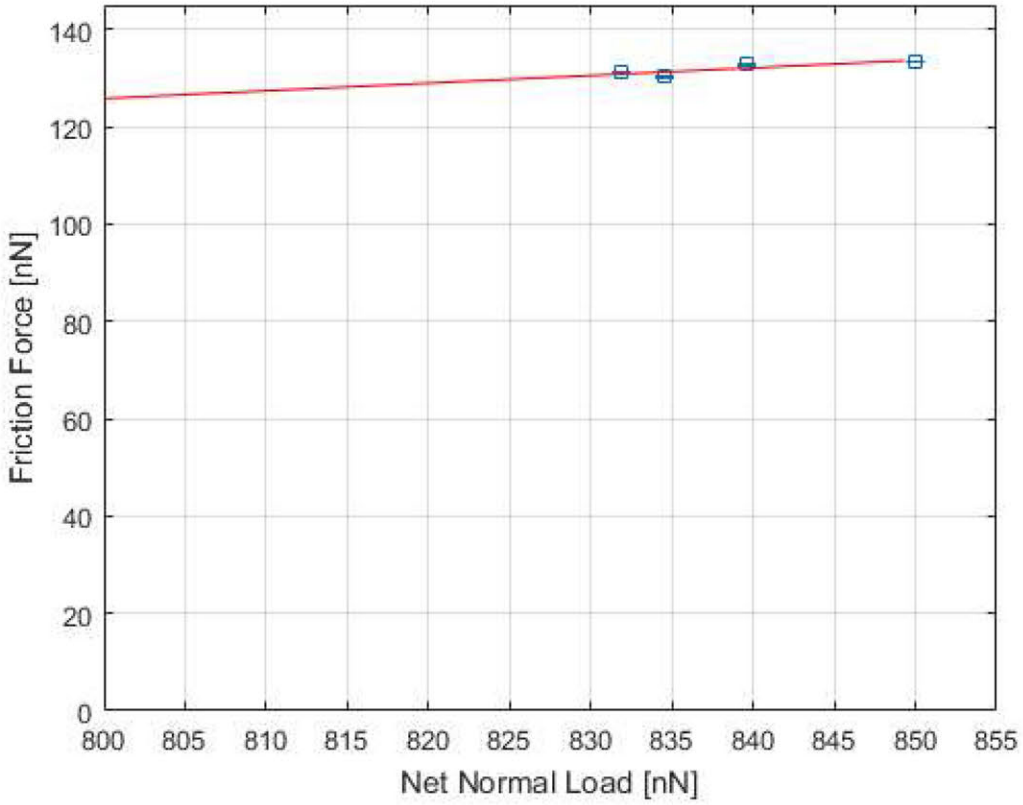

Figure 3-5: Friction force measured from upper control surface versus net normal load at the interface, for two steel surfaces passivated with oxygen in dry sliding contact.

3.3.3 Steel-Steel Contact

Simulations were also run for two different sets of steel counterfaces for comparison. One set was passivated with hydrogen atoms and the other set was passivated with oxygen atoms. As with the previous simulations, these sets of passivated steel counterfaces were simulated in dry sliding friction, with a range of applied normal forces to the lower surface. Once again we observe from the results in Figures 3-4 and 3-5 that there is a linear increase in the friction force as the applied normal load increases. However, unlike in the case of the DLC-DLC or the DLC-Steel simulations of dry sliding contact, the amount of adhesion between the surfaces is much greater than when one or both of the surfaces are passivated DLC. Additionally, during these simulations the hydrogen and oxygen passivated steel surfaces were able to form chemical bonds with the opposing counterface, which contributed to the high friction forces observed at all applied normal forces. In the case of hydrogen passivated steel, the fit resulted in an estimated adhesion force between the surfaces of 1100 ± 50nN. With oxygen passivated steel the adhesion force was found to be 810 ± 24nN.

Even though the adhesion between the two steel surfaces is very large, the actual COF for each case is still within the expected range of values for steel surfaces in dry sliding contact [73]. The COF for the hydrogen passivated steel was determined to be 0.13 ± 0.01, while the COF for oxidized steel was found to be 0.20 ± 0.01.

3.3.4 DLC - Steel Contact

Additional simulations were run using a combination of a steel counterface with a DLC counterface, the latter having an sp^3 percentage of 90%. In order to compare these results to the most common experiments of dry sliding friction between DLC and steel surfaces, the two combinations of passivation layers chosen were oxidized steel in dry sliding contact with hydrogen passivated DLC (Figure 3-6) and oxidized steel in dry sliding contact with oxidized DLC (Figure 3-7). As in the other dry fiction simulations discussed in this chapter, there is a linear relation between the amount of friction measured and the applied normal load. When simulating the contact between

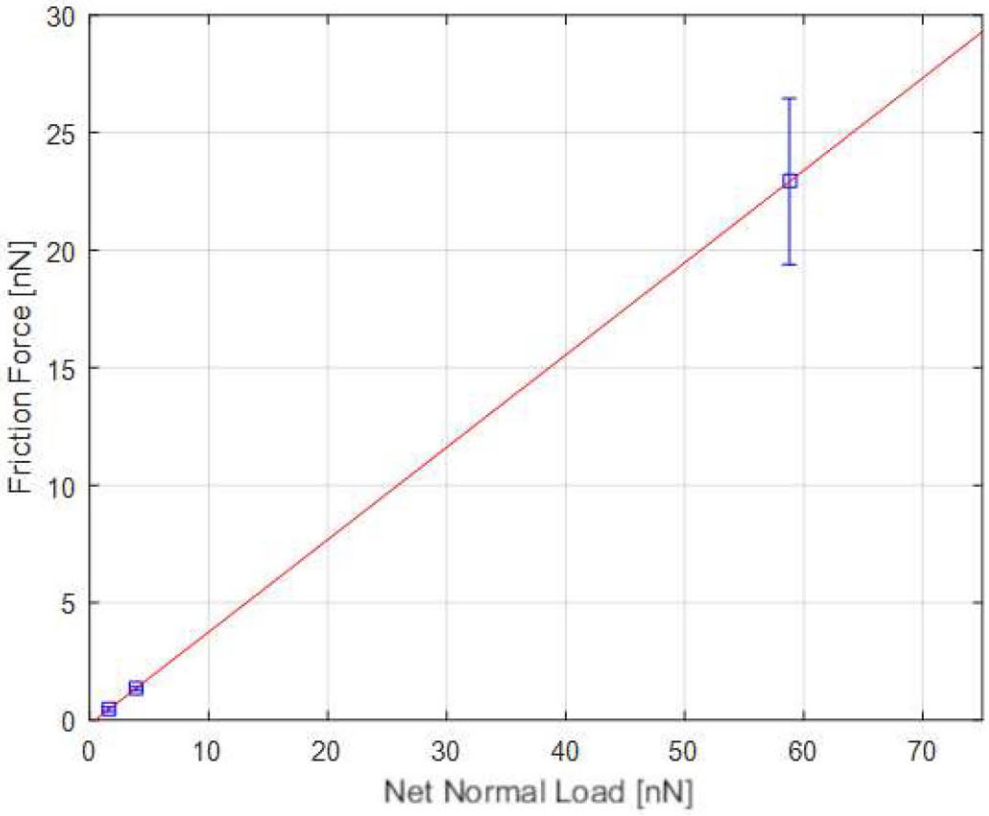

Figure 3-6: Friction force measured from upper control surface versus net normal load at the interface, for DLC and steel counterfaces passivated with hydrogen.

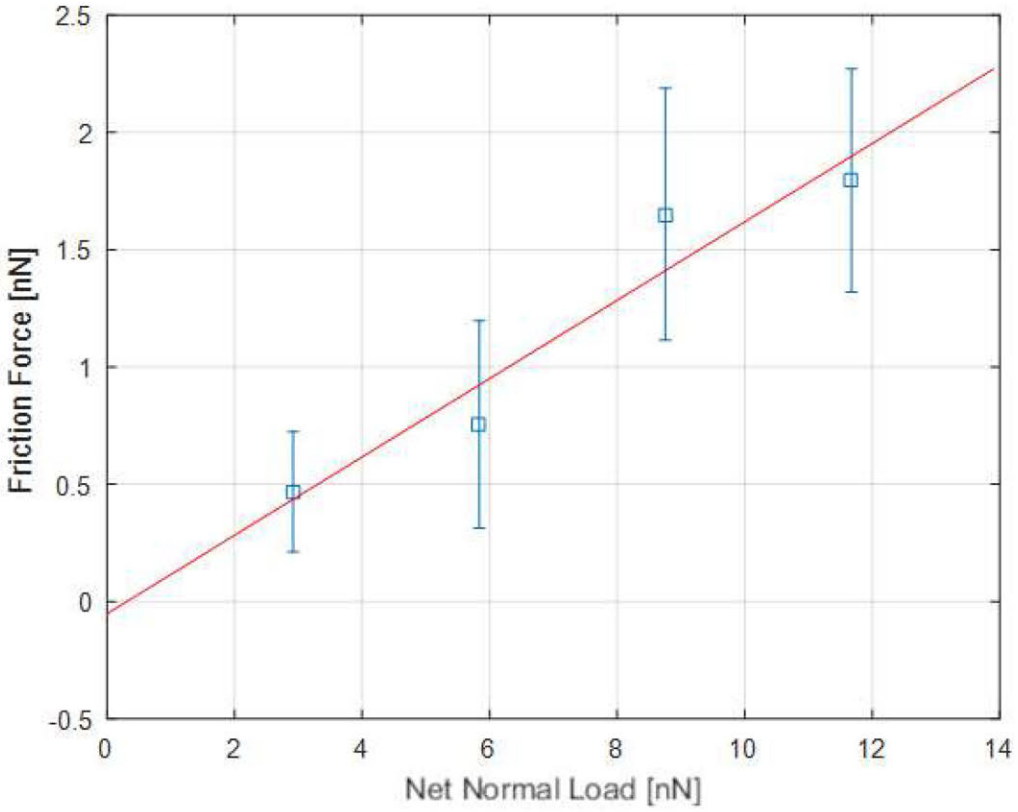

Figure 3-7: Friction force measured from upper control surface versus net normal load at the interface, for DLC and steel counterfaces passivated with oxygen.

oxidized DLC and oxidized steel, the adhesion between the surfaces was negligible and the COF was found to be $0.15 \pm .06$. Experimental values for the COF in the literature for this combination range from 0.14 to 0.20 [60].

The simulation of oxidized steel in dry sliding contact with hydrogenated DLC is intended to model a hydrogentated DLC surface in dry sliding contact with a steel plate that has formed an iron oxide layer due to being exposed to oxygen in the air. From Figure 3-7 we can determine that there is negligible adhesion between the surfaces, and using a linear fit a COF of 0.38 ± 0.04 was obtained. Unfortunately this a fair bit higher than the values for hydrogenated DLC in sliding contact with steel surfaces found in the literature, which can be as low as 0.10 [61, 14]. However, there are some caveats about how strongly the simulation models what is happening in the laboratory experiments. For instance, DLC will invariably adsorb a thin layer of water when it is placed in atmospheric conditions (assuming the relative humidity is greater than zero). This will be explored in much greater detail in Chapter 5.

3.4 Discussion

In this chapter we have generated a large number of model DLC and steel counterfaces, and used MD simulations of these models to study how these surfaces interact in dry sliding friction at atomistic length scales. We accounted for the additional adhesion forces between surfaces by measuring the friction force at several different applied loads and then fitting the resulting friction data to the formula in equation 3.3. This allowed us to estimate not only the COF, but also the amount of adhesive force between the two surfaces.

Using this analysis we are able to obtain a number of new insights. First, the passivation layer on the surface of the counterfaces is very important for determining the tribological properties of the material. In addition to being responsible for preventing DLC surfaces from chemically bonding/welding to the opposing counterface, the passivation layer can have a dramatic impact on the strength of adhesion forces between the two surfaces. This can result in very large differences in the resulting

friction force, even if the COF is unchanged.

The second is that changing the bulk sp^3 percentage of the DLC can have a dramatic impact on the tribological properties of the DLC. However, this impact is dependent on how the bulk change in material properties affects the passivation layer. As we saw in Section 3.3.2, decreasing sp^3 percentage of Hydrogen passivated DLC resulted in a smaller COF. This was a result of the decreased rigidity of the DLC's passivation layer allowing the hydrogen atoms to slip past each other more easily. However, decreasing the sp^3 percentage of the oxygen passivated DLC in Section 3.3.2 ended up resulting in a higher COF. Reducing the rigidity of the charged oxygen atoms the oxidized passivation layers allowed for the surfaces to come closer together and allowed for more interaction between the surfaces.

Finally, we were able to show that these dry sliding friction simulations were able to reproduce accurate COF values for self mated DLC surfaces and self mated steel surfaces in dry sliding contact. In general we found that (excluding sp^3 percentages above 80%) hydrogen passivated DLC had the smallest COF, while oxygen passivated DLC had a friction coefficient much closer to that of steel surfaces. Unfortunately, the dry sliding friction model currently being used was unable to accurately reproduce the experimentally determined COF values that occur with steel surfaces in contact with hydrogenated DLC when exposed to air. This is likely because the model dry friction model does not take into account the humidity that is naturally present in ambient conditions, which can provide a source of water molecules for lubrication.

Chapter 4

Thin Film Lubrication and Wear

4.1 Introduction

In this chapter, we use MD simulations of a model asperity and a flat counterface in relative motion, initially separated by a thin layer of lubricant in order to investigate the origins of the enhanced resistance to scuffing wear associated with DLC coated surfaces [69, 70, 71]. We performed these simulations in the presence of model lubricants such as water, n-eicosane, and 9-octyl-eicosane, and observed how the presence of thin films of these model lubricants modified both the friction and wear properties of both the bulk materials and the passivation layers that formed when those surfaces were exposed to the lubricants. More specifically, by measuring both the material stress at the point of contact as well as estimating the wear rate of the counterfaces, we are able to quantify the extent to which the lubricants and the passivation layer they induce on the DLC surfaces protect the counterfaces from scuffing and wear damage. By comparing and contrasting our observations to the behavior of steel counterfaces under the same conditions, we gain molecular insight into what makes DLC an effective coating for reducing friction and wear.

4.2 Methods

4.2.1 Simulation Setup

Our setup follows the general setup described for the "sinusoidal" counterfaces in section 2.3.4. We now discuss elements of this setup that are specific to the present simulations.

We performed MD simulations of two counterfaces in relative motion, initially separated by a thin layer of lubricant. The relative motion includes a tangential component (25 m/s) and a small normal component (2.5 m/s); the latter serves to reduce the gap height, squeezing out the lubricant film, until material failure is observed. Using the "sinusoidal" counterface geometry allows for easier identification of displaced (worn) atoms while also helping to reduce the number of lubricant molecules trapped between the counterfaces as the gap decreases in size. Additionally a large vent is introduced in the upper counterface to allow excess fluid to escape during the simulation and prevent the pressure from reaching extreme values.

The temperature control layer was set to maintain a temperature of 350K. This is sufficient to maintain a temperature between 350K and 400K in the region adjacent to the tip of the model asperity for the duration of the simulations. The only exception to this is during the final part of the DLC simulations where as a result of the extreme pressures the DLC counterfaces break down catastrophically, causing the temperatures to exceed 1000K.

In order to track the wear in the system, we estimate the number of displaced atoms throughout the duration of the simulation. The displacement is defined with respect to each atom's expected position based on its position at the beginning of the simulation and the velocity of the counterface on which it belongs. An atomic displacement of more than two unit cells (7.1 angstroms total for DLC and 5.7 angstroms total for steel) is considered to be beyond the nominal value resulting from elastic deformation and is used as the threshold for signaling permanent deformation in the form of plastic deformation/wear.

It is also important to note that these stress measurements in this chapter also

include any pre-stress in the material. For the passivated DLC surfaces, the initial normal stress (zz component) was 2.0 GPa, while the initial shear stress (xz component) was 0.21 GPa when passivated with hydrogen atoms. When passivated with a 2:1 ratio of hydrogen and oxygen atoms, the initial normal stress was 1.5 GPa and the shear stress was -1.2 GPa. For the steel counterfaces, we measured an initial normal stress of 1.8 GPa and shear stress of 0.09 GPa when passivated with hydrogen atoms, while when passivated with a 2:1 ratio of hydrogen and oxygen atoms the normal stress was 0.5 GPa and the shear stress was -0.03 GPa. We note that although these quantities are quite large in absolute terms, they are small compared to the stresses to which the materials are subjected to during the course of the simulations performed in this chapter.

In order to account for this effect, we first measure this internal stress at the contact point for each passivated surface before contact. In all results presented below, the contact point pressure refers to the corrected pressure from which the internal normal stress has been subtracted. Additionally, a similar adjustment has been applied to the shear stress when used to estimate the applied shear force at the contact point (such as when calculating the COF).

4.2.2 Model Lubricants

We consider three model lubricants, namely, water, n-Eicosane, and 9-octyl-eicosane. These were chosen due to their relatively simple molecular structure, which at the same time is quite varied in terms of types of atoms, molecular weight, polarity, and shape.

While water is not a commonly chosen as a lubricant in a mechanical system, it is important to consider when studying friction. This is because DLC, steel, and many other materials have the ability to adsorb water molecules from the surrounding air [62, 63]. The thickness of this layer depends on the relative humidity of the surrounding environment, but this layer of water can be several angstroms thick [64].

n-Eicosane was chosen because it is more similar to a traditional lubricant. It is nonpolar, with higher molecular weight, and is more viscous than water. In principle,

this means that it should require more force to squeeze out from between the two counterfaces and is thus expected to provide better wear protection [66]. Since n-eicosane is a hydrocarbon, hydrogen-based passivation layers were used on the surface of the DLC and steel counterfaces for this lubricant.

The final model lubricant tested is 9-octyl-eicosane. It is a branched alkane that is larger and has a higher molecular weight than n-eicosane, in principle making it even more difficult to squeeze out from between the counterfaces and thus, in principle, the most protective of the three lubricants. This lubricant was tested using the same hydrogen based passivation layer as n-eicosane.

4.2.3 Disjoining Pressure

An important factor to consider during these simulations is the strength of the adhesion between the lubricant molecules and each of the counterfaces. This is because in addition to the strong Van der Waals attraction between two surfaces, there is also a strong attraction between the individual lubricant molecules and the surfaces. This presents itself as a disjoining pressure, the difference between the pressure in a region adjacent to a surface and the pressure in the bulk phase. The van der Waals contribution to the disjoining pressure for a liquid on a flat surface in contact with a cylinder can be approximated by [65]:

$$\Pi_{vdw} = -\frac{CL}{16\delta^{5/2}} \tag{4.1}$$

where C is the Hamaker constant between the two counterfaces, L is the diameter of the cylinder, and the lubricating layer and δ is the liquid film thickness. In order to estimate the disjoining pressure of our lubricants we used the Hamaker constant values from [67, 68] and the geometric mean approximation for the combining rules. From this we find that when using DLC surfaces, the disjoining pressure reaches a maximum of approximately -250 MPa when there is one layer of water molecules remaining between the surfaces and -280 MPa when using n-eicosane. With steel surfaces we find that a maximum disjoining pressure of approximately -210 MPa for

water and -245 MPa for n-eicosane. When comparing these results to the simulation results in the following section, we found that these disjoining pressures to be much smaller than the bulk fluid pressure, which are on the order of GPa.

4.3 Results

Simulations with either DLC or steel counterfaces were run with each of the three lubricants, namely, water, n-eicosane, and 9-octyl-eicosane. The number of worn atoms was tracked as a function of time, allowing for comparisons to the contact point pressure, shear stress, and the surface separation. Below we discuss the results for the three lubricants. The separation measure shown in the figures below is the nominal separation between the surfaces, based on the locations of the position control layers, and does not account for the deformation of the counterfaces.

4.3.1 Water

The simulation results for two steel counterfaces, two DLC counterfaces, and one steel and one DLC counterface in sliding contact using water as a lubricant are shown in figures 4-1, 4-2, and 4-3. As we can observe in figure 4-1, the pressure at the contact point generally increases over the course of the simulation. If we define wear as occurring when the rate of displaced atoms exceeds 1 Atom per picosecond, then according to figure 4-2, this threshold is exceeded at a separation of $\sim$ 2.3 angstroms for steel counterfaces (point A), a separation of $\sim$ -2.4 angstroms for DLC counterfaces (point C), and a separation of $\sim$ 3.2 angstroms for mixed surfaces (point E).

From figure 4-1 we can determine that for steel counterfaces the contact point pressure increased from 5.8 GPa at the baseline to 12 GPa at point A, while for DLC counterfaces the contact point pressure increased from 38 GPa (baseline) to 66 GPa at point C. With mixed counterfaces the pressure increased from a baseline of 5.3 GPa to 12.9 GPa at point E. The baseline value here accounts for the surface tension effects in the lubricant and adhesion between the lubricant molecules and the surfaces which is different in each simulation; in this work, it has been taken to be the pressure

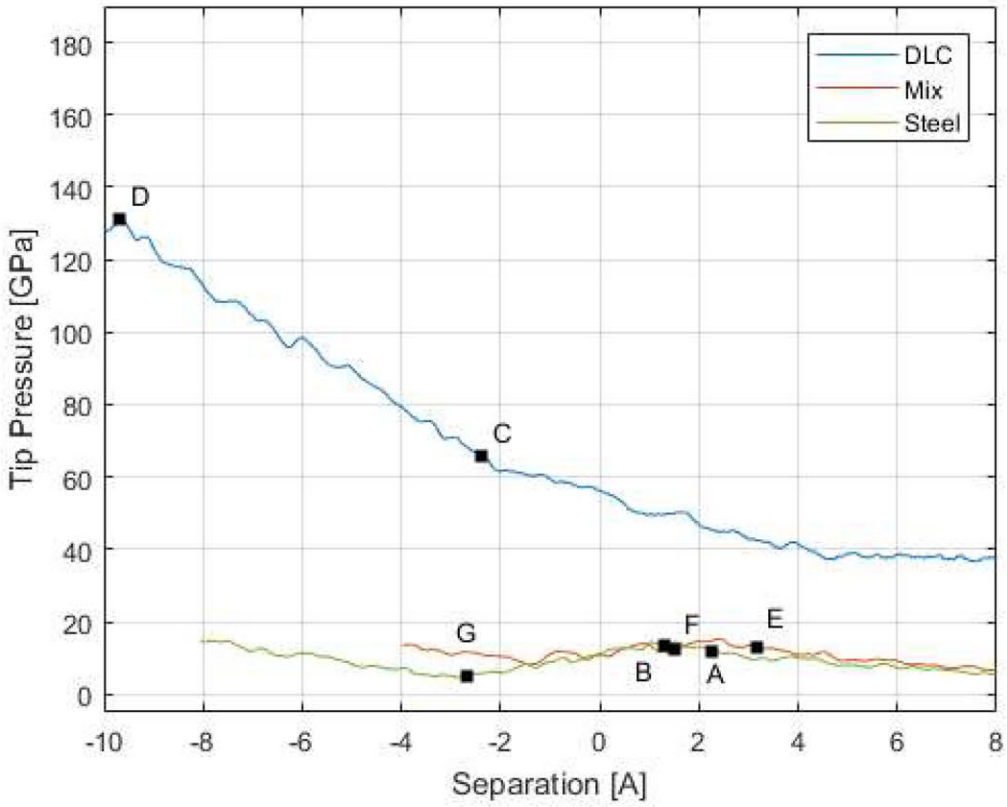

Figure 4-1: Contact point pressure versus gap height (negative heights correspond to compression of the counterface materials) when using water as a lubricant. DLC results are shown in blue, steel in green, and mixed surfaces in red. Points of interest A through G are discussed in the text.

value at a separation of 8 angstroms.

As can be seen in figure 4-4 the steel counterfaces begin to experienced bonding at the interface, which began when the gap between the tip of the asperity and the lower counterface became sufficiently small for chemical bonds to begin forming between the two surfaces. This chemical bonding is likely contributing to the mechanical failure of the passivation layer by increasing the amount of friction between the counterfaces. From the figures we can determine that once the steel counterfaces reach the wear threshold at point B, the pressure exhibits a sudden drop even as the wear rate continues to increase. This pressure drop between points A and G, indicates that the contact point pressure is not directly responsible for the onset of wear. Instead, from figure 4-5, we can observe that the wear is a result of the two surfaces bonding

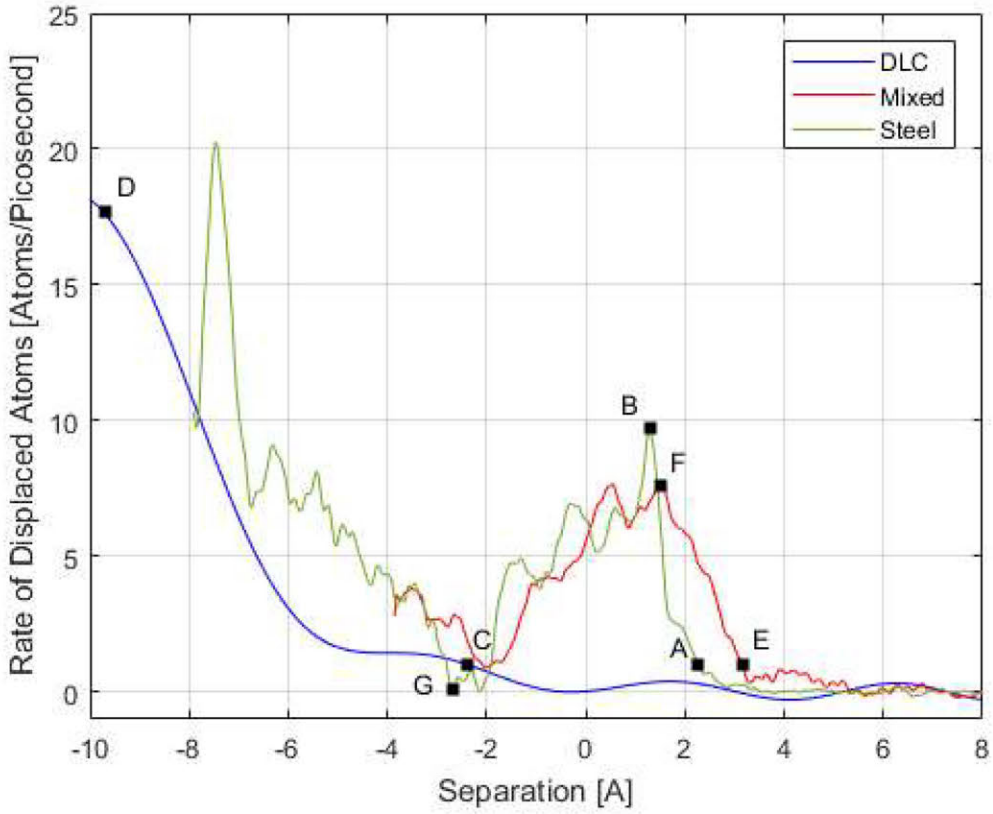

Figure 4-2: Rate at which atoms are becoming displaced versus gap height (negative heights correspond to compression of the counterface materials), when using water as a lubricant. DLC results are shown in blue and steel in green, and mixed surfaces in red. Points of interest A through G are discussed in the text.

together and then being sheared. As shown in figure 4-3, the shear stress during this section of the simulation is fairly consistent around a value of 4 GPa, with a maximum shear stress of 5 GPa at point B. This is fairly close to the ideal shear strength of iron for slip along a $< 1\ 1\ 0 >$ plane of 7.8 GPa found by Clatterbuck [72]. Reducing the number of atoms in the detection region, that is, restricting the atoms that contribute to this average value to those closest to the contact point yields a value of 7.0 GPa for the shear stress, suggesting that the failure mechanism is indeed related to the shear stress and that the slightly lower values obtained here are due to finite size of the averaging region. Following the onset of wear in steel both the wear rate and contact point pressure continue to increase until a maximum wear rate of 21 Atoms/ps is reached at a pressure of 17 GPa (although the pressure does first

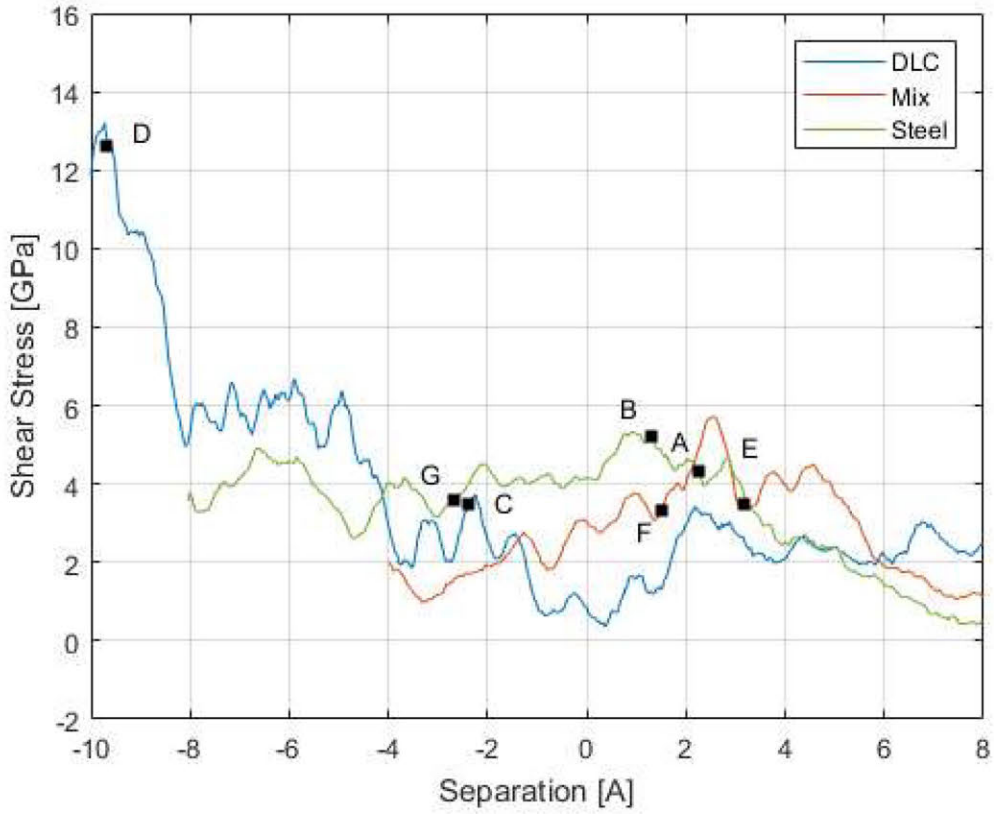

Figure 4-3: Shear stress at contact point versus gap height (negative heights correspond to compression of the counterface materials), when using water as a lubricant. DLC results are shown in blue and steel in green, and mixed surfaces in red. Points of interest A through G are discussed in the text.

decrease before monotonically increasing after point G). This point of maximum wear coincides with the catastrophic failure of the material.

Comparatively, the DLC counterfaces did not experience significant wear until much higher pressures were applied. Unlike the case of steel counterfaces, the DLC passivation layers were not reactive with each other even under high pressures, which significantly reduces the tendency to form chemical bonds. From figure 4-2, atom displacement starts at a contact point pressure of 66 GPa at point C, from which the displaced atom rate increases steadily from the threshold of 1 Atom/ps to 18 Atoms/ps by the end of the simulation when the pressure exceeds 130 GPa at point D. However, we cannot directly characterize these displaced atoms as worn material in the traditional sense. This is because not all of these displaced atoms at high

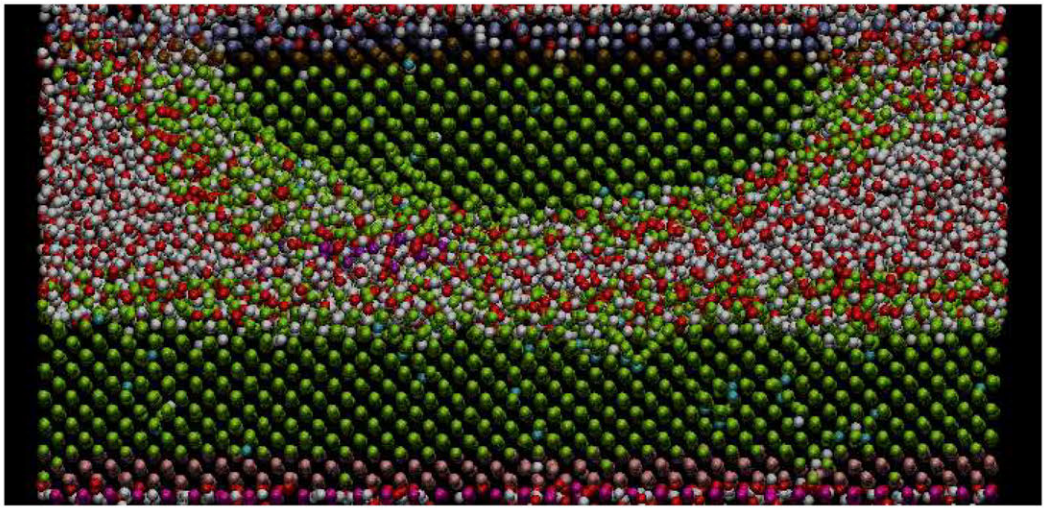

Figure 4-4: Wear behavior of steel counterfaces when lubricated with water at point A. The oxygen atoms making up the lubricant are shown in red and the hydrogen atoms are shown in white.

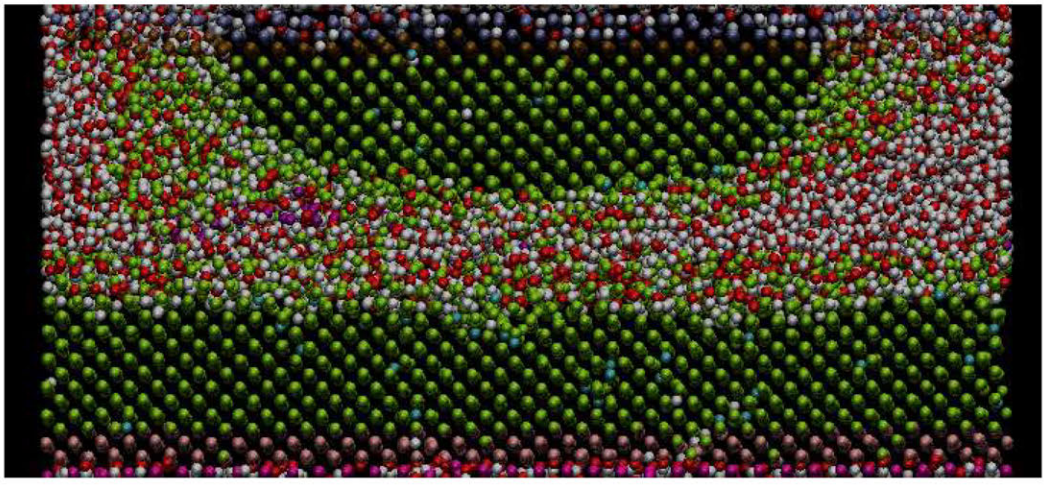

Figure 4-5: Wear behavior of steel counterfaces when lubricated with water at point B. The oxygen atoms making up the lubricant are shown in red and the hydrogen atoms are shown in white.

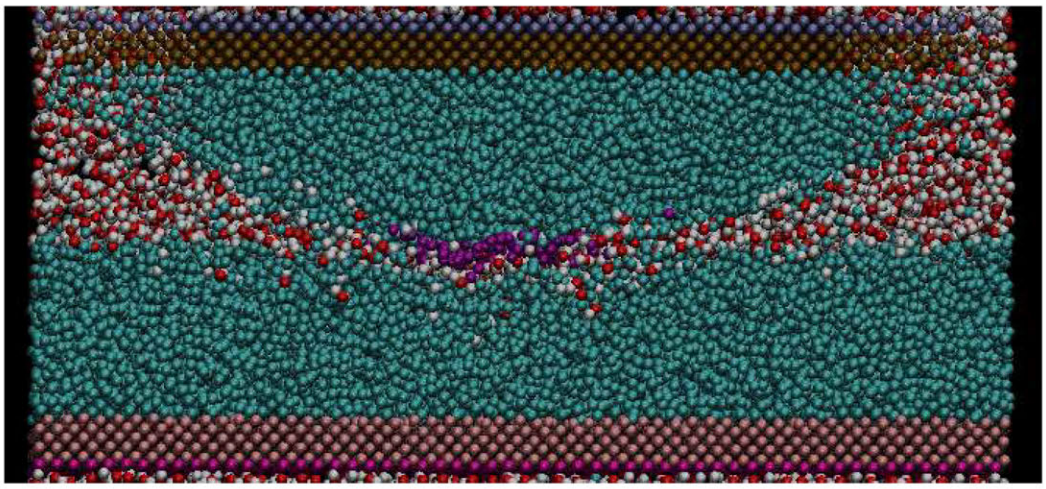

Figure 4-6: Wear behavior of DLC counterfaces when lubricated with water at point C. The oxygen atoms making up the lubricant are shown in red and the hydrogen atoms are shown in white.

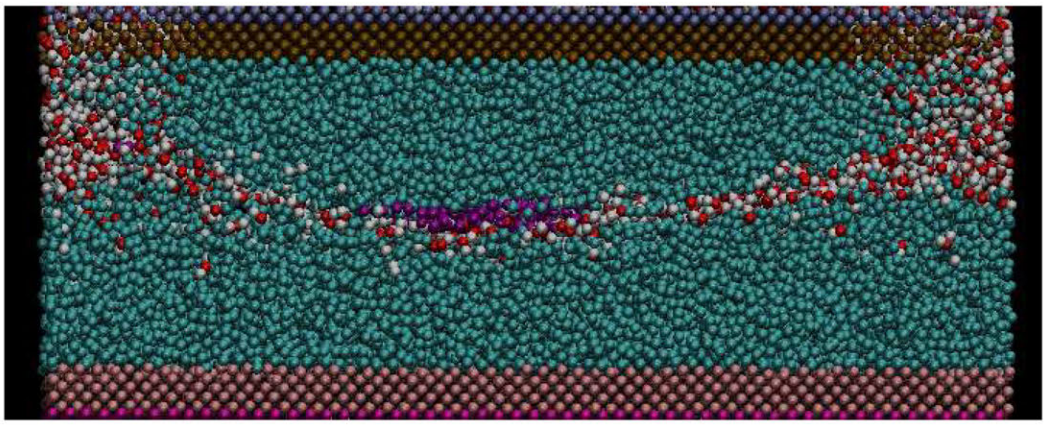

Figure 4-7: Wear behavior of DLC counterfaces when lubricated with water at point D. The oxygen atoms making up the lubricant are shown in red and the hydrogen atoms are shown in white.

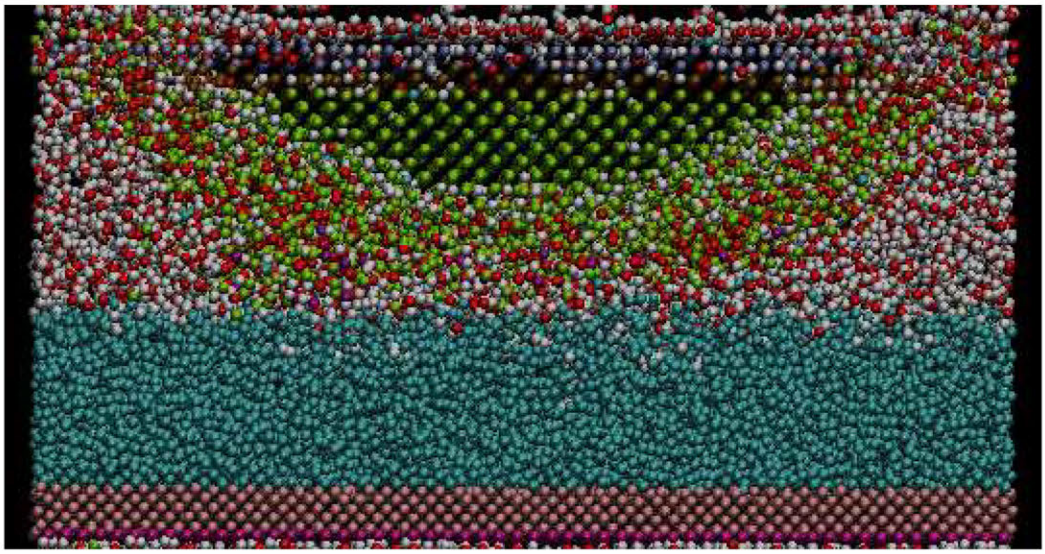

Figure 4-8: Wear behavior of mixed counterfaces when lubricated with water at point E. The oxygen atoms making up the lubricant are shown in red and the hydrogen atoms are shown in white.

pressures can be attributed to plastic deformation, which can be seen in figure 4-6. For pressures greater than ~100 GPa, the atomic structure of the DLC compresses in the normal direction sufficiently for significant numbers of atoms to meet the criteria for being displaced (having moved more than two unit cells), while the material can still regain its original configuration if the pressure is reduced. Significant plastic deformation and catastrophic wear in the DLC counterfaces does not occur until the pressure at the contact point reaches ~135 GPa at point D, at which point the extreme forces are enough to overcome the bonds between carbon atoms in the DLC, as shown in figure 4-7.

Additionally, the lack of chemical bonding between the DLC counterfaces resulted in relatively small amounts of friction, leading to a relatively low amount of shear stress at the contact point; the latter ranged from 2 GPa to 6 GPa as the contact point pressure increased from 73 GPa to 135 GPa. This leads to an estimated COF value in the range of 0.03 to 0.06, which is comparable to experimental COF results for DLC sliding friction in humid air [64, 62].

When performing the same simulation with mixed counterfaces, the resulting pressure and wear data were very similar to those obtained when using steel counterfaces,

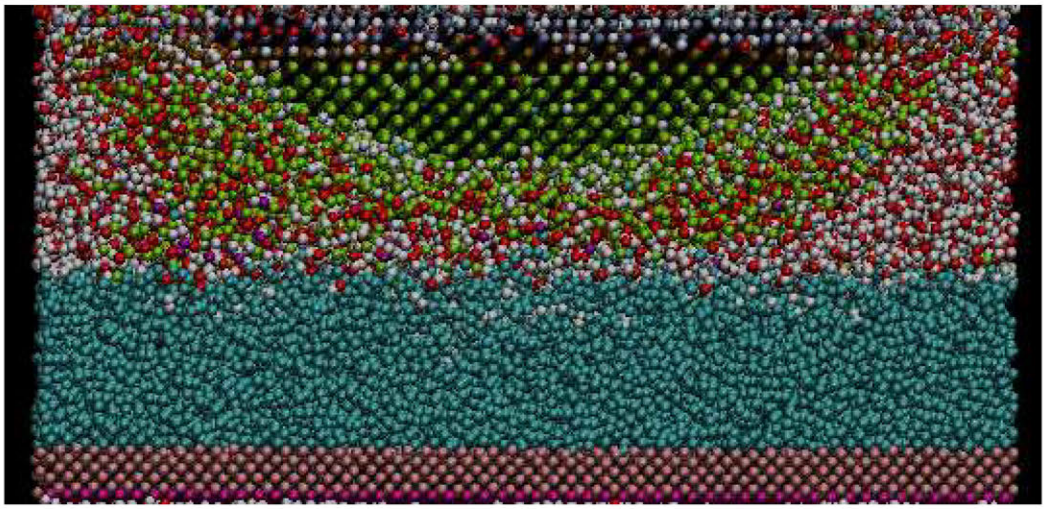

Figure 4-9: Wear behavior of mixed counterfaces when lubricated with water at point F. The oxygen atoms making up the lubricant are shown in red and the hydrogen atoms are shown in white.

and the tip pressures are within the margin of error. In figures 4-1 and 4-2, we can determine that wear begins occurring at 13 GPa at point E, before the pressure levels off and the wear rate reaches a maximum of 7.6 Atoms/ps at point F. The wear rate and pressure then drop off as the material in contact is worn away. The major differences between the results with mixed counterfaces compared to with steel counterfaces can be observed in figure 4-8 and 4-9. From these images we can see that all of the wear is concentrated in the upper steel surface, due to the steel surface being scraped away by the harder DLC counterface. Additionally, we can see from 4-3 that the shear rate after wear begins is noticeably smaller in the case of mixed surfaces. This is likely due to very few chemical bonds forming between the iron atoms in the upper steel counterface and the passivated DLC, even after wear begins damaging the passivation layer on the steel counterface.

4.3.2 n-Eicosane

The simulation results for two steel counterfaces, two DLC counterfaces, and one steel and one DLC counterface in sliding contact using n-eicosane as a lubricant are shown in figures 4-10, 4-11, and 4-12. These figures show that the steel counterfaces were better protected by n-eicosane than water. The separation distance at which

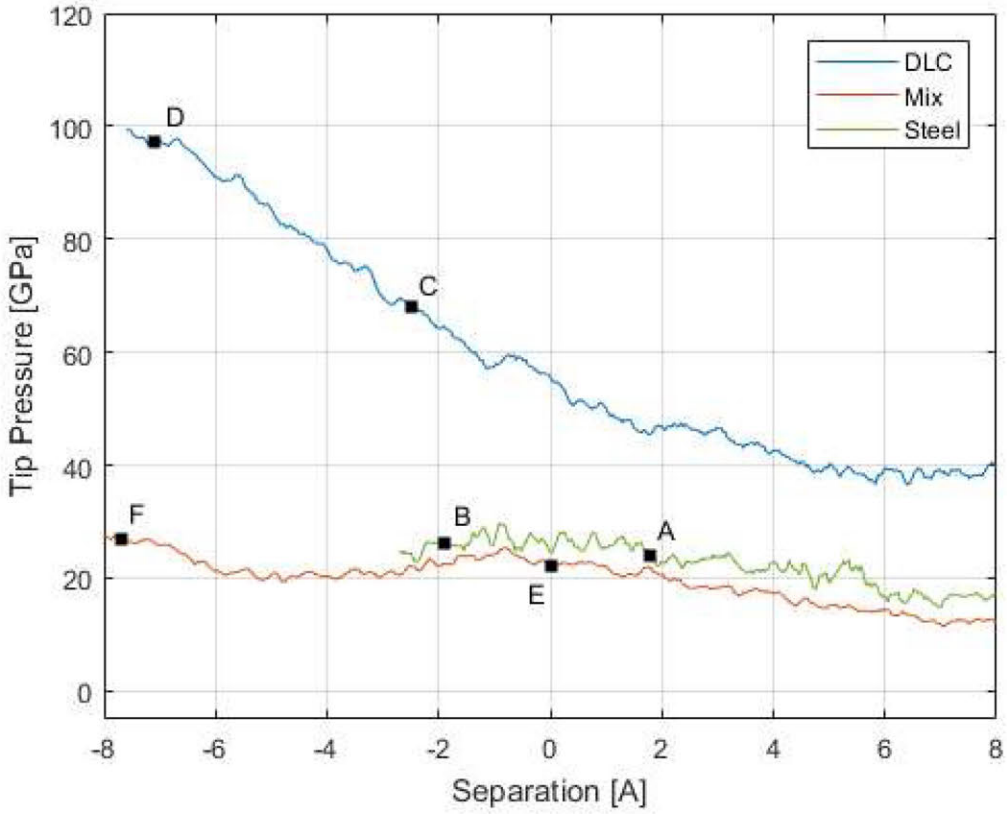

Figure 4-10: Contact point pressure versus gap height (negative heights correspond to compression of the counterfaces) when using n-eicosane as a lubricant. DLC results are shown in blue, steel in green, and mixed surfaces in red. Points of interest A through F are discussed in the text.

the rate of displaced atoms exceeds 1 atom per picosecond is 1.8 angstroms for steel counterfaces. This corresponds to an increase in pressure from 17 GPa at the baseline separation of 8 angstroms to 25 GPa when the wear rate first exceeds the threshold at point A. This means that an increase of 8 GPa was required before wear began, compared to the increase of 6.2 GPa when water was used as the lubricant. In the DLC simulation, wear began when the separation reached -2.5 angstroms. The pressure at the contact point rose from 38 GPa at the baseline to 68 GPa when wear began at point C. This is an increase of 30 GPa, which is slightly higher compared to the 28 GPa increase that was observed when using water as the lubricant. With mixed counterfaces the pressure increased from a baseline of 12 GPa to 24 GPa at point E, which corresponds to an increase in pressure of 12 GPa before wear was able to begin.

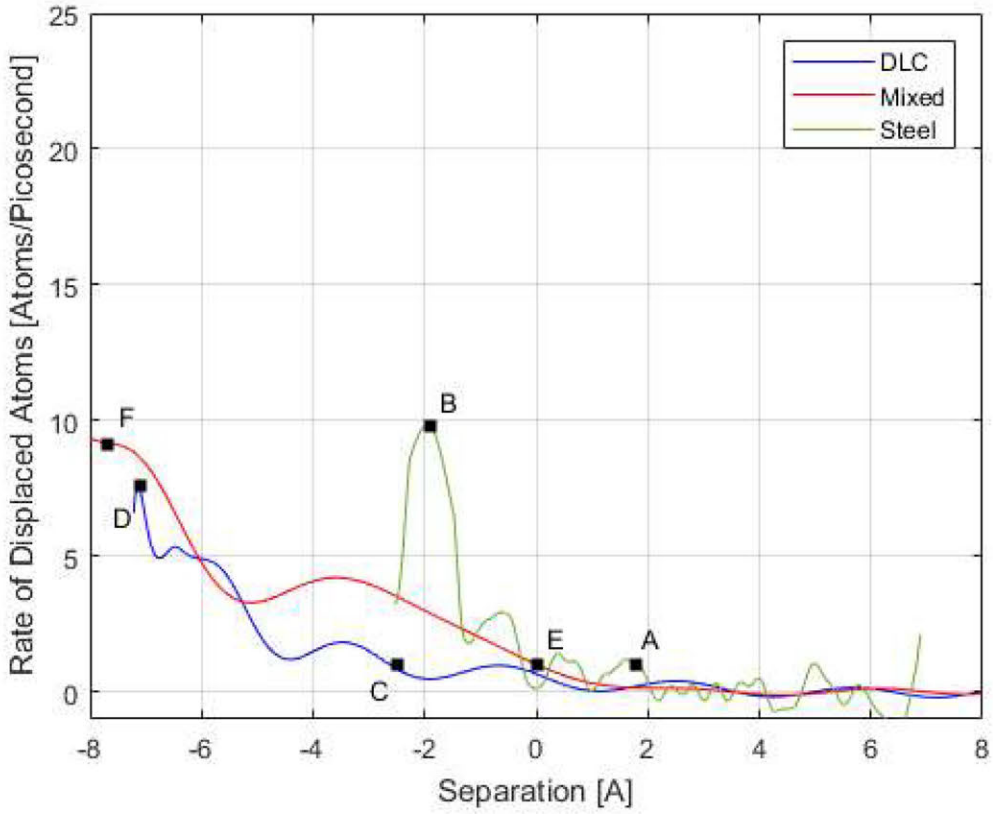

Figure 4-11: Rate at which atoms are becoming displaced versus gap height (negative heights correspond to compression of the counterface materials), when using n-eicosane as a lubricant. DLC results are shown in blue, steel in green, and mixed surfaces in red. Points of interest A through F are discussed in the text.

This is larger than the 7.3 GPa increase in pressure required for wear to begin when simulating mixed surfaces lubricated with water. For each set of surfaces, the use of n-eicosane provided greater wear protection from scuffing and wear by increasing the amount of normal force needed to cause the initial onset of wear.

While the iron atoms in the steel counterfaces eventually began forming bonds between the two surfaces once the pressure at the contact point reached 25 GPa at point A, the shear stress at the contact point was just 3.0 GPa; using a reduced detection region size causes the shear stress measurement to increase only slightly to 4.5 GPa, making failure due to the shear stress unlikely. Observing figure 4-13, we can see the formation of bonds across the counterfaces is a result of the last layer of n-eicosane being squeezed out, bringing the passivation layers into close contact.

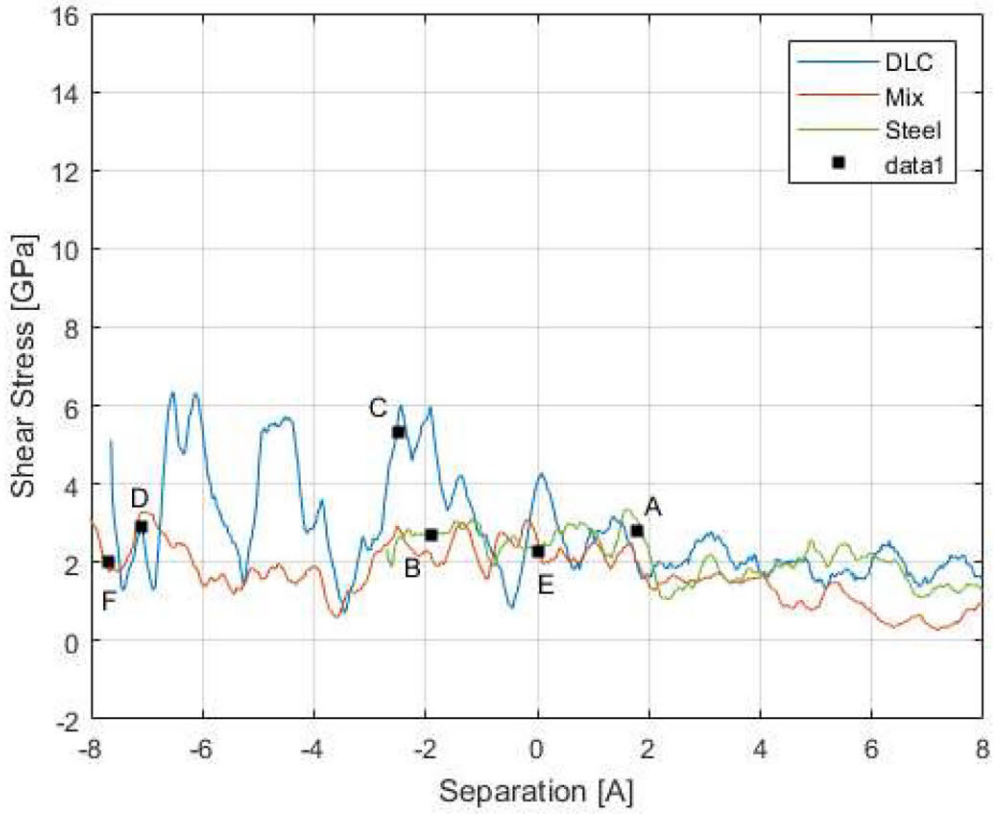

Figure 4-12: Shear stress at contact point versus gap height (negative heights correspond to compression of the counterface materials), when using n-eicosane as a lubricant. DLC results are shown in blue, steel in green, and mixed surfaces in red. Points of interest A through F are discussed in the text.

However, the majority of the wear is due to the bcc lattice beginning to deform under the high compressive load, which rises to exceed the strength of the lattice and result in the counterfaces quickly reaching catastrophic failure and a maximum wear rate of 9.8 Atoms/ps at point B (shown in figure 4-14). The maximum wear rate observed when lubricating with n-eicosane is roughly the same as the corresponding simulation with water lubrication. However, the required pressure rise to cause this wear increased significantly with n-eicosane as the lubricant. This points to the larger n-eicosane molecule distributing the load over a greater surface area compared to water.

The results from the simulations using DLC counterfaces show very similar results to those observed when using water as the lubricant. As shown in figure 4-15 even

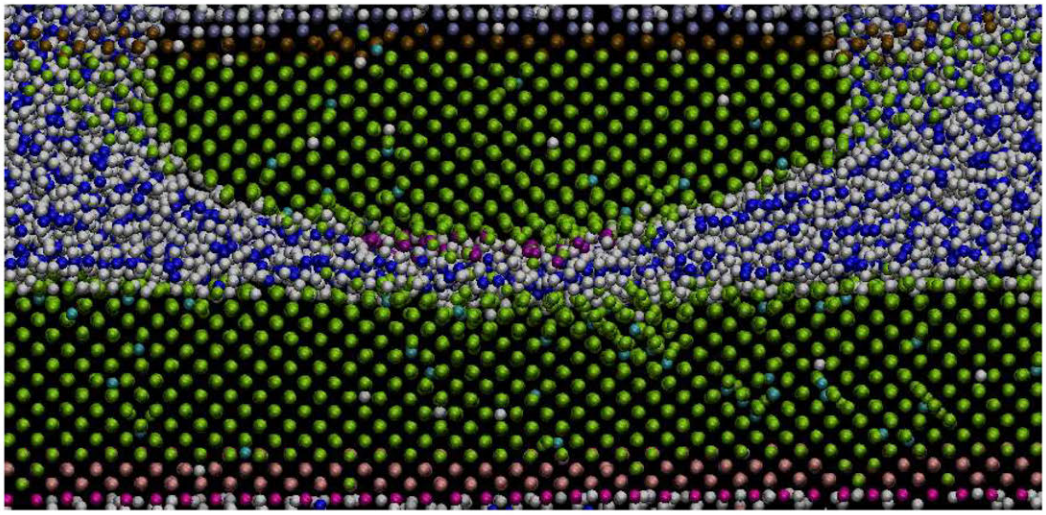

Figure 4-13: Wear behavior of steel counterfaces when lubricated with n-eicosane at point A. The carbon atoms making up the lubricant are shown in dark blue and the hydrogen atoms are shown in white.

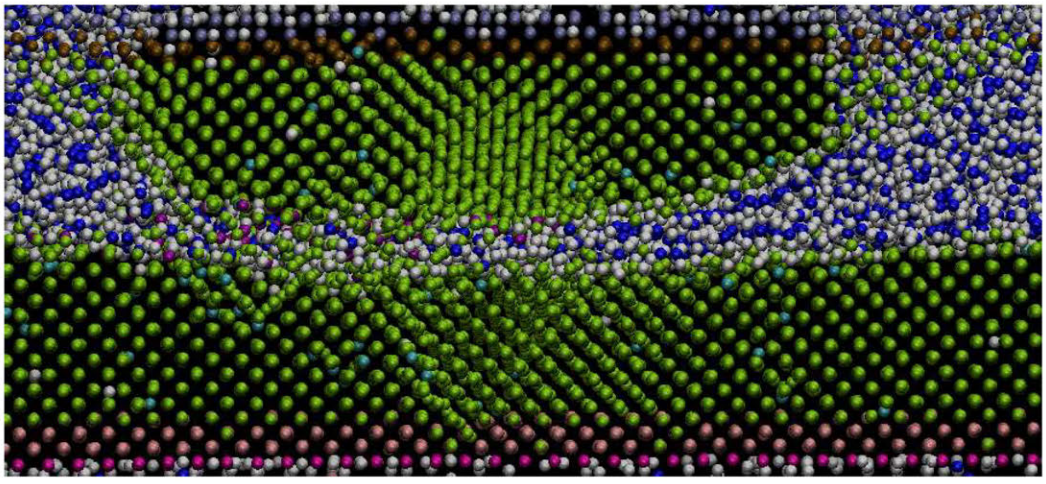

Figure 4-14: Wear behavior of steel counterfaces when lubricated with n-eicosane at point B. The carbon atoms making up the lubricant are shown in dark blue and the hydrogen atoms are shown in white.

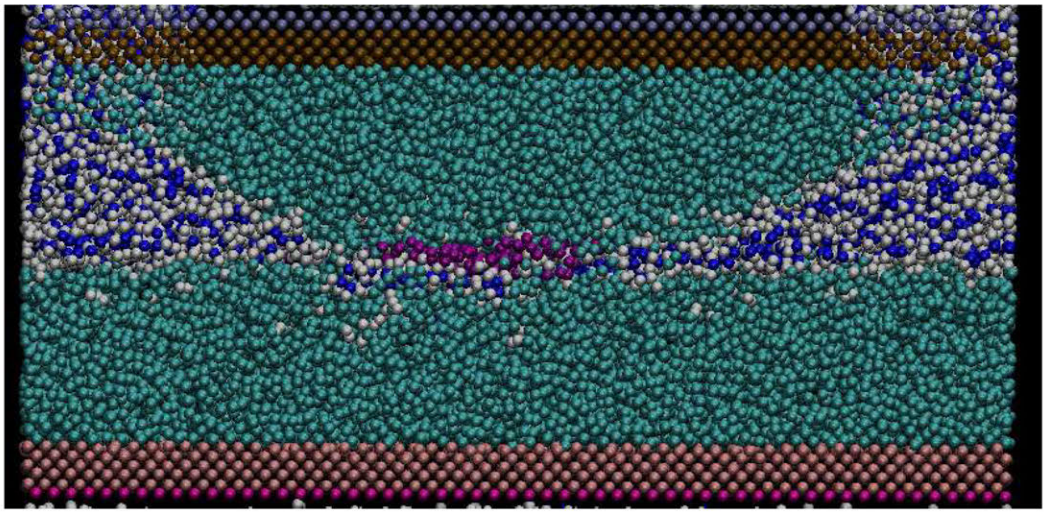

Figure 4-15: Wear behavior of DLC counterfaces when lubricated with n-eicosane at point C. The carbon atoms making up the lubricant are shown in dark blue and the hydrogen atoms are shown in white.

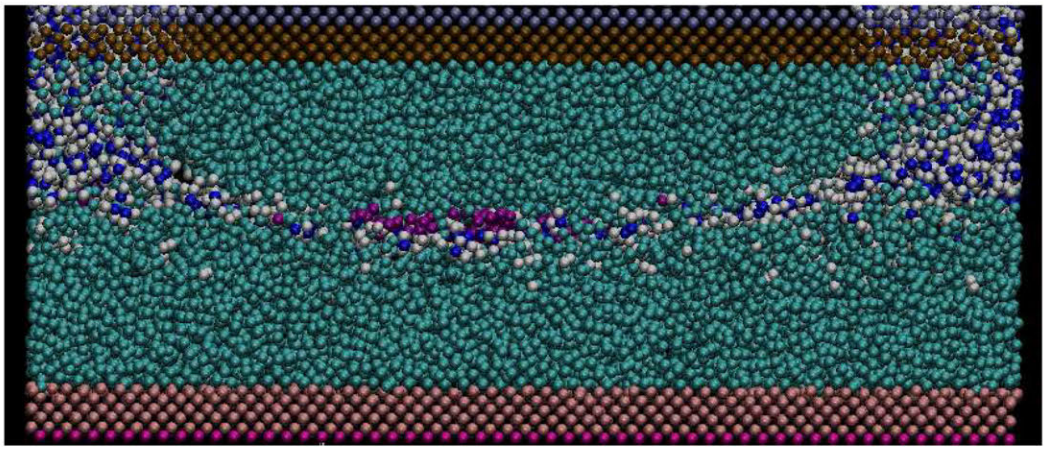

Figure 4-16: Wear behavior of DLC counterfaces when lubricated with n-eicosane at point D. The carbon atoms making up the lubricant are shown in dark blue and the hydrogen atoms are shown in white.

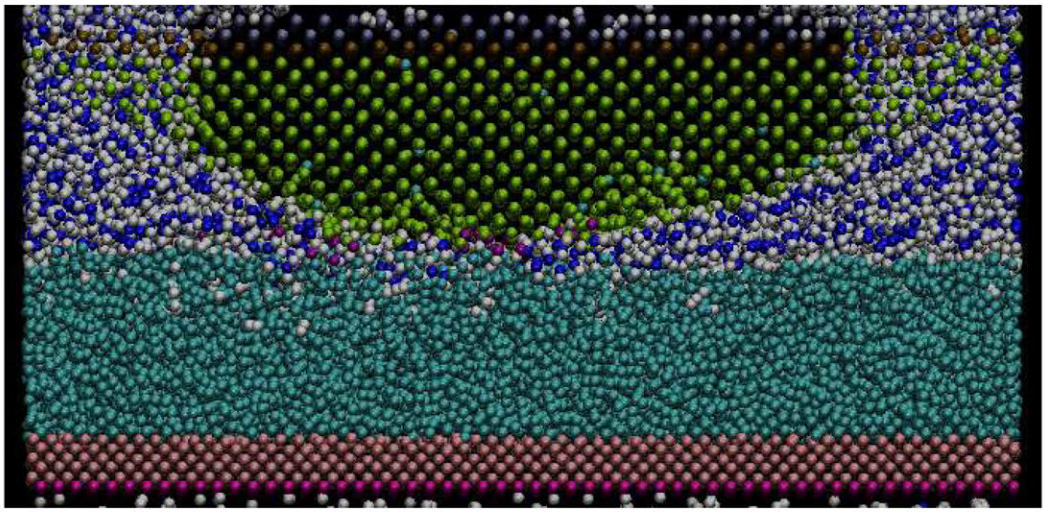

Figure 4-17: Wear behavior of mixed counterfaces when lubricated with n-eicosane at point C. The carbon atoms making up the lubricant are shown in dark blue and the hydrogen atoms are shown in white.

when the lubricant has been squeezed out from between the counterfaces, the passivation layers once again prevent any chemical bonding from occurring. The number of displaced atoms begins to increase as the tip pressure approaches ~100 GPa and is primarily due to the high pressure causing elastic deformation of the counterfaces (as seen in figure 4-16). This results in a displaced atom rate that increases to more than 7.6 Atoms/ps by the end of the simulation (see figure 4-11). Large scale plastic deformation in the DLC counterfaces reached its peak when the contact point pressure reached 97 GPa at point D, at which point the extreme forces are enough to overcome the bonds between carbon atoms in the DLC. As before, the low friction between the counterfaces results in very low shear stress at the contact point. The shear stress was found to be 3 GPa and 5 GPa for contact point pressures of 68 GPa and 97 GPa. This corresponds to a range of COF from 0.03 to 0.07, which is similar to the dry sliding friction for hydrogen passivated DLC [59].

When performing the same simulation with mixed counterfaces, the resulting pressure and wear data were in between those obtained for the DLC and the steel simulations. We can see from figure 4-17 that the wear in this case is due to a combination of the softer steel surface being scraped away by the harder DLC surface and the high pressure of the lubricant. In figures 4-10 and 4-11, we observe that wear begins

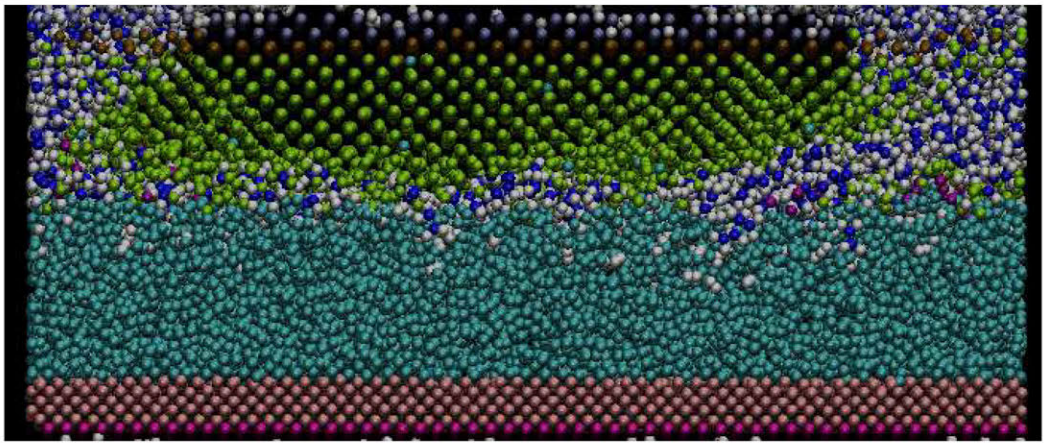

Figure 4-18: Wear behavior of mixed counterfaces when lubricated with n-eicosane at point D. The carbon atoms making up the lubricant are shown in dark blue and the hydrogen atoms are shown in white.

occurring at 24 GPa at point E, a smaller increase over the baseline than with steel. However, unlike with the steel, the wear rate continues to increase until it reaches a wear rate of 9 Atoms/ps. Unlike what we observed with the water lubricated mixed surfaces, from figure 4-12 we can determine that the shear rate for steel and mixed surfaces are nearly identical. This is a result of the hydrogen passivation layer of the DLC not being able to completely prevent bonding with the iron atoms from the upper counterface, once the onset of wear damages the steel counterfaces passivation layer. This limited bonding between the surfaces can be observed in figure 4-18.

4.3.3 9-Octyl-Eicosane

The simulation results for two steel counterfaces, two DLC counterfaces, and one steel and one DLC counterface in sliding contact using 9-octyl-eicosane as a lubricant are shown in figures 4-19, 4-20, and 4-21. These figures show that 9-octyl-eicosane offers the same or slightly better protection from the onset of wear than n-eicosane for all three combinations of counterfaces. The separation distance at which the rate of displaced atoms exceeds 1 atom per picosecond is 1.4 angstroms for steel counterfaces (point A). This corresponds to an increase in pressure from 11 GPa at the 8 angstrom separation baseline to 21 GPa when the wear exceeds the threshold of 1 atom/ps at point A. The observed pressure rise of 10 GPa is a small increase compared to the

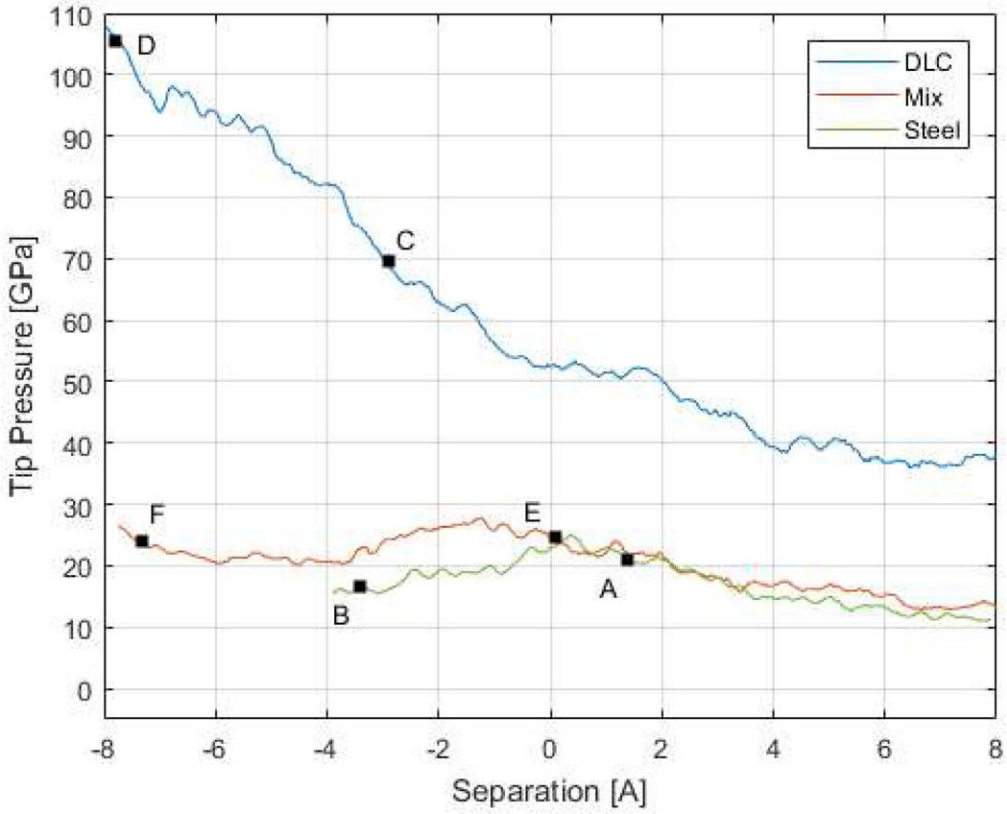

Figure 4-19: Contact point pressure versus gap height (negative heights correspond to compression of the counterfaces) when using 9-octyl-eicosane as a lubricant. DLC results are shown in blue, steel in green, and mixed surfaces in red. Points of interest A through D are discussed in the text.

rise in contact point pressure required for wear to begin with n-eicosane. In the DLC simulation, wear began when the separation reached -2.9 angstroms. This required a pressure rise at the contact point from 37 GPa at the baseline to 70 GPa when wear began at point C. This increase of 33 GPa is a small improvement in preventing wear over using n-eicosane or water as the lubricant. With mixed counterfaces the pressure increased from a baseline of 13 GPa to 25 GPa at point E. This corresponds to an increase in pressure of 12 GPa before the onset of wear, the same as we observed when using n-eicosane as the lubricant.

With 9-octyl-eicosane as the lubricant, the iron atoms in the steel counterfaces eventually began forming bonds between the surfaces once the pressure at the contact point reached 21 GPa at point A, which can be observed in figure 4-22. This corre-

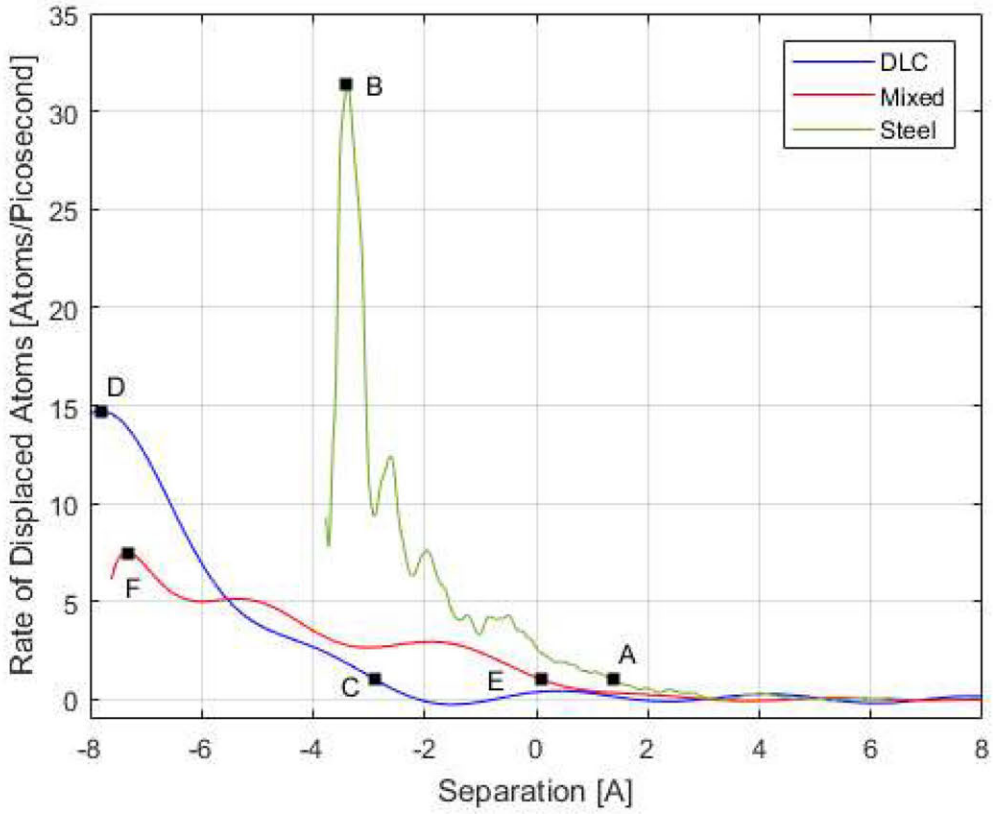

Figure 4-20: Rate at which atoms are becoming displaced versus gap height (negative heights correspond to compression of the counterfaces), when using 9-octyl-eicosane as a lubricant. DLC results are shown in blue, steel in green, and mixed surfaces in red. Points of interest A through D are discussed in the text.

sponds to the point at which the final layer of 9-octyl-eicosane molecules is squeezed out, bringing the counterfaces into close contact. The material begins to fail catastrophically once the contact point pressure reaches its peak at 24 GPa, and bonding begins to occur between the two steel surfaces. From this point onwards the wear rate continues to increase until it peaks at 31 Atoms/ps when the steel counterfaces fail catastrophically at point B due to the high normal load and high fluid pressure, which causes the distortions in the BCC lattice seen in figure 4-23. Once bonding begins to occur between the surfaces, we observe a fairly consistent shear stress between 2 GPa and 3 GPa.

The DLC counterfaces show very similar wear behavior to that observed when using the other two model lubricants. From figure 4-24, we can observe that even once

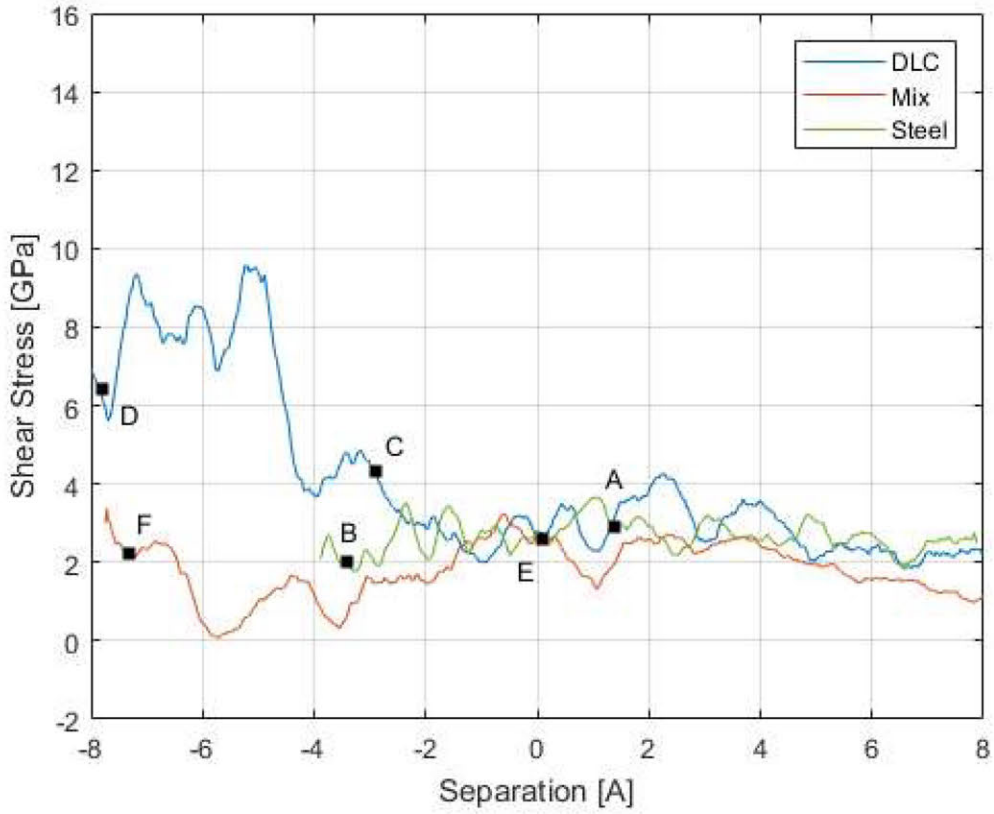

Figure 4-21: Shear stress at contact point versus gap height (negative heights correspond to compression of the counterface materials), when using 9-octyl-eicosane as a lubricant. DLC results are shown in blue, steel in green, and mixed surfaces in red. Points of interest A through F are discussed in the text.

the lubricant has been squeezed out from between the surfaces, the passivation layers once again prevent any chemical bonding from occurring. The number of displaced atoms begins to increase for pressures above 70 GPa (point C), again primarily due to elastic deformation of the counterfaces at these high pressures. This results in a displaced atom rate that steadily increases to 15 Atoms/ps at point D. This also corresponded to reaching an interface pressure of 104 GPa, at which point the applied forces were enough to overcome the bonds between the carbon atoms (seen figure 4-25). As before, the low friction between the counterfaces results in very low shear stress at the contact point, relative to the amount of normal stress being applied. The shear stress was found to be 3 GPa and 9 GPa for interface pressures of 70 GPa and 104 GPa. This corresponds to a range of COF from 0.04 to 0.09, which is in the

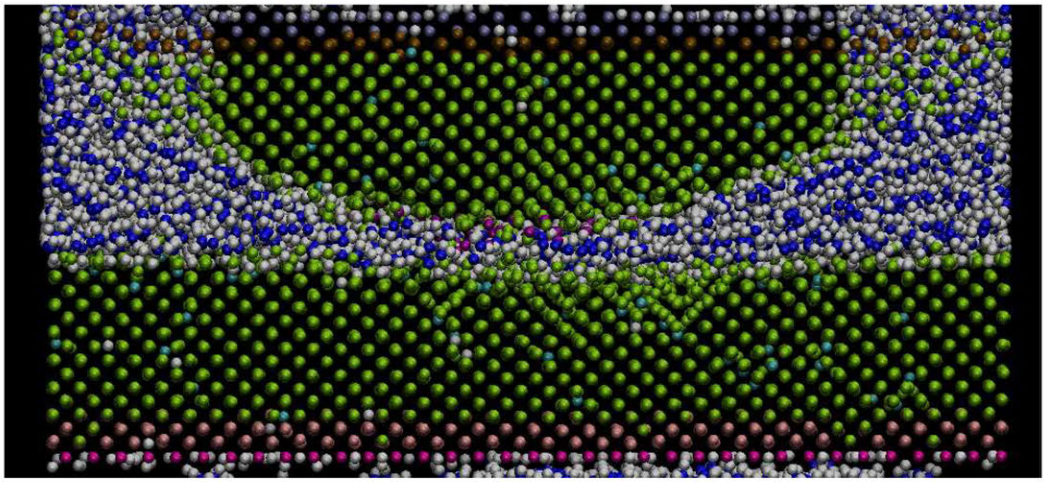

Figure 4-22: Wear behavior of steel counterfaces when lubricated with 9-octyl-eicosane at point A. The carbon atoms making up the lubricant are shown in dark blue and the hydrogen atoms are shown in white.

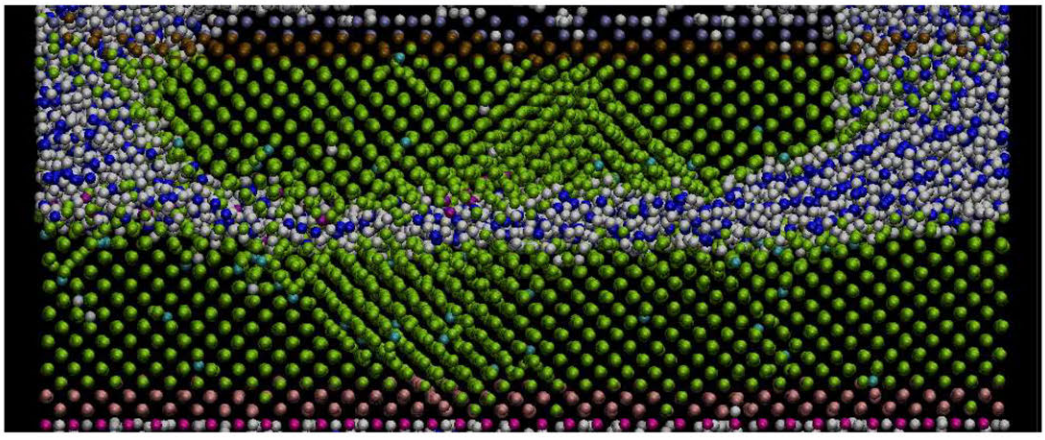

Figure 4-23: Wear behavior of steel counterfaces when lubricated with 9-octyl-eicosane at point B. The carbon atoms making up the lubricant are shown in dark blue and the hydrogen atoms are shown in white.

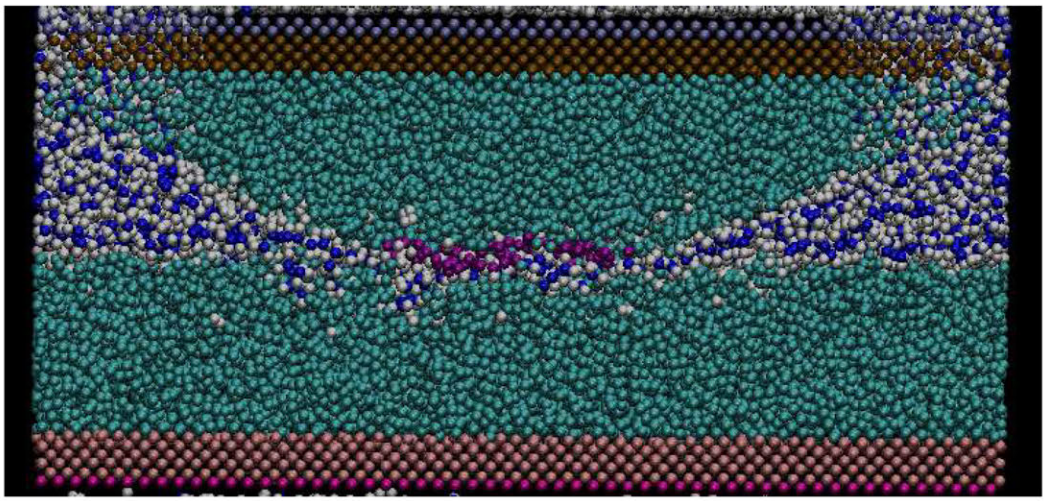

Figure 4-24: Wear behavior of mixed counterfaces when lubricated with 9-octyl-eicosane at point C. The carbon atoms making up the lubricant are shown in dark blue and the hydrogen atoms are shown in white.

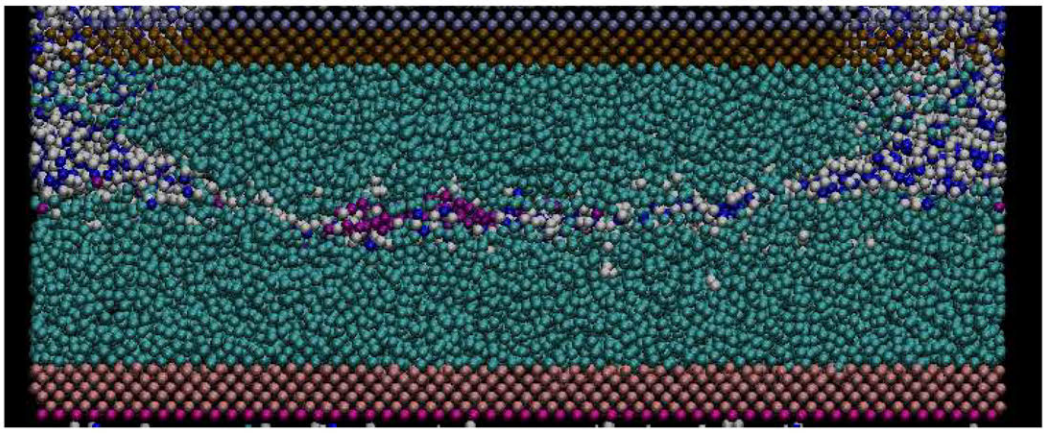

Figure 4-25: Wear behavior of mixed counterfaces when lubricated with 9-octyl-eicosane at point D. The carbon atoms making up the lubricant are shown in dark blue and the hydrogen atoms are shown in white.

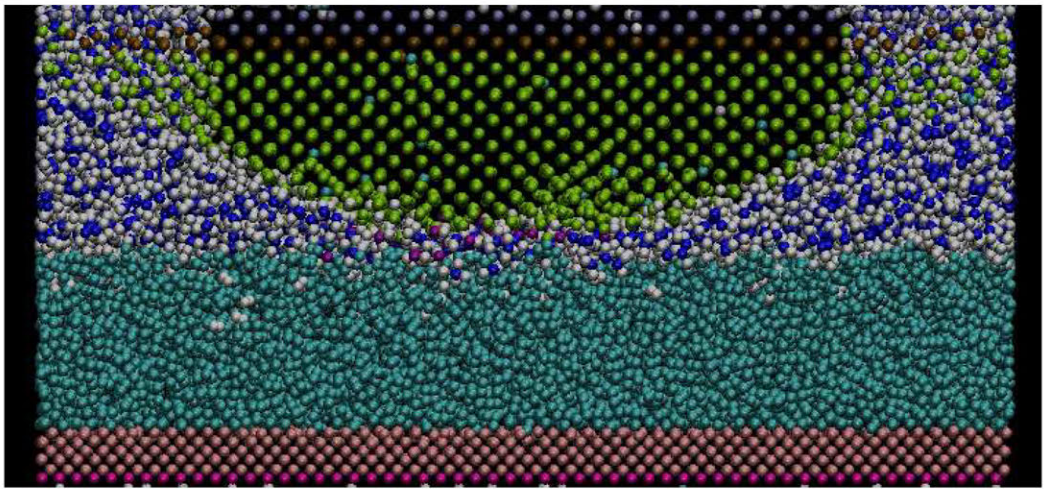

Figure 4-26: Wear behavior of mixed counterfaces when lubricated with 9-octyl-eicosane at point C. The carbon atoms making up the lubricant are shown in dark blue and the hydrogen atoms are shown in white.

range we would expect for the dry sliding COF for DLC with a hydrogen passivation layer [59].

When simulating mixed counterfaces lubricated with 9-octyl-eicosane, we once again observe very similar results to the simulations using n-eicosane as the lubricant. Figure 4-26 indicates that the wear in this case is due to a combination of the softer steel surface being scraped away by the harder DLC surface and the high pressure of the lubricant. As before, the resulting pressure and wear data were in between those obtained for the DLC and the steel simulations. In figures 4-19 and 4-11, the measurements indicate that wear begins occurring at 25 GPa at point E, at which point the pressure stops increasing as separation continues to decrease. After the onset of wear, the wear rate steadily increase until it reaches a peak of 7.5 Atoms/ps. Similar to the previous section, we can determine from figure 4-21 that the amount of shear in the steel and mixed cases are very similar, with the shear in the mixed counterfaces being slightly smaller. As before, this is likely a result of the hydrogen passivation layer of the DLC not being able to completely prevent bonding with the iron atoms from the upper counterface after the onset of wear, as seen in figure 4-27.

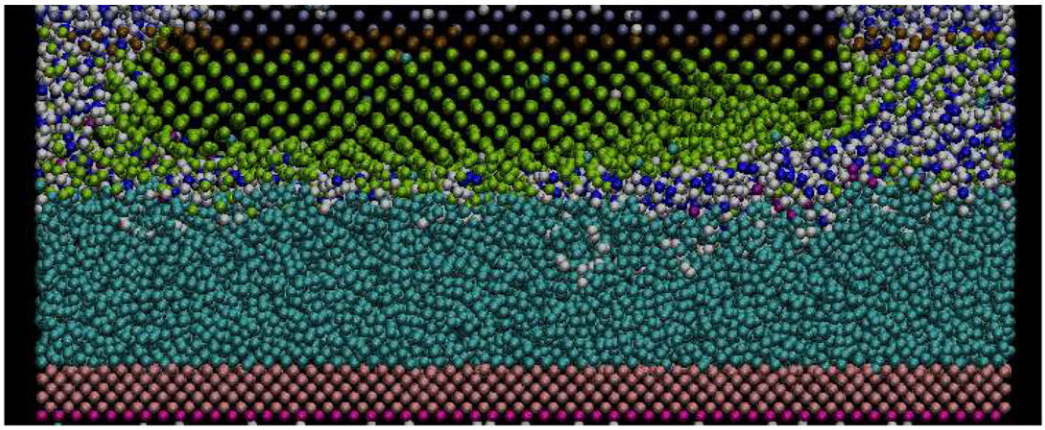

Figure 4-27: Wear behavior of mixed counterfaces when lubricated with 9-octyl-eicosane at point D. The carbon atoms making up the lubricant are shown in dark blue and the hydrogen atoms are shown in white.

4.4 Discussion

From these computational experiments, steel surfaces experienced large amounts of friction and wear due to several reasons. First, the passivation layers that formed on the steel countersurfaces were able to chemically react with each other. This bonding resulted in high friction forces which contributed to high shear stresses at the contact point. In the case of water as a lubricant, the counterfaces failed due to this shear stress. The friction and wear performance of steel was greatly improved by using more realistic lubricants like n-eicosane and 9-octyl-eicosane. These lubricants did not react with the steel passivation layers and increased the pressure needed to bring the surfaces close enough to begin bonding. We also saw that as the size of the molecular weight of the lubricant molecule increased, wear, measured via the rate of displaced atoms, decreased significantly.

In contrast, DLC has a number of properties that conspire to produce significantly more favorable behavior, namely, considerably lower wear and low friction. The first component that contributes to these properties is the passivation layer that forms when the DLC is exposed to the environment. This layer protects the DLC from any further chemical reactions with the environment. Additionally, unlike the passivation layers that form on steel counterfaces, due to the very strong bonds between carbon and the passivation elements (O or H), the DLC passivation layers prevent the surface

from creating chemical bonds to the counterface. In other words, the energy barrier for damaging the passivation layer is high. The passivation layer could only be damaged if it came into contact with carbon atoms with dangling bonds, i.e., an unpassivated DLC surface. However, due to the high reactivity of unpassivated DLC, this is unlikely outside of a vacuum.

Another contributor to the DLC performance is its high material strength. The large number of strong sp^3 bonds, especially in ta-C, makes it very difficult for the carbon atoms to detach from the structure. This protects high sp^3 DLC from damage by the very high contact point pressure. In simulations with lower sp^3 a-C, high pressures have been shown to lead to conversion of sp^2 bonds to sp^3 bonds [31]. Additionally DLC's amorphous structure means that the strength of the material is not effected by the plane on which stress is applied.

When simulating the combination of a steel and a DLC surface, we generally saw contact point pressure and wear rate results that were close to what we would expect for two steel surfaces. However, the results obtained for the shear stress were not as clear cut. When lubricated with a hydrocarbon based lubricant the shear stress was nearly identical to that of two steel surfaces, but the shear stress was noticeably lower when using water as a lubricant. This was because the passivation layer that forms on DLC when exposed to water was able to prevent iron atoms from bonding to the DLC surface even after the model iron asperity had begun experiencing wear. The passivation layer preventing bonding from occurring is likely a major contributing factor to DLC's resistance to scuffing wear.

While adding lubricants to softer counterfaces, like the model steel counterfaces, can result in reduced wear at a given pressure, the protective effects of using a lubricant with DLC are not as readily apparent. However, in theory they could provide some benefits, like providing a way to affect the composition of the passivation layer and reducing the peak pressures encountered at the contact point due to their larger size.

We observe that water, n-eicosane, and 9-octyl-eicosane affect the friction and wear experienced by the counterfaces in two different ways. First, each of these lubricants

has different fluid properties (e.g. viscosity), which play a dominant role in friction before the surfaces come into contact. Here, due to the very small thickness of the fluid layer, the adhesion between a molecules of a given lubricant type and a particular type of surface is also important, as this controls how much pressure is needed to squeeze out the fluid molecules and bring the surfaces into contact [66]. Larger lubricant molecules also tend to distribute the load over larger areas, thus reducing peak loads. Second, hydrocarbons like n-eicosane and 9-octyl-eicosane provide only a source of hydrogen for creating a passivation layer, while water provides a source of hydrogen and oxygen. This results in the formation of different types passivation layers, which play a significant role in the friction and wear between the surfaces after they make contact. While both of these types of environment result in a very stable passivation layer for the DLC counterfaces, the passivation layer created on the steel surface was not as effective at preventing bonding, particularly when comprised of hydrogen (resulting from exposure to hydrocarbons). Instead, when using steel counterfaces, the hydrocarbon lubricants were able to reduce wear significantly entirely through their fluid properties.

Chapter 5

Couette Flow

5.1 Introduction

In this chapter, we use MD simulations to study in more detail the transition from lubricated to dry friction. The manner in which this transition takes place is of great fundamental importance and many open questions still remain. In particular, although the two limiting processes, namely nanoconfined flow or solid-solid friction, have received enormous attention *individually*, the transition from the former, a rate dependent process, to the latter, a rate-independent process, has yet to be fully understood.

In the interest of simplicity, the discussion below refers to the simplest geometry, namely, planar shear of two atomically flat solid surfaces. The MD simulations for this work will also be performed in this geometry.

Recent work on this topic has proposed [74] that this transition takes place across three distinct regimes of behavior. For sufficiently large surface separations, friction (resistance to motion of the solid surfaces) is purely hydrodynamic; in the geometry considered here this corresponds to traditional Couette flow. As the surface separation becomes smaller, the layer of lubricant becomes too thin to act as a bulk fluid; this new regime, in which the effect of the fluid-solid interfaces becomes important is referred to as interfacial. Finally, as the surface separation becomes so small that no lubricant exists in liquid form between the solid surfaces, the surfaces slide past each

other via slip; for this reason, this regime is referred to as the slip regime.

The authors of [74] constructed the following model for describing the frictional force required to sustain the shearing action:

$$\frac{1}{\gamma} = \frac{AU_0}{F_f} = \frac{1}{\gamma_{slip}} + \frac{1}{\gamma_{interfacial}} + \frac{1}{\gamma_{bulk}} \tag{5.1}$$

In the above, A is the solid surface area, U_0 is the velocity of the moving counterface, and F_f is the friction force acting on each counterface.

This relation effectively assumes that the three mechanisms may be combined as a network of resistances in parallel. Although the rationale for this composition is not provided in [74], it is understood that this arrangement leads to the correct behavior in the limiting case where each mechanism is primarily active in a well-defined regime.

Expression 5.1 was found to be in very good agreement with in-house MD simulation results for a system comprised of water and two polar decanol $CH_3(CH_2)_9OH$ bilayers [74]. These molecules were modeled using the SPC/E force field, which represents groups of atoms using Van der Waals interaction cites and electrostatic point charges. These Couette flow simulations were performed at a pressure of 1 MPa and a temperature of 300K. The counterfaces in these computational experiments were translated in the x direction a constant velocity which was varied between 10×10^{-4} m/s to 0.5 m/s for dry friction and between 0.05 m/s and 5 m/s for lubricated friction. The constant velocities used were increased with increasing fluid heights, which allowed the authors to optimize their simulations to reduce the computational cost. However, this also required taking great care when setting up each individual simulation to select velocities within the linear friction regime.

Here we note that in this validation by Schlaich et al [74], each of the terms γ_{slip}, $\gamma_{interfacial}$, γ_{bulk} was expressed in an ad-hoc form that included adjustable constants with channel-height dependence. In addition to providing ample flexibility for fitting the MD results, that functional form also ensured that each mechanism became quickly negligible beyond the range of channel heights in which it was "active". In addition to the ad hoc functional dependence of the three terms on the channel height,

overall eight fitting parameters were used.

In this work, we would like to use the insights gained from the MD simulations of Schlaich et al., as well as our simulations to propose a much simpler, rational model that can explain our results using fewer fitted parameters. Although we believe that there is much valuable insight in the "decomposition" used in [74], here we find that a much simpler model with a much smaller number of adjustable constants describes our MD simulation results quite well. The difference may perhaps be due to the different fluid-solid system considered here, which leads to slightly different behavior. More research is needed to clarify these questions.

5.2 Methods

5.2.1 Simulation Setup

Our setup follows the general setup described for flat counterfaces in section 2.3.4. We now discuss elements of this setup that are specific to the present simulations.

We performed MD simulations of two flat DLC or steel counterfaces in relative motion, separated by a model lubricant. The height of the lubricant was controlled by changing the number of lubricant molecules between the two surfaces. A constant normal force was applied in the vertical direction on the lower counterface to set an external pressure of 500 MPa. The lower counterface was also translated at a constant velocity in the horizontal direction (25 m/s) while the upper counterface was held stationary. The temperature control layer was set to maintain a temperature of 350K. The resulting friction force was measured from the control surface of the fixed (upper) counterface.

In order to control the amount of fluid separation in each of the simulations, the simulations are initialized with a different number of lubricant molecules trapped between the two counterfaces. During the initialization these loosely placed molecules are compressed down from a vapor and excess kinetic energy is periodically removed to allow the lubricant molecules to condense into a fluid. Additionally, the coordinates

of the lubricant molecules are tracked throughout the simulation in order to generate velocity profiles and density profiles of the lubricant in order to study lubricant interaction with the passivated surfaces.

5.2.2 Model Lubricants

The results for this chapter are split into two parts. In the first part, section 5.3.1, we will be looking at DLC and steel counterfaces separated by water. The small molecular size and relatively low viscosity of water makes it easier to observe all the nanoconfined flow regimes, as well as compare these results to those obtained in the literature. In order to simulate water as accurately as possible in these simulations, we will be making use of the Aqueous ReaxFF potential.

In the second part, section 5.3.2, we study the wall shear/friction results of hydrogen passivated DLC surfaces separated by a range of alkanes (n-decane, n-eicosane, and 9-octyl-eicosane) and its dependence on the size of the lubricant molecule. Due to the incompatibility between the Aqueous ReaxFF with hydrocarbons, for the Couette flow simulations lubricated with alkanes, we will be relying on the combustion branch ReaxFF model used in the previous chapters.

5.3 Results

In this section we discuss our results.

5.3.1 Water

The friction results for the MD simulations of water for DLC and steel counterfaces are shown in figure 5-1. Simulations were run with fluid heights up to approximately 50 angstroms, before the computational cost of obtaining additional data points became too large to continue with our current computational resources. However, our current resources are sufficient to observe the beginning of the transition from interfacial flow to bulk-like flow and thus we were able to observe all three regimes. From the

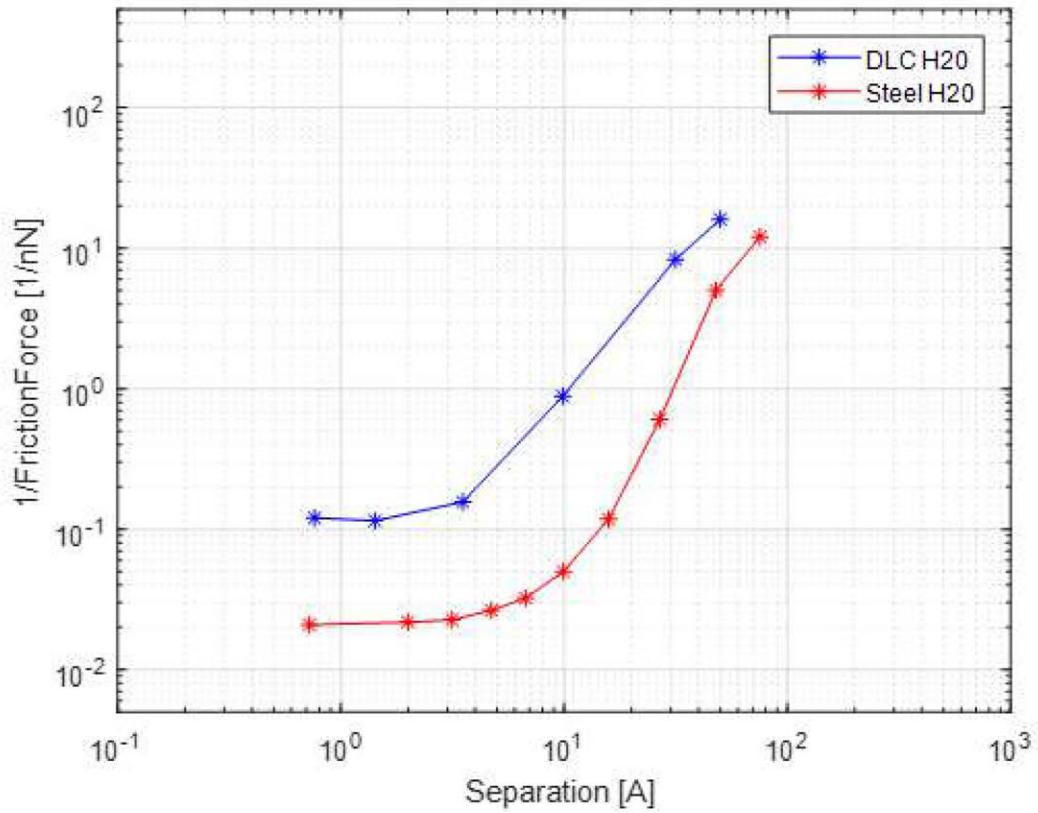

Figure 5-1: Inverse of friction force versus fluid height when using water as a lubricant. The results for DLC surfaces are shown in blue and the results for steel surfaces are shown in red.

figure we can observe that the DLC counterfaces are associated with a lower friction force at every fluid height simulated compared to the steel counterfaces. However, it is also important to note that, as expected, the difference in the friction forces diminishes as the fluid height increases and bulk-like flow becomes the dominant source of friction. Additionally, we can observe that the transition from sliding friction to interfacial friction occurs at approximately 5 angstroms with DLC counterfaces, but this transition is delayed noticeably when steel counterfaces are used. Conversely, we do not observe as significant a difference between the two surface types when looking at the transition to bulk-like flow, which begins at around 50 angstroms.

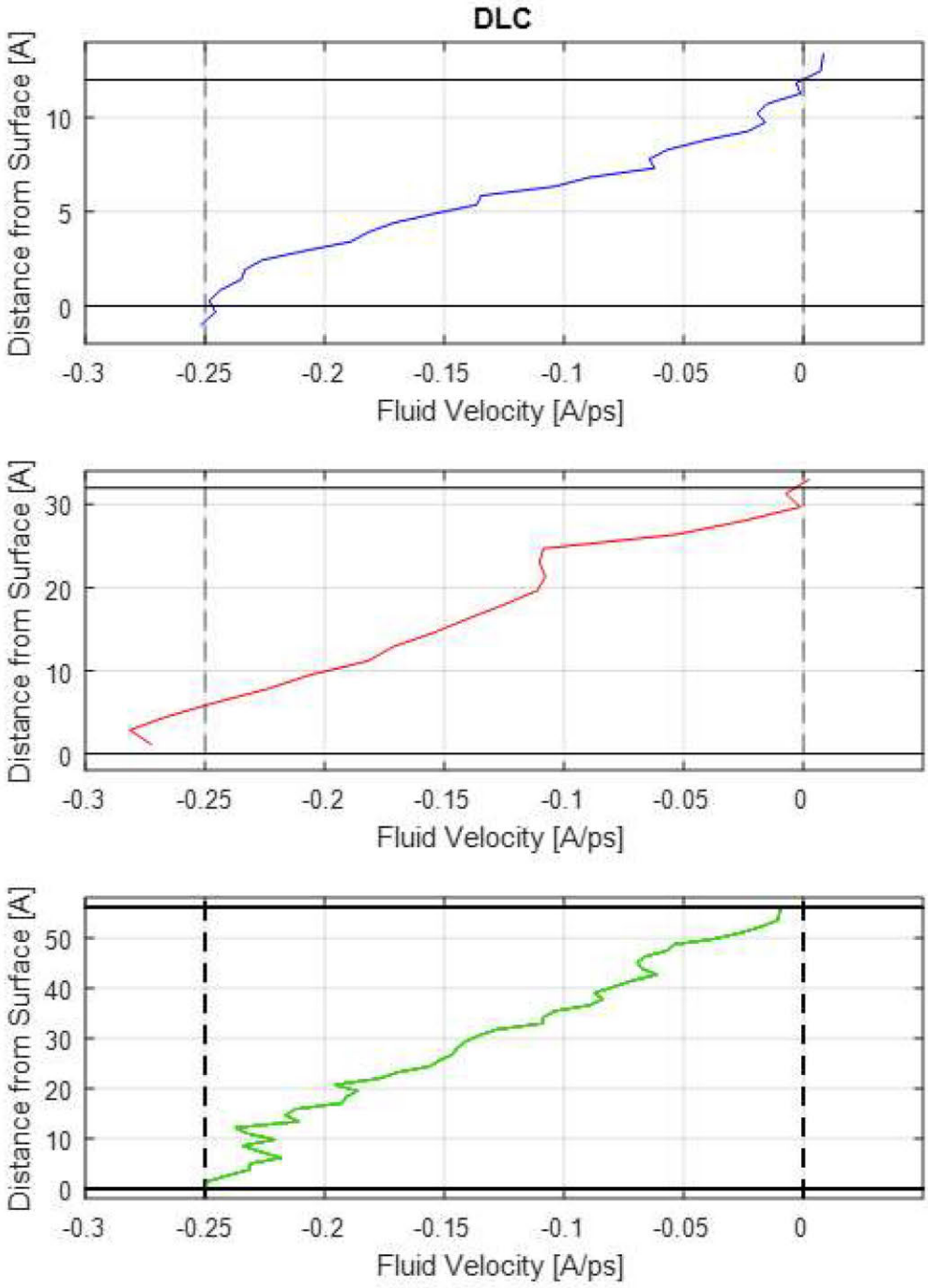

Figure 5-2: Selection of velocity profiles for water between two DLC surfaces. Top) 12 angstroms of fluid height. Middle) 32 angstroms of fluid height. Bottom) 56 angstroms of fluid height. The solid lines indicate the height of each passivated surface, and the dotted lines indicate the x velocity of each counterface.

Velocity and Density Profiles

In order to obtain a better understanding of the source of the differences between the DLC and steel simulations, we study the velocity profiles within the water, as shown in figures 5-2 and 5-3. Figure 5-2 shows three velocity profiles for three increasing heights of water (1200 water molecues/12 Angtsoms, 3600 water molecues/32 angstroms, and 5800 water molecules/56 angstroms) separating DLC counterfaces. From this data we can observe that the water molecules near each passivation layer are moving at the same velocity as the counterface they are adjacent to, even for relatively small fluid heights. This indicates that there is a strong adhesion between the water molecules and the passivation layer that forms on DLC when it is passivated in water. Additionally, we can also determine that there is some thickness of lubricant near each interface that is relatively immobile with respect to the nearby solid. From the figure we can observe that the thickness of this interfacial layer that is influenced by the proximity to the passivated surface appears to grow with increasing fluid height.

The resulting velocity profiles for 1200 water molecules (12 angstroms), 3600 water molecules (27 angstroms), and 6000 water molecules (49 angstroms) when paired with steel counterfaces are shown in figure 5-3. We similarly observe that there is an extended interfacial layer that keeps water atoms near each surface at approximately the same velocity as the wall. However, unlike the DLC case, this interfacial layer is much thicker and is a result of the formation of iron-oxyhydroxide at the interface between the steel counterfaces and the water. This disperses iron atoms into the water and results in a much more gradual transition from solid to liquid. As with the DLC simulations, this interfacial layer appears to grow with the total fluid height at least up until bulk-like flow begins to take over at fluid heights over 56 angstroms.

Additional insight is obtained by looking at the density profiles of the water lubricating layers as a function of the distance between the counterfaces. Density profiles for DLC and steel counterfaces separated by 3600 water molecules are shown in figures 5-4 and 5-5, respectively. From these two figures we can get an even clearer picture of

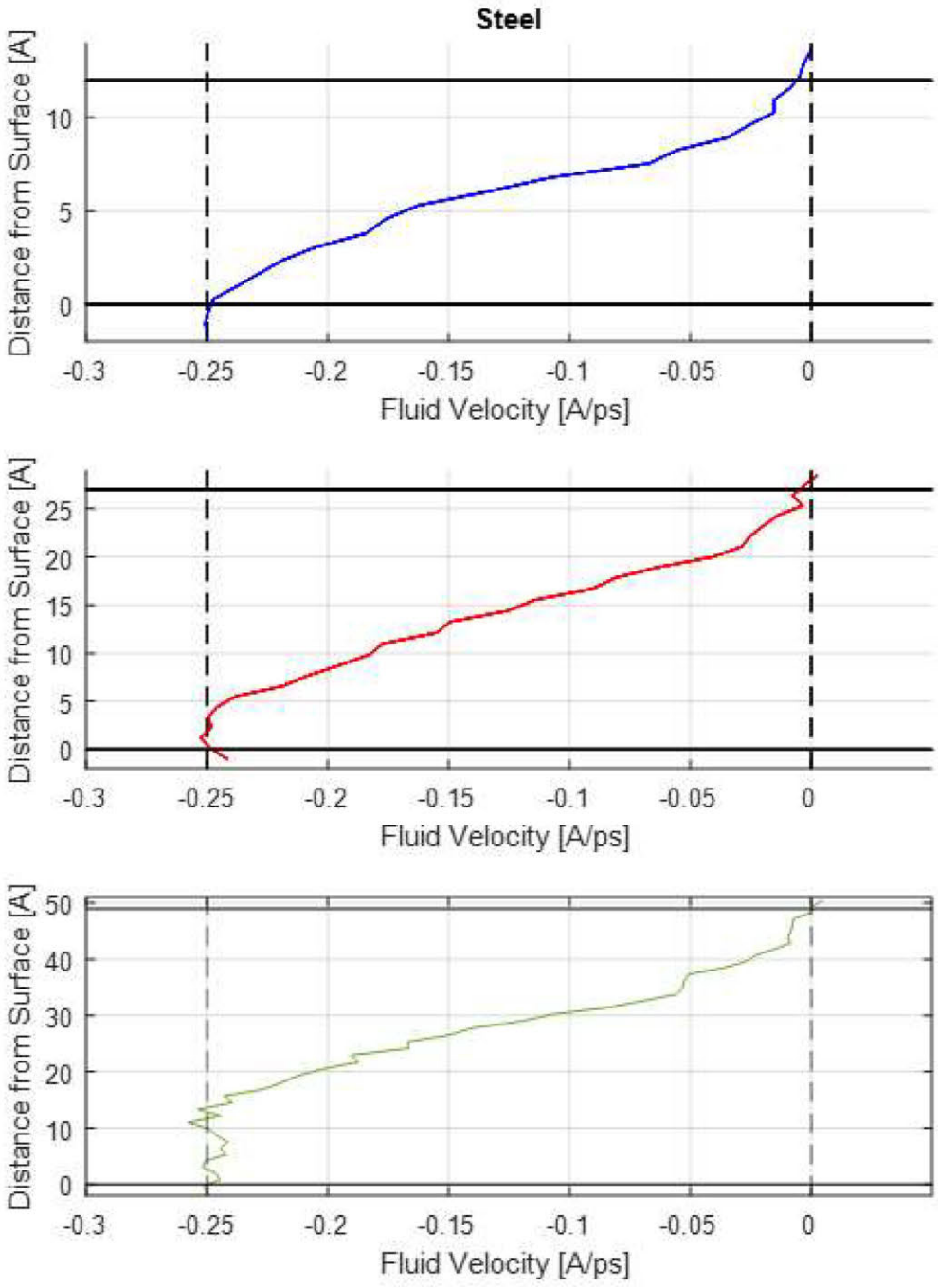

Figure 5-3: Selection of velocity profiles for water between two steel surfaces. Top) 12 angstroms of fluid height. Middle) 27 angstroms of fluid height. Bottom) 49 angstroms of fluid height. The solid lines indicate the height of each passivated surface, and the dotted lines indicate the x velocity of each counterface.

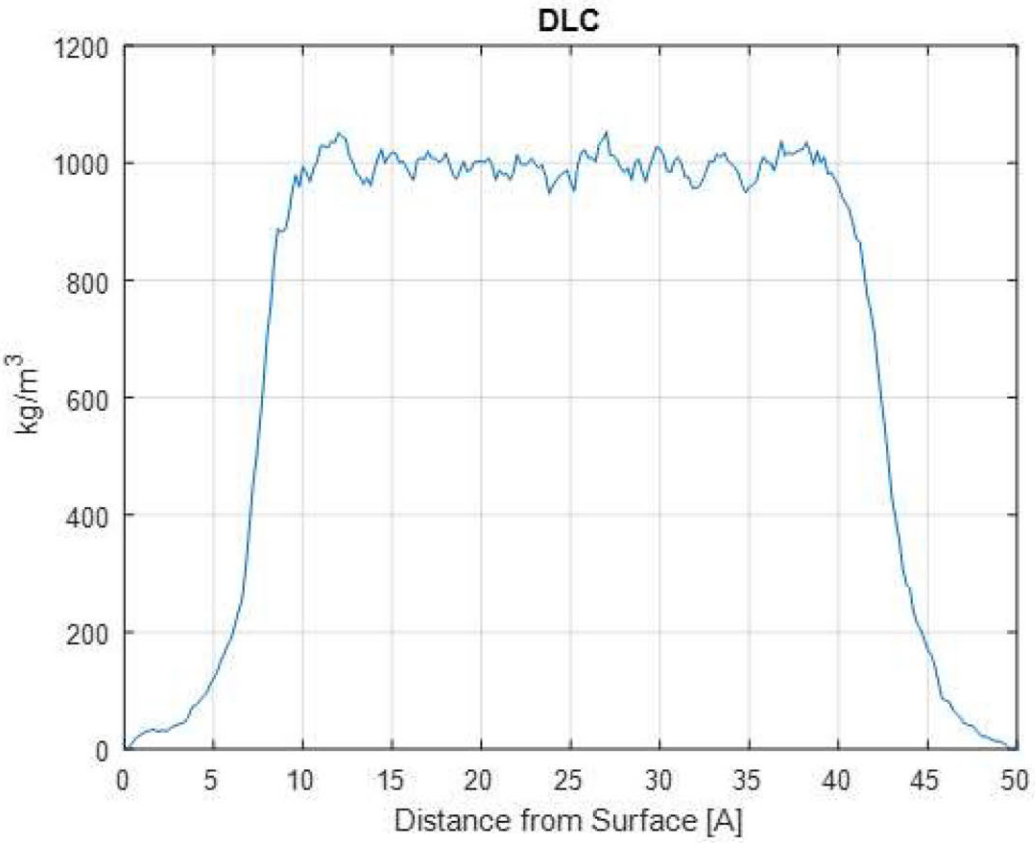

Figure 5-4: Density profile results for water 350K water at 500 MPa between two DLC surfaces.

the structure of these interfacial layers. For DLC surfaces we observe that as the distance from the surface increases, the density of the water remains significantly lower than expected up until approximately 10 angstroms from each of the counterfaces. However, in the case of steel counterfaces, the data indicates that the bulk density of the fluid is not reached until 20 angstroms from either of the steel counterfaces. The stepped transition in the density of water molecules observed in figure 5-5 is due to the formation of iron-oxyhydroxide at the surface, which allows iron atoms to mix into the lubricating layer near the interface.

It is also important to note that even far from these interfacial layers, the bulk density of water is found to be 992 kg/m^3 for DLC counterfaces and 999 kg/m^3 for steel counterfaces, due to the molecular potential model being used. This is about 10% less than the expected bulk density of water under these conditions (1120

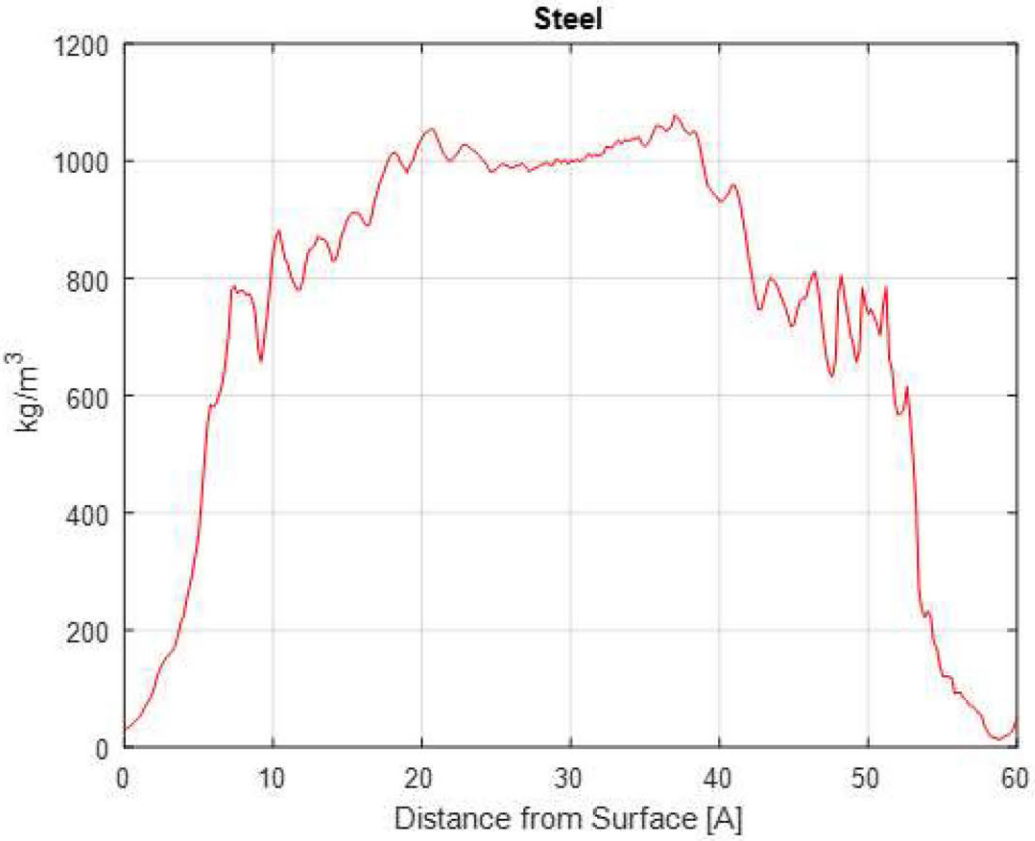

Figure 5-5: Density profile results for water 350K water at 500 MPa between two steel surfaces.

kg/m^3), but is expected to have a significant impact on the water viscosity, due to the strong relation between the density of fluids and their viscosity [76]. Similarly, the atomic scale non-uniformity of the density observed in the results may also impact the viscosity of the water in the simulations.

5.3.2 Alkanes

Additional simulations were run using hydrogen passivated DLC counterfaces with a selection of hydrocarbon lubricants (n-Decane, n-Eicosane, 9-Octyl-Eicosane). The friction force was measured for lubricant layers of various heights and the results are shown in figure 5-6. As with the Couette flow simulations lubricated with water, the computational cost of running ever larger simulations prevented us from being able to simulate lubricant layers larger than 100 to 200 angstroms in height. Unfortunately,

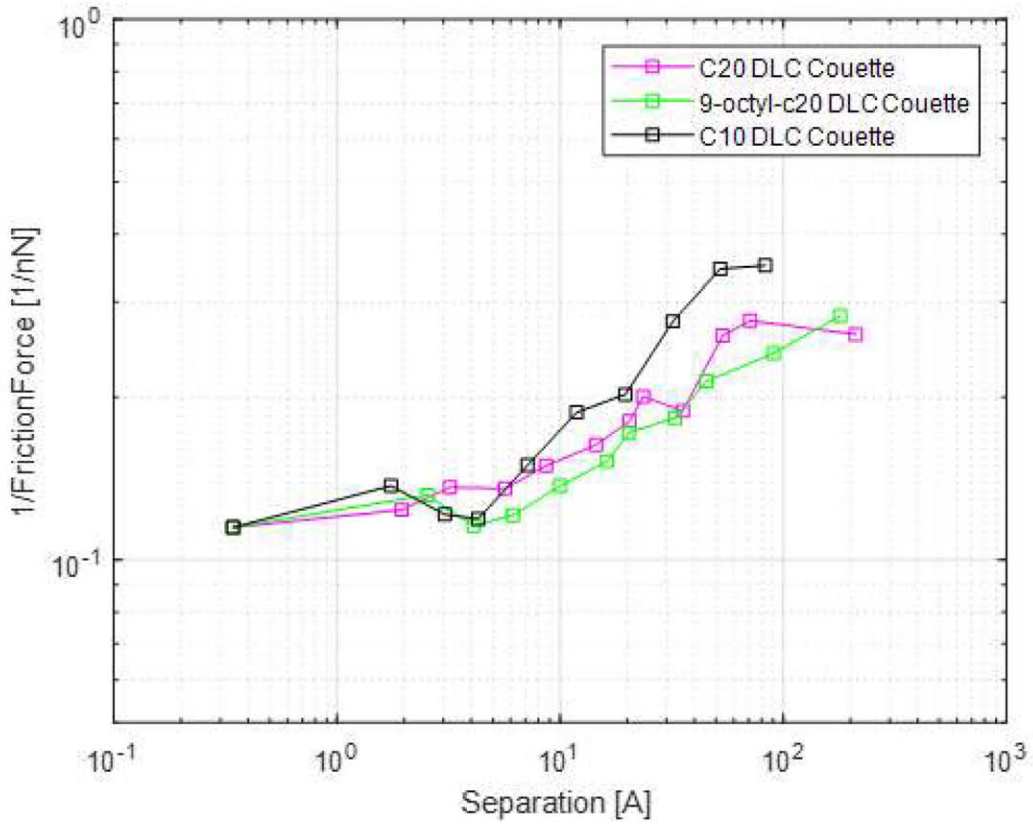

Figure 5-6: Inverse of friction force versus fluid height for hydrogen passivated DLC counterfaces lubricated with n-Decane (Black), n-Eicosane (Magenta), 9-Octyl-Eicosane (Green).

in the alkane case, the transition to interfacial flow occurs at larger channel heights, which occurs due to two related reasons. The first and most obvious is that physically the molecules in the interfacial layer are just significantly larger. The second is that larger molecules generally have higher viscosities [77, 78]; as shown in section 5.3.3 higher viscosities will cause the transition to interfacial flow to occur at larger gap heights As a result, we were unable to simulate all of the expected flow regimes; as figure 5-6 shows, we were able to measure the slip friction and the beginning of the transition to the interfacial regime.

From the data in figure 5-6, we can determine that 9-octyl-eicosane generally had the highest friction, followed by n-eicosane, and then n-decane. In other words, the larger the molecule size the higher the resulting friction force. However, this is

not just a result of the higher viscosity increasing the amount of shear stress in the system. Given that the Couette flow data is primarily in the slip regime and the start of the interfacial regime, the increase in size of the interfacial layer is more likely to have a significant effect on the friction force than the viscosity itself. In other words, delaying the onset of interfacial flow results in an extended slip friction regime and will increase the friction force for a given channel height.

5.3.3 A rational model for the friction

In this section we propose an expression for describing wall shear in our nanoconfined Couette flow simulations. The proposed expression is a modified form of relation 5.1 proposed by [74]. The modifications are in part due to our preference for a model which is simpler and does not use many adjustable (fitting) constants, but also because the physics of the system used in this work appears to be slightly different than those investigated in [74]. This expression superposes a slip term with a bulk Couette term that has a reduced channel width due to the interfacial layers observed in the preceding simulations. As the width of these interfacial layers was found to be dependent on the gap height (see figures 5-2 and 5-3), the amount by which the gap width is reduced is dependent on the gap width itself. Mathematically, the above can be written in the following form

$$\frac{1}{F_{wall}} = C_1 + C_2 \left(L - 2H(L)\right) \tag{5.2}$$

where

$$C_1 = \frac{1}{F_{slip}} \tag{5.3}$$

and

$$C_2 = \frac{1}{A\mu U_0} \tag{5.4}$$

Here, C_1 represents the inverse of the slip friction term, while C_2 is the standard bulk Couette flow coefficient that incorporates the surface area (A), the viscosity of the lubricant (μ) and the translational velocity of the moving counterface (U_0). The

height of the interface layer $H(L)$, which is a function of the separation between the two counterfaces L, is described by the form

$$H(L) = \left(\frac{1}{(L/2)^3} + \frac{1}{H_\infty^3} \right)^{-1/3} \tag{5.5}$$

which was shown in the work of Schlaich et al. to capture this phenomenon quite well. Here H_∞ is the maximum thickness of the interfacial layer, which would occur during bulk Couette flow. In other words, the model has three unknown parameters (C_1, C_2, and H_∞) that can be determined by fitting simulation results.

Applying this model to the results from section 5.3.1, results in good agreement as shown in figure 5-7. This fitting process provides more than numerical values for the unknown coefficients. It also provides insight into the manner in which DLC and steel counterfaces interact with water and how that affects the behavior of the lubricant. When fitting the data generated using DLC counterfaces, H_∞ was found to be approximately 5.3 angstroms. This agrees with the previous estimates of the maximum thickness of the interfacial layer based on the velocity and density profiles in section 5.3.1, and indicates that water lubricated DLC surfaces results in a relatively thin interfacial layer. Additionally, we can use the value of C_2 to estimate the viscosity of water; the fit shown in the figure results in the value 0.33 mPa s.

Fitting the simulation data for steel counterfaces lubricated with water, we obtain a much larger H_∞ of 19 angstroms. This is consistent and in fact in good agreement with the visual observations of the size of the interfacial layers observed from the velocity and density profiles. This larger passivation layer is a result of the formation of iron-oxyhidroxide on the steel surface, which results in a much more gradual transition from solid to liquid. Using this simplified model, we can estimate the viscosity of the water to be 0.38 mPA s.

The viscosity estimates we obtained are significantly smaller than the expected viscosity of water at 500 MPa and 350K. However, as we noted in section 5.3.1, the bulk density of water was significantly lower. If we compare our estimates to the viscosity of water at 350K and a density of 1000 kg/m^3, namely 0.39 mPa s

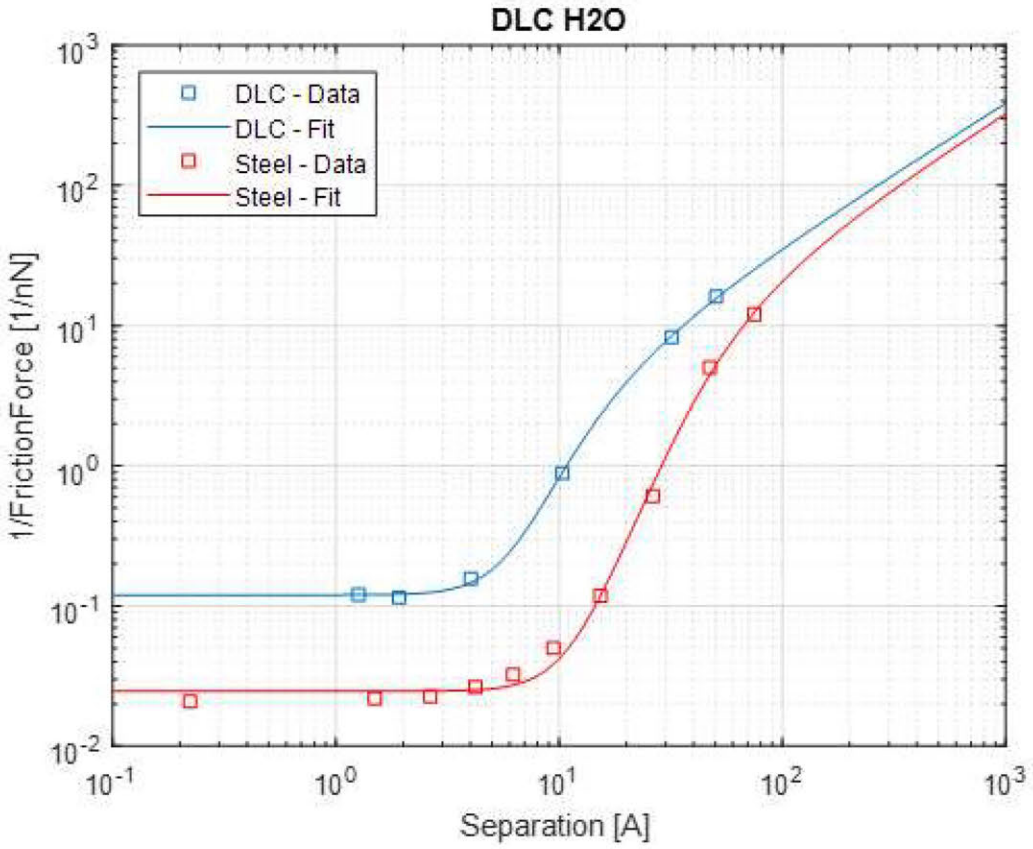

Figure 5-7: Inverse of friction force versus fluid height when using water as a lubricant. DLC results are shown in blue and steel surfaces in red. Solid lines are the result of fitting the model proposed here (eq. (5.2)) to the data for each surface.

[75], the agreement is much better. The deviation in these results is possibly due to the limited amount of simulations with large fluid heights and/or the atomic scale variations in the density and viscosity of fluids, as well as modeling error originating in the interaction potential.

Unfortunately, due to the high computational cost of running ever larger simulations using hydrocarbon lubricants, we were unable to simulate the interfacial or bulk-like regimes of nanoconfined flow for these cases. As a result, there is insufficient data for fitting the new model to the simulations discussed in section 5.3.2. However, combining the available simulation results for n-decane with the experimentally determined viscosity of the lubricant from the literature [79], we can use the model to estimate the value of H_∞ for these lubricants.

We start by evaluating equation 5.2 for $H = H_\infty$:

$$\frac{1}{F^*} = \frac{1}{F_{slip}} + \frac{0.0385 H_\infty}{A\mu U_0} \tag{5.6}$$

Using the experimental viscosity of n-eicosane and the values for F_{slip}, A and U_0 from the MD simulations, we can estimate H_∞ by reading $1/F^*$ from the simulation data. Using our simulation results, we estimate H_∞ for DLC surfaces lubricated with n-eicosane to be approximately 45 angstroms. This indicates that simulations with a channel height of several hundred angstroms would be necessary to model all three regimes in this case.

Additionally, we can rewrite equation 5.6 in the form

$$H_\infty = (26.0 A\mu U_0)\left(\frac{1}{F^*} - \frac{1}{F_{slip}}\right) \tag{5.7}$$

which demonstrates that H_∞ increases proportionally with the viscosity, as previously mentioned in section 5.3.2. This also implies that the necessary simulation sizes would increase in proportion with the viscosity. Note that this proportionality to the viscosity assumes that the molecules are otherwise sufficiently similar and have effectively identical interactions with the counterfaces.

5.4 Discussion

In this chapter we have used MD simulations of Couette flow to study the interactions between thin films of various lubricants and passivated DLC or steel counterfaces. These interactions between the passivated surfaces and the molecules of lubricant become increasingly important as fluid film thickness decreases. Previous work [74] has suggested that three distinct regimes can be identified as the thickness of the lubricating layer decreases, namely bulk-like flow, interfacial flow and slip friction.

In these computational experiments we were able to observe the transitions between these different flow regimes for both DLC and steel counterfaces when using water as the lubricating layer. Unfortunately, the hydrocarbon lubricants tested were

too large and viscous to reach interfacial or bulk-like flow before the computational costs of running larger simulations became infeasible. We then used viscosity and density profiles of the lubricating layer to gain insight into the underlying mechanics of the origins of these flow regimes. The primary feature of these profiles was the existence of an interfacial layer of fluid in close proximity to each surface that had a density lower than the bulk density of the fluid and was also relatively immobile with respect to the nearest solid. These interfacial layers were found in the simulations using both DLC and steel counterfaces; however, some key differences exist. In the case of DLC surfaces the passivation layer is thin and the transition to the water was sharp; at the same time, the passivated surface is very hydrophilic and strongly attracts water molecules. In contrast, the much thicker passivation layer that formed in the case of steel counterfaces was a result of the formation of iron-oxyhydroxide on the steel surface, which resulted in a much less sharp transition from solid to liquid.

Using this information we developed a model for the friction in nanoscale Couette flow that captures the transition between the three regimes mentioned above. By fitting this model to the data collected from the simulations in section 5.3.1, we were able to find that the layer of water molecules adhering to the surface have a maximum thickness of 5 angstroms with the DLC surfaces and a maximum thickness of 19 angstroms with the steel surfaces. Additionally, the proposed model allowed us to estimate the viscosity of the water to be approximately between 0.33 and 0.38 mPa s. These viscosity measurements are close to the true viscosity of water at a temperature of 350K and density of 1000 kg/m^3.

Additional simulations were run using hydrogen passivated DLC counterfaces with n-Decane, n-Eicosane, and 9-Octyl-Eicosane as the model lubricants. The measured friction force at every fluid height generally increased with the molecule size of the lubricant being used, which is also correlated with the viscosity of each lubricant. This results in a larger H_∞, which means that a larger fluid height is necessary for the system to transition to interfacial and bulk-like flow regimes, which are associated with significantly reduced friction.

Chapter 6

Conclusion

6.1 Summary and conclusions

In this thesis we have used MD simulations with a reactive force field for the purpose of investigating the tribological properties of DLC under dry, lubricated and mixed lubrication conditions. We have shown that the tribological properties of DLC in dry sliding friction are heavily dependent on both the structure of the DLC as well the passivation layer that forms under different environmental conditions. We investigated the role the passivation layer on the DLC counterface allows it the latter to resist scuffing and wear by preventing bonding as the thin film of lubricant is squeezed out at the point of contact. Additionally, we developed a simplified model for describing the frictional force in nanoconfined Couette flow, and using that model investigated how the surface chemistry of DLC and its passivation layer impact the fluid dynamic properties of thin layers of model lubricants.

In Chapter 3, we describe MD simulation results of dry sliding friction between pairs of DLC, steel, and mixed surface counterfaces. From these simulations we were able to determine that the passivation layer on the surface of the counterfaces is very important for determining the tribological properties of the material. This layer is particularly strong and durable in DLC, and acts to prevent passivated surfaces from chemically bonding/welding to the opposing counterface. Additionally, the passivation layer can have a dramatic impact on the strength of adhesion forces between

the two surfaces. The passivation layer is crucial for limiting adhesion between the two counterfaces as well as preventing the surfaces from chemically bonding together. However, in addition to being affected by the chemical makeup of the passivation layer, the tribological properties of DLC can also be impacted by the bulk sp^3 percentage of the DLC. In addition to changing the hardness and strength of the bulk material, modifying the sp^3 percentage can significantly change the properties of the passivation layer that forms on the surface of the DLC.

In Chapter 4, we used MD simulations for investigating, at the atomistic level, friction and wear between like surface pairs of DLC and steel counterfaces in lubricated contact. We considered water, n-eicosane, and 9-octyl-eicosane lubricants, while paying particular attention to the passivation layer they induce on the sliding solid surfaces. These simulations provide molecular insight into the key differences in behavior between the two materials as the lubricant is squeezed out at the point of contact. Specifically, steel surfaces were found to be very susceptible to bonding, which causes high friction, wear and ultimately material failure; the latter can be either due to high stress or wear, depending on the lubricant. In contrast, DLC forms a very strong and chemically inert passivation layer, which, when combined with the DLC high strength, make it an effective coating for reducing friction and wear.

In Chapter 5, we used MD simulations of Couette flow to study the interactions between thin films of various lubricants and passivated DLC or steel counterfaces. These interactions between the passivated surfaces and the molecules of lubricant become increasingly important as fluid film thickness decreases, which results in the three different regimes of nanoconfined flow that depend on the thickness of the lubricating layer. As the thickness of the layer decreases, the type of friction transitions from bulk-like flow, to interfacial flow, and then finally to slip friction. By studying the behavior of the lubricant molecules in these simulations, we were able to observe an interfacial layer that was relatively immobile with respect to the nearest solid. Using this information we developed a simplified model for the fiction in nanoscale Couette flow. Using this proposed model with these simulation results, we were able to estimate both the bulk viscosity of a lubricant and the maximum thickness of the

interfacial layer that would form for a given combination of lubricant and counterface.

Overall, we can attribute the majority of DLC's excellent tribological properties to the passivation layers that form when it is exposed to water or hydrocarbon molecules. DLC's passivation layers are very effective at preventing adhesion and bonding between surfaces in close contact, while also being highly durable. In fact, they are so effective, that DLC was found to behave nearly identically in mixed lubrication and wear regardless of which lubricant was used. Additionally, the compact nature of DLC's passivation layers results in a relatively small interfacial layer, which allows for lubricated DLC surfaces to approach bulk-like flow, yielding smaller friction forces, even at very small counterface separations.

6.2 Outlook and Suggestions for Future Work

The work in this thesis was targeted at developing models and techniques for investigating the tribological properties of a system composed of a fairly common tetrahedral amorphous DLC surface and a selection of easy to simulate model lubricants. Fully understanding the tribological properties of DLC and its interactions with lubricants will require a study expanding to the full range of DLC variants, including those with low sp^3 percentages, as well as those doped with light elements (B, Si, N, O, F), or alloyed with different metals (Ti, W, Cu, Cr), in order to modify their tribological properties [80].

Similarly, a lot could be learned from observing the interaction between DLC and lubricants in additional detail. In particular, modeling the strength of the adhesion and wettability between various real-world lubricants and DLC surfaces could provide additional information about the strength of the wear protection provided by various lubricants and how much fluid is required for bulk like flow to develop. In addition, real world lubricants are frequently combined with friction and wear modifying additives. There is little known about how these oil additives interact with DLC surfaces or how combining DLC and these additives might affect both the lubricated and unlubricated friction between counterfaces.

In the present thesis we did not investigate the effects of temperature. Introducing temperature as variable may modify some of our results and will be valuable in understanding how the high temperatures seen in engines affect the longevity and durability of DLC coatings. In particular this would involve looking at the effect of temperature on the DLC wear rate, what the maximum safe temperature for DLC coatings is depending on the desired properties, and whether various lubricants would moderate the effects of high temperature on DLC.

Another interesting area of study would be the formation of DLC passivation layers and which passivation layer properties result in improved tribological performance. This would involve studying how different lubricants or environmental conditions impact the formation of the passivation layer and if it is possible to develop a particularly advantageous passivation layer that could significantly reduce the coefficient of friction or wear rate.

Bibliography

[1] Erdemir, A. and Donnet, C., "Tribology of diamond-like carbon films: recent progress and future prospects" J. Phys. D Appl. Phys., 36, R311, 2006.

[2] R. Zahid, et al., "Effect of Lubricant Formulation on the Tribological Performance of Self-Mated Doped DLC Contacts: a Review" Tribol Lett, 58, 32, 2015.

[3] J. Araujo and R. Banfield , "DLC as a Low Friction Coating for Engine Components." SAE Technical Paper, 36, 0255, 2012.

[4] M. Kano, "Overview of DLC-Coated Engine Components." In: Cha S., Erdemir A. (eds) Coating Technology for Vehicle Applications. Springer, 2015.

[5] C.S. Bhatia , E. Rismani-Yazdi, S.K. Sinha, and A.J. Danner. "Applications of DLC in Magnetic Recording." In: Q.J. Wang, YW. Chung (eds) Encyclopedia of Tribology. Springer, Boston, MA, 2013.

[6] M.I. Jones, et al., "Protein adsorption and platelet attachment and activation, on TiN, TiC, and DLC coatings on titanium for cardiovascular applications." J. Biomed. Mater. Res, 52, 413-421, 2000.

[7] R. Hauert, et al., "Analysis of the in-vivo failure of the adhesive interlayer for a DLC coated articulating metatarsophalangeal joint." Diam. Relat. Mater, 25, 34âĂŞ39, 2012.

[8] B. Vengudusamy, J.H. Green, G.D. Lamb, and H.A. Spikes. "Behaviour of MoDTC in DLC/DLC and DLC/steel contacts." Tribol. Int, 54, 68-76, 2012.

[9] D.C. Pham, H.S. Ahn, J.E. Oh, and E.S. Yoon,"Tribochemical interactions of Si-doped DLC film against steel in sliding contact." J. Mech. Sci. Technol, 21, 1083-1089, 2007.

[10] H. Li, et al., "Friction-induced physical and chemical interactions among diamond-like carbon film, steel ball and water and/or oxygen molecules." Diam. Relat. Mater, 15, 1228-1234, 2006.

[11] Sutton, D.C., Limbert, G., Stewart, D., and Wood, R.J.K., "The friction of diamond-like carbon coating in a water environment" Friction, 1, 210, 2013.

[12] Ronkainen, H., Varjus, S., and Holmberg, K., "Friction and wear properties in dry, water- and oil-lubricated DLC against alumina and DLC against steel contacts" Wear, 222, 120, 1998.

[13] Jiang, J., Zhang, S., and Arnell, R.D., "The effect of relative humidity on wear of a diamond-like carbon coating" Surf. Coat. Technol., 167, 221, 2003.

[14] Marino, M.J., Hsiao, E., et al., "Understanding run-in behavior of diamond-like carbon friction and preventing diamond-like carbon wear in humid air" Langmuir, 27,12702, 2011.

[15] Alder, B.J. and Wainwright, T.E., "Studies in Molecular Dynaics. I. General Method" J. Chem. Phys., 31, 459, 1959.

[16] Israelachvili, J.N,*Intermolecular and Surface Forces*, Academic Press, 2015.

[17] Gnecco, G. and Meyer, E., *Fundamentals of Friction and Wear*, Springer, 2008.

[18] Gnecco, G., Bennewitz, R., et al. "Friction and Wear on the Atomic Scale," *Nanotribology and Nanomechanics*, Springer, 2007.

[19] T.P. Senftle, et al., "The ReaxFF reactive force-field: development, applications and future directions." npj Comput. Mater, 2, 15011, 2016.

[20] M. Meuwly, "Reactive molecular dynamics: From small molecules to proteins." WIREs Comput. Mol. Sci, 9, 1386, 2019.

[21] S. Nouranian , et al., "An interatomic potential for saturated hydrocarbons based on the modified embedded-atom method." J. Biomed. Mater. Res, 16, 6233-6249, 2014.

[22] Kajita, S., and Righi, M.C., "A fundamental mechanism for carbon-film lubricity identified by means of ab initio molecular dynamics" Carbon, 103, 193, 2016.

[23] Bal, S., Onodera, T., et al., "Friction Reduction Mechanism of Hydrogen- and Flourine-Terminated Diamond-Like Films Investigeated by Molecular Dynamics and Quantum Chemical Simulation" J. Phys. Chem. C, 116, 12559, 2012.

[24] Haashi, K., Tezuka, K., et al., "Tribochemical Reaction Dynamics Simulation of Hydrogen on a Diamond-like Carbon Surface based on Tight-Binding Quantum Chemical Molecular Dynamics" J. Phys. Chem. C, 115, 22981, 2011.

[25] T.M.M. Homelle, and N.G. Hadjiconstantinou, "A low-variance deviational simulation Monte Carlo for the Boltzmann equation." J. Comp. Phys, 226, 2341-2358, 2007.

[26] A.C. Ferrari and J. Robertson, "Raman spectroscopy of amorphous, nanostructured, diamond-like carbon, and nanodiamond." Phil. Trans. R. Soc. Lond, A362, 2477-2512, 2004.

[27] A. Al-Azizi, et al., "Vapors in the ambient-A complication in tribological studies or an engineering solution of tribological problems?" Friction, 3, 85-114, 2015.

[28] A. Al-Azizi, et al., "Surface Structure of Hydrogenated Diamond-like Carbon: Origin of Run-In Behavior Prior to Superlubricious Interfacial Shear" Langmuir, 31, 1711-1721, 2015.

[29] J. Jiang, S. Zhang, and R.D. Arnell, "The effect of relative humidity on wear of a diamond-like carbon coating." Surf. Coat. Tech, 167, 221-225, 2003.

[30] S. Kajita and M.C. Righi, "A fundamental mechanism for carbon-film lubricity identified by means of *ab initio* molecular dynamics." Carbon, 103, 193-199, 2016.

[31] X. Li, A. Wang and K.R. Lee, "Insights on low-friction mechanism of amorphous carbon films from reactive molecular dynamics study." Tribol. Int, 131, 567-578, 2019.

[32] X. Li, A. Wang and K.R. Lee, "Atomistic understanding on friction behavior of amorphous carbon films induced by surface hydrogenated modification." Tribol. Int, 136, 446-454, 2019.

[33] G.T. Gao, P.T. Mikulski and J.A. Harrison, "Molecular-Scale Tribology of Amorphous Carbon Coatings: Effects of Film Thickness, Adhesion, and Long-Range Interactions." J. Am. Chem. Soc, 124, 7202-7209, 2002.

[34] T. Kunze, et al., "Wear, Plasticity, and Rehybridization in Tetrahedral Amorphous Carbon." Tribol. Lett, 53, 119-126, 2014.

[35] L. Bai, et al., "Wear and friction between smooth or rough diamond-like carbon films and diamond tips." Wear, 372, 12-20, 2017.

[36] K. Hayashi, et al., "Tribochemical Reaction Dynamics Simulation of Hydrogen on a Diamond-like Carbon Surface Based on Tight-Binding Quantum Chemical Molecular Dynamics" J. Phys. Chem. C, 115, 22981-22986, 2011.

[37] T. Kuwahara, et al., "Mechano-chemical decomposition of organic friction modifiers with multiple reactive centres induces superlubricity of ta-C." Nat. Commun, 10, 151, 2019.

[38] H.M. Aktulga, J.C. Fogarty, S.A. Pandit, and A.Y. Grama, "Parallel reactive molecular dynamics: Numerical methods and algorithmic techniques." Parallel Comput, 38, 245-259, 2012.

[39] H.M. Aktulga, et al., "Optimizing the performance of reactive molecular dynamics simulations for many-core architectures." Int. J. High Perform. C, 33, 304-321, 2018.

[40] A.C.T. van Duin, S. Dasgupta, F. Lorant, and W.A. Goddard, "ReaxFF: A reactive force field for hydrocarbons." J.Phys. Chem. A, 105, 9396-9409, 2001.

[41] T.P. Senftle, et al., "The ReaxFF reactive force-field: development, applications, and future directions." Npj Comput. Mater, 2, 15011 (2016).

[42] S. Plimpton, "Fast parallel algorithms for short-range molecular dynamics." J. Comput. Phys, 117, 1, 1995.

[43] L. Verlet, "Computer "Experiments" on Classical Fluids. I. Thermodynamical Properties of Lennard-Jones Molecules". Phys Rev. 159, 98âĂŞ103, 1967.

[44] S. Nosé, "A unified formulation of the constant temperature molecular dynamics methods." J. Chem. Phys, 81, 511, 1984.

[45] W. G. Hoover, "Canonical dynamics: Equilibrium phase-space distributions." Phys. Rev. A, 31, 1695, 1985.

[46] K. Chenoweth, A.C.T. van Duin, and W.A. Goddard, "ReaxFF reactive force field for molecular dynamics simulations of hydrocarbon oxidation." J. Phys. Chem. A, 112, 1040-1053, 2008.

[47] C. Zou, A.C.T van Duin, and D. Sorescu, "Theoretical investigation of hydrogen adsorption and dissociation on iron and iron carbide surfaces using the ReaxFF reactive force field method." Top. Catal, 55, 391-401, 2012.

[48] H.A. Castillo, E. Restrepo-Parra, and P.J. Arango-Arango, "Chemical and morphological difference between TiN/DLC and a-C:H/DLC grown by pulsed vacuum arc techniques." Appl. Surf. Sci, 257, 2665-2668, 2011.

[49] S.J. Bull, "Tribology of carbon coatings: DLC, diamond and beyond." Diam. Relat. Mater, 4, 827-836, 1995.

[50] E.J. Caule and M. Cohen, "The Formation of Thin Films of Iron Oxide" Can. J. Chem, 33, 288-305, 1955.

[51] Y. Wang, et al., "Tight-Binding Quantum Chemical Molecular Dynamics Study on the Friction and Wear Processes of Diamond-Like Carbon Coatings: Effect of Tensile Stress." ACS Appl. Mater. Inter, 9, 34396-34404, 2017.

[52] A.C.T van Duin, et al., "A ReaxFF Reactive Force Field for Proton Transfer Reactions i Bulk Water and Its Applications to Heterogeneous Catalysis." Comput. Catal., 14, 223, 2013.

[53] A. Ramasubramaniam, M. Itakura, and E.A. Carter, "Interatomic potentials for hydrogen in α-iron based on density functional theory." Phys. Rev. B, 79, 174101, 2009.

[54] M. Aryanpour, A.C.T van Duin, and J.D. Kubicki, "Development of a Reactive Force Field for Iron-Oxyhydroxide Systems." J. Phys. Chem. A, 114, 6298-6307, 2010.

[55] H.M. Aktulga, J.C. Fogarty, S.A. Pandit, and A.Y. Grama, "Parallel reactive molecular dynamics: Numerical methods and algorithmic techniques." Parallel Comput, 38, 245-259, 2012.

[56] A.K. Rappe and W.A. Goddard III, "Charge Equilibration for Molecular Dynamics Simulations, J. Phys. Chem, 95, 3358-3363, 1991.

[57] A. Nakano, "Parallel multilevel preconditioned conjugate-gradient approach to variable-charge molecular dynamics." Comput. Phys. Commun, 104, 59-69, 1997.

[58] G.L. Klimchitskaya, U. Mohideen, andV.M. Mostepanenko, "Casimir and van der Waals forces between two plates or a sphere (lens) above a plate made of real metals." Phys. Rev. A, 61, 062107, 2000.

[59] A. Erdemir, O.L. Eryilmaz, , and S.H. Kim, "Effect of tribochemistry on lubricity of DLC films in hydrogen." Surf. Coat. Technol., 257, 241, 2014.

[60] Cloutier, M., Harnagea, C., et al., "Long-term stability of hydrogenated DLC coatings: Effects of aging on the structural, chemical and mechanical properties." Diam. Relat. Mater., 48, 65, 2014.

[61] A. Al-Azizi, O. Eryilmaz, A. Erdemir, and S.H. Kim, "Surface Structure of Hydrogenated Diamond-like Carbon: Origin of Run-In Behavior Prior to Superlubricious Interfacial Shear." Langmuir, 31, 1711-1721, 2015.

[62] M. Tagawa, et al., "Effect of water adsorption on microtribological properties of hydrogenated diamond-like carbon films." Tribol Lett, 17, 575-580, 2004.

[63] S. Lee and R. W. Staehle, "Adsorption of Water on Copper, Nickel, and Iron." Corros. Sci, 53, 33-42, 1997.

[64] A. Al-Azizi, et al., "Nano-texture for a wear-resistant and near frictionless DLC." Carbon, 73, 403-412, 2014.

[65] E.C. Donaldson and W. Alam, "Surface Forces". *Wettability.* Gulf Publishing Company, 57-119, 2008.

[66] I.M. Sivebaek, V.N. Samoilov and B.N.J. Persson, "Squeezing molecular thin alkane lubrication films between curved solid surfaces with log-range elasticity: Layering transitions and wear." J. Chem. Phys, 119, 2314, 2003.

[67] J.N. Israelachvili, "van der Waals dispersion force contribution to works of adhesion and contact angles on the basis of macroscopic theory." J. Chem. Soc, Faraday Trans. 2, 69, 1729-1738, 1973.

[68] C.-J. Tsai, D.Y.H. Pui, and B.Y.H. Liu, "Elastic Flattening and Particle Adhesion." Aerosol Sci. Tech, 15, 239-255, 1991.

[69] S. Usui, H. Kato, H. Nakajima, and K. Shimokawa, "Effect of Diamond-Like Carbon Coating on Anti-Scuffing Characteristics of Piston Pins." SAE Technical Paper, 2019-01-0184, 2019.

[70] P. Obert, H.-J. Fusser, and D. Bartel, "Oil distribution and oilfilm thickness within the piston ring-liner contactmeasured by laser-inducedfluorescence in a reciprocating model test understarved lubrication conditions." Trib. Int, 129, 191-201, 2019.

[71] P. Obert, T. Muller, H.-J. Fusser, and D. Bartel, "The influence of oil supply and cylinder liner temperature on friction,wear and scuffing behavior of piston ring cylinder liner contactsâĂŞAnew model test." Trib. Int, 94, 306-314, 2016.

[72] D.M. Clatterbuck, D.C. Chrzan, and J.W. Morris Jr., "The ideal strength of iron in tension and shear." Acta Mater, 51, 2271-2283, 2003.

[73] F. Saeidi, B. Meylan, P. Hoffmann, and K. Wasmer, "Effect of surface texturing on cast iron reciprocating against steelunder starved lubrication conditions: A parametric study." Wear, 348, 17-26, 2015.

[74] A. Schlaich, J. Kappler, and R.R. Netz, "Hydration Friction in Nanoconfinement: From Bulk via Interfacial to Dry Friction." Nano Lett, 17, 5969-5976, 2017.

[75] K.E. Bett and J.B. Cappi, "Effect of Pressure on the Viscosity of Water." Nature, 207, 620-621, 1965.

[76] F. Llovell, R.M. Marcos, and L.F. Vega, "Free-Volume Theory Coupled with Soft-SAFT for Viscosity Calculations: Comparison with Molecular Simulation and Experimental Data." J Phys. Chem. B, 117, 8159-8171, 2013.

[77] E.F. Cooper and A.-F.A. Asfour, "Densities and Kinematic Viscosities of Some C6-C16 n-Alkane Binary Liquid Systems at 293.15 K." J. Chem. Eng. Data, 36, 25-288, 1991.

[78] E. Kiran and Y.L. Sen, "High-Pressure Viscosity and Density of n-Alkanes." Int. J. Thermophys, 13, 412-442, 1992.

[79] A.L. Lee and R.T. Ellington, "Viscosity of n-Decane in the Liquid Phase." J. Chem. Eng. Data, 10, 346-348, 1965.

[80] J.C. Sanchez-Lopez and A. Fernandez, "Doping and Alloying Effects on DLC Coatings." In: Donnet C., Erdemir A. (eds) *Tribology of Diamond-Like Carbon Films*. Springer, 2008.